ARISTOTLE UNIVERSITY OF THESSALONIKI

FACULTY OF SCIENCES
SCHOOL OF GEOLOGY
DEPARTMENT OF GEOPHYSICS

KALOGIROU E. ELENI
GRADUATED GEOLOGIST

STUDY ON GROUND SURFACE FISSURES IN THE BROADER AREA OF THE LIGNITE MINES OF MAVROPIGI VILLAGE, EORDAIA PREFECTURE, NORTHERN GREECE

MASTER THESIS

POSTGRADUATE PROGRAM OF GEOLOGY SCHOOL
FIELD OF SPECIALIZATION: GEOPHYSICS

THESSALONIKI, 2014

KALOGIROU E. ELENI
Graduated Geologist

STUDY ON GROUND SURFACE FISSURES IN THE BROADER AREA OF THE LIGNITE MINES OF MAVROPIGI VILLAGE, EORDAIA PREFECTURE, NORTHERN GREECE

Submitted to the Department of Geology under the postgraduate program Studies 'Geology and Geo-environment'
Department of Geophysics

THREE-MEMBER CONSULTING AND EXAMINING COMMITTEE

Tsapanos Theodoros	Professor A.U.TH.
Karakostas Vassilios	Professor A.U.TH.
Marinos Vassilios	Assis. Professor A.U.TH.

Number Annex Scientific Yearbook of Department of Geology N °

Contents

PREFACE

The present dissertation was a part of a research program held in the area of Mavropigi settlement of the Eordaia municipality. This program concerns the appearance of surface ruptures both in the village and the surrounding area, caused by the operation and in general the excavation nearby the mine. The **scope** of the present work is to determine whether fissures concern the tectonic activity of the area or the mine exploitation.

In the ***first chapter*** an introduction and a reference to similar phenomena of surface ruptures in Greece and all around the world is made together with a general reference to the landslides and their distinction from the explosions.

The ***second chapter*** presents the geology and tectonic regime of Greece, generally, in the broader area and finally in the examined area.

The ***third chapter*** deals with the seismicity of the region from ancient times to the present and its analysis with the Gutenberg – Richter method.

The ***fourth chapter*** describes the installation of a temporary seismological network and the analysis of data derived from that. This analysis includes two velocity models, which are analyzed and compared. The chapter concludes with a demonstration of the earthquake waveforms collected during the testing period.

In the ***fifth chapter***, the waveforms produced by the explosions in the mine Kardia, which is located South-East of Mavropigi are presented.

The ***sixth chapter*** analyzes the geotechnical research done, simultaneously with the seismological research.

In the end of the dissertation the conclusions of this research are mentioned and discussed.

Acknowledgements

I would like to thank, primarily, the three members of the consulting and examining committee for their assistance during the elaboration of the present work, and the seismological station personnel, who helped me each time that was necessary. I would also like to thank the PPC for the assignment of the times and dates of the eruptions that took place in the mine during the four-month operation of the local network. Finally, I would like to thank my relatives for their precious moral and economical support and George, who gave me the inspiration to move on.

CHAPTER 1- INTRODUCTION

1.1 GENERAL PURPOSE

During July 2010 a ground fissure was observed in the field, near the village of Mavropigi and in its Northwest (NW) side. Local authorities gave a plethora of interpretations while trying to explain the phenomenon. After few months (beginning of September), one more ground fissure close and almost parallel to the previous one and very close to the limits of the lignite exploitation by the Public Power Corporation (PPC) was discovered.

The present thesis aims to investigate the connection of these events with the tectonics of the area or to the mine activities (e.g. blasts, excavations, etc).

Surface fissures have caused serious damages to existing buildings regardless age. Some of these buildings are in danger of collapse, with the obvious risk of serious injury to their occupants.

For these assessment, detailed geological, geophysical and seismological studies of the broader area were conducted.

In the following section some examples related to surface ground fissures from Greece and all over the world are stated.

1.2 EXAMPLES OF SURFACE FISSURES RELATED TO OVER-EXPLOITATION, TECTONIC REASONS AND EARTHQUAKES

Water over-exploitation , tectonic reasons and earthquakes have widely caused fissure phenomena on the Greek surface, but also all around the world. Hereby, some of the most important examples.

1.2.1 Case studies

It has been demonstrated that surface fissures can be associated with surface geological events over-exploitation of groundwater aquifers as well. In some distinct cases, large earthquakes appear to linked with this complex tectonic and hydrological phenomenon.

1. Surface fissures related to over-exploitation : Phenomena of soil surface fissures appearance, attributed to over-exploitation of ground water, have been observed in several US states such as Arizona (Holzer, 1979), Texas (Holzer, 1984a&b), Nevada (Holzer and Gabrysch, 1987) and California (Holzer and Pampeyan, 1981). The affected areas in U.S.A. are leastwise fourteen (14) regions in six (6) states and have a total area of more than 22.000 km^2 (Holzer, 1986). In several cases it has been established the combined effect of tectonic (pre-existing faults) and hydrologic causes (over-exploitation). In other cases of related phenomena without the tectonic deformation (Holzer and Pampeyan, 1981).

2. Surface fissures caused by tectonic reasons: Sliding on the faults surface without any seismic event is known as **creep**. Non seismic creep is related to tectonic causes which are prevalent in nature. St. Andrea's fault in California is one example (Goulty and Gilman, 1978;Burford and Harsh, 1980). One additional example of non seismic creep is the fault of Taiwan, before and after, the earthquake of September 20^{th} 1999 (figure 1.1), M=7.6 (USGS).

Figure (1.1) : Effects of the 20th September of 1999, M=7.6, Taiwan (after Lekkas, 1999).

3. Surface fissures related to earthquakes: Surface fissures, are often considered to be a precursor of a seismic event (e.g. : China). However, in some sporadic cases, surface fissures can occur during the after-shock period (Muir-Wood and King, 1993). The fault formation is associated with changes in the hydrological state of the region (Kovach et al., 1975). Nevertheless, sometimes liquefactions can occur without any seismic event (Holzer and Clark, 1993). Concluding, surface fissures are strongly related to seismic events, however in most cases is hard to identify the triggering mechanism.

1.2.2 Studies in Greece

1. Kalochori, Thessaloniki: In this case the over-exploitation caused an extensive subsidence of the soil surface (Andropoulos et al., 1991). Additional phenomena of sliding in pre-existing faults, related to hydrological and geotechnical causes, during the last forty (40) years (Stiros, 2001) exist.

2. Basin area of Thessaly: The phenomenon of surface fissures (figure1.2) began in 1992 and continues until today. It is well established the correlation between the rate of displacement and the end of the irrigation season. Furthermore there is a non-seismic slip on pre-existing faults. Despite the fact that the original reason for the surface ruptures was differential subsidence due to over-exploitation, these faults are still considered to be a potential risk for the region. Their formation is extraneous to the decrease in aquifer parameters and lies in tectonic causes. Continued deformation caused very serious damages to the settlements of the region resulting severe problems for buildings and infrastructures (Zouros et al., 1994).

Figure (1.2) : *Images* of the surface ground fissure in the basin area of Thessaly (after Zouros et al., 1994).

3. Gerakarou, Thessaloniki: Two surface fissures, which intersect the national highway of Thessaloniki-Kavala, with at least seven (7 cm) centimeters of non seismic displacement. Due to their location and orientation, are considered characteristic instances of creep. Relocation accounts for almost the 50 % of the seismic faults' displacement occurred in 1978 in that specific location.

4. Peraia, Thessaloniki: The surface ground fissures in the region of Peraia, shown in figure (1.3), it is mainly associated with :
    - the pre-existing tectonic structure
    - the drawn-down of the aquifer and
    - the type of the sedimentary deposits.

Extensive construction of the region masks the fault, hence it is not visible on the surface. The evaluation of geological mapping, drillings and geophysical prospection proved the nature of the fault as normal and confirmed the existence of sedimentologicaal structure (Neogene-Quaternary deposits), and therefore the differentiation of the substratum (especially the foundation substratum) on either sides of the fault. The fault dips to the North with high angles (60^0-70^0). The Neogene layers are almost horizontal with very small slopes (5^0-10^0) to South (Pavlides, 2007).

a) **b)**

Figure (1.3) : Images of the surface ground fissure in village Peraia, a) on the surface of the road and b) on a stone fence (after Pavlides, 2007).

5. Anargyroi, Florina: The first fissure on the ground soil appeared in late 1998 and 1999. This feature was later observed on some buildings as well. While the front head of the mine excavation of the PPC (Public Power Coorporation) had reached within less than about 700 m from the Eastern boundary of the village, the depth of the excavation had been estimated around 100 m. Today forehead excavation is approximately 400 m from the nearest house in the village , and the excavation depth is greater than 140 m (Soulios, 2009).

Figure (1.4) : Image of the surface fissures in Anargyroi village (after Soulios, 2009).

The cracks on the ground and the buildings are constantly increasing (figure 1.4), and today about 80 % of the buildings in the village present damages. Measurements have shown that the upper level of the aquifer use to be at a depth of about 2-5 m. For lignite exploitation purposes, the PPC (Public Power Coorporation) decreased the water level in the aquifer by at least 100 m, using pumping devices. This was an extremely important intervention to the hydro-geological conditions of the area. The first abstraction for drainage began in 1993, with 2,4 $\cdot 10^6$ m^3. Since then, this number grew reaching a value of 6-7 $\cdot 10^6$ m^3 of water pumped out between 2007 and 2008. Concluding, the surface ground fissures were caused by sinking of the aquifer together with extensive mining activity.

6. Lagyna, Municipality of Lagkadas: In this case, the surface ground fissures were provoked by a non seismic slide of a pre-existing fault. Among the reasons, not only tectonic reconfiguration but hydro-geologic mutation of the region as well (figure 1.5). In figure 1.5b the detachment of a column of a fence is shown, with a measureddisplacement of 12 cm. The gap on the top is 5 cm and 3 cm on the base of the fence (Tsapanos, 2006).

a) b)

Figure (1.5) : Images (a and b), where fissures on the surface and on the walls are distinguished (Soulios, 2009).

1.3 BASIC TERMS AND GENERAL DEFINITIONS

Landslide is a general term, which describes the down-slope movement of soil, rock and organic materials under the effect of gravity, triggered by natural or human causes (Highland and Bobrowsky, 2008). The landslide expresses the result of searching for a new equilibrium state for the soil. Human intervention is possible to stop completely or slow down this phenomenon.

Movements of the soil can generally affect the following :

- Mountainous and low-land villages, but also large urban areas
- Mines
- Roads and tunnels
- Dams, landslides occur in the ridges or in its reservoir
- Public utility networks and seabottom structures (e.g. failure of slopes due to undersea earthquakes).

1.4 LANDSLIDES MECHANISMS

The mechanisms causing landslides are frequently referred as “triggering” conditions. Despite the contribution of human activities to the formation of landslides, the vast majority is caused by natural processes. The landslides triggered either by natural causes or human mediation are illustrated in table (1.1).

Table 1.1: Landslides mechanisms caused by natural and human triggers (after King, 2006).

	Natural causes	**Human causes**
Removal of support	Erosion at the base of the slope, waves, glaciers, etc.	Excavation at the base of the slope or the hill
Removal of vegetation	Forest fires	Timbering
Addition of moisture	Rainfall	Broken water pipes
Addition of weight	Heavy snowfall, landslides, etc.	Placement of fill
Oversteepening	(this term sometimes is used to describe also the removal of support)	By placing additional fill gradients exceeding the angle of response
Vibrations	Earthquakes, thunders	Blasting, operation of heavy equipment

The processes referred in table 1, are described thoroughly in the next paragraph (King, 2006).

Removal of support: excavation or erosion in the base of the slope can result in unstable situations. This loss of support can cause immediate or late landslides.

Removal of vegetation: Changes in vegetation can form landslides in two different ways.

1. Vegetation removes the water from the soil.
2. The root system supports and provides stability to the soil.

Areas, subjected to fires or uncontrollable logging, are more vulnerable to landslides.

Addition of moisture: Many soils, especially clays, despite hard when dry, transform into soft when a small amount of moisture is added: the water pressure within the porosity of a soil has the effect of "inflating" the pore spaces and reducing the frictional forces between soil particles. These process results in landslides formation and is the most common natural trigger.

Addition of weight: Weight addition on the top of the slope has the same effect as increased gravity. When the added weight exceeds the shear strength of the slope, land sliding can occur.

Over steepening: The maximum angle under which the material is still hold together called "angle of response". When the angle of the slope exceeds the angle of response, land sliding can occur. The term is often used to describe a situation were landslides are triggered by excavation or erosion.

Vibrations: In many cases, sudden movements, force the grains of the soil to lose their contact one with another. The frictional forces bounding the material together are lost and the slope is sliding. Earthquakes, explosions, heavy equipment and loud noises can trigger landslides.

1.5 TYPES OF LANDSLIDES

Five main types of landslides and a sixth complex type, that consists of at least two of the main types, have been proposed by Varnes, (1978). These six (6) types are shown in figure (1.6) as classified by Hungr et al., 2014 (Figure (1.6)) and presented by the British Geology Survey (B.G.S.) Note that this classification is based on the studies, first, made by Varnes, (1978) and afterwards by Cruden and Varnes (1996). All six (6) types are shown in figure (2) and described thoroughly below (Highland and Bobrowsky, 2008).

1. **Falls**, freefall of pieces of rock, debris or earth.

2. **Topples**, a topple is defined as the forward rotation, of a mass of soil or rock, around a point or axis, below the center of gravity of the initially displaced mass.

3. **Slides**: a) Rotational slide, a landslide on which the surface rupture is curved upward (spoon-shaped) and the slide movement is more or less rotational about an axis, that is the contour of the slope, b) Translational slide, translational landslide where the mass moves outward, or downward, along a relatively planar surface with little rotational movement or backward tilting. This type of slide may progress over considerable distances if the surface rupture is sufficiently inclined, in contrast to rotational slides, which tend to restore the slide equilibrium.

4. **Spreads:** an extension of a cohesive soil or rock mass, combined with the general subsidence of the fractured mass of cohesive material into softer underlying material.

5. **Flows:** a spatially continuous movement in which the surfaces of shear are short-living, closely spaced, and usually not preserved. The velocity components of the displacing mass in a flow resemble those in a viscous liquid. Often, gradual mutation from slides to flows is observed, depending on the water content, mobility, and evolution of the movement.

6. **Complex**: These are landslides featuring two or more of the basic types of landslides simultaneously, or at different times during the onset of slope failure.

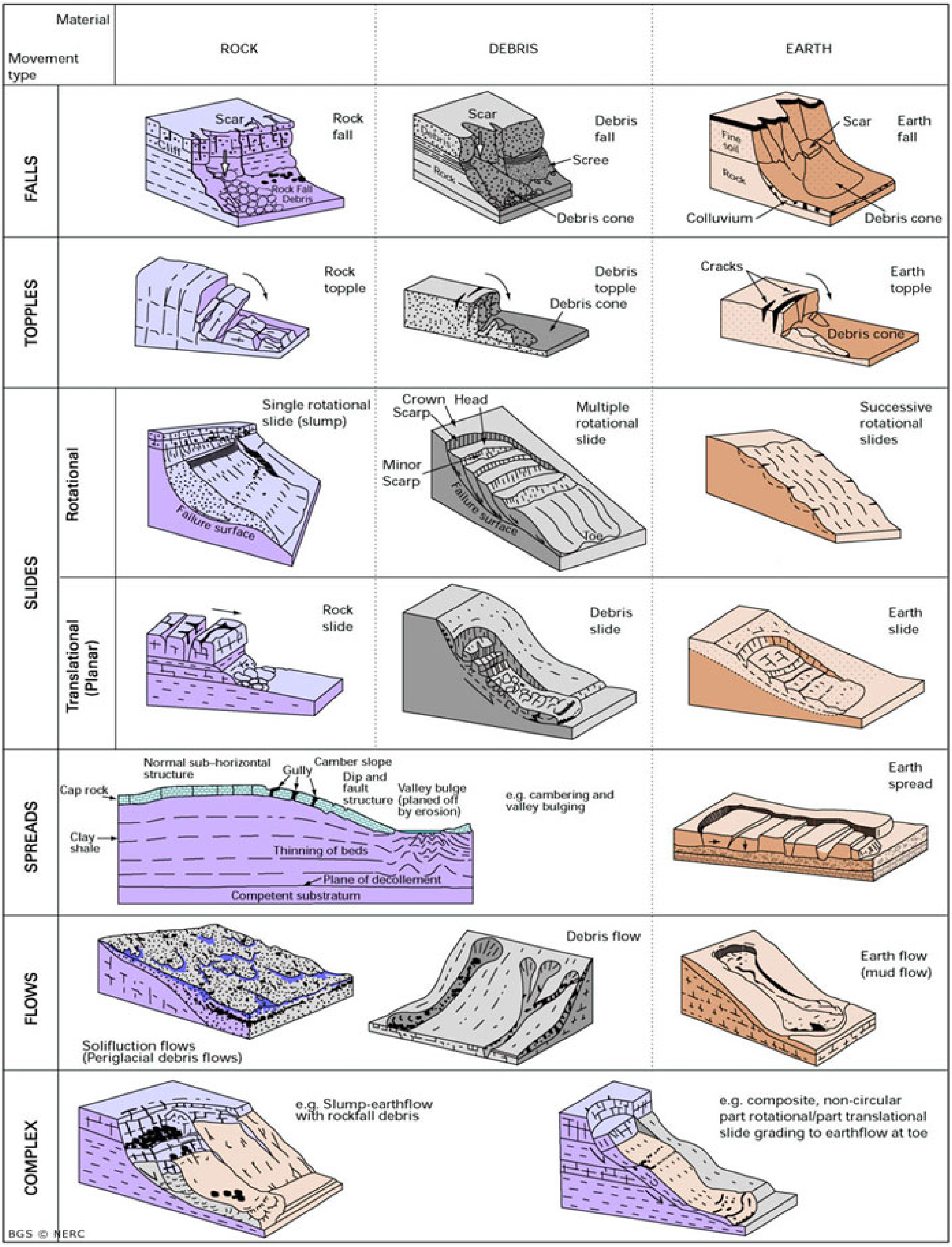

Figure (1.6): Classification of landslides (after B.G.S;Hungr et al., 2014).

1.6 LANSLIDES RELATED TO EARTHQUAKES

From literature can be concluded that seismic events contribute substantially to landslides formation. Some instances of landslides can cause heavy and/or catastrophic damages.

For example, in **Northridge**, **California,** on January 17th 1994, an earthquake of magnitude **M=6.7** occurred. The Northridge earthquake triggered landslides (figure1.7) over an area of about 10.000 km^2. The limit of landslides is defined by small rock and soil falls from very susceptible slopes such as steep road cuts (Sassa, 1999).

Figure (1.7) : Dense concentration of disrupted slides and falls triggered by the 1994 Northridge, California, earthquake (Harp and Jibson, 1996)

On **Alaska**, November 3rd 2002, was afflicted by an earthquake with magnitude **M=7.9**. The landslides, in this case, were primarily rock falls and rock slides ranging in volume from a few cubic meters to forty (40) million-cubic-meter rock avalanches, mostly concentrated in a narrow zone ~ thirty (30) km wide that straddled the fault rupture zone over its entire three hundred (300) km length. Large rock avalanches were all clustered at the western end of the rupture zone, where acceleration levels were reported to be extremely high. Liquefaction effects, consisting of sand blows, lateral spreads, and settlement contributed to the formation as well (Harp et al., 2003). All the types of landslides are depicted in figure (1.8)

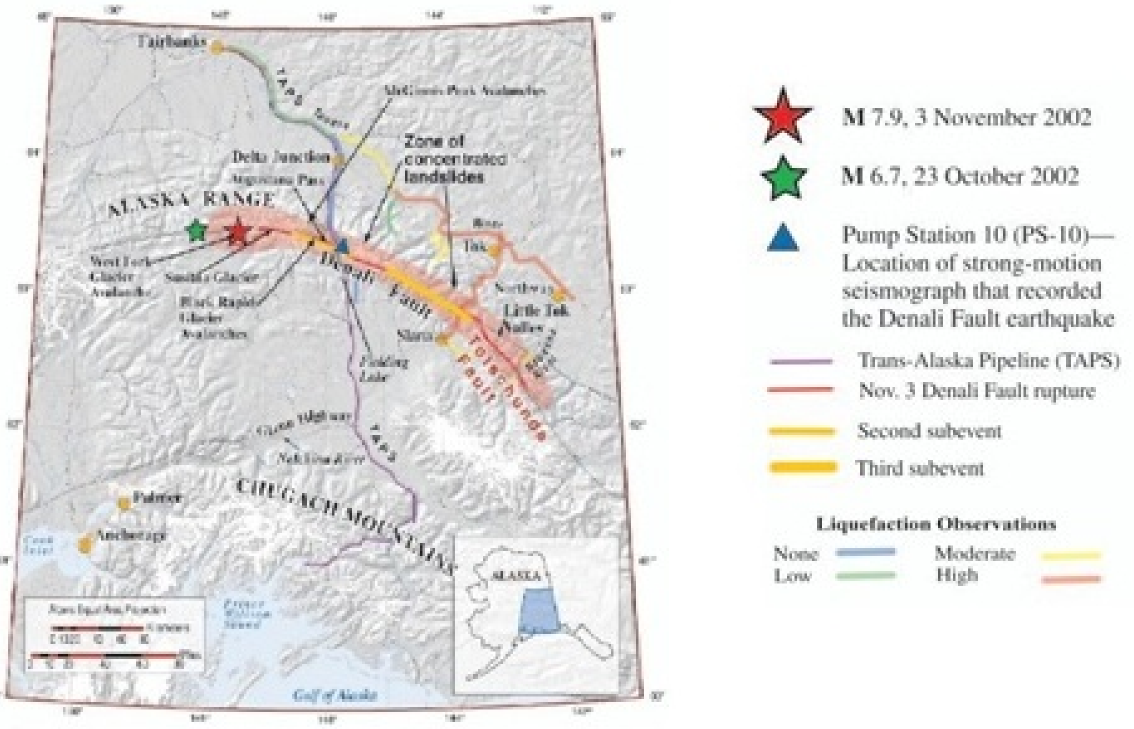

Figure (1.8) : Map showing main shock, foreshock, zone of fault rupture, landslides, triggered by the Denali Fault earthquake of 3 November 2002 (after Harp et al., 2003).

In the Chinese region known as **Sichuan**, figure (1.9), an earthquake with magnitude **M 8.0** occurred in May 12^{nd} 2008. This earthquake engendered more than 15.000 landslides such as rockfalls and debris flows, which resulted in about 20.000 deaths (Yin et al., 2008).

Figure (1.9) : Landslide of Sichuan, China, 12 May 2008, earthquake M 8.0 (after Agu, 2008).

Beichuan, which laterally translates to “North of the river”, was the city principally affected by the seismic event, accounting more than 15.000 deaths (roughly half of the population). Heavy damages caused the city to be rebuilt on a different location, about 20 km from the former site. The destroyed city now is an open museum.

Keefer (1984) was the first who studied the connection between earthquake occurrence and landslides generation. In this respect, he identified fourteen types of landslides with the most common being (Keefer, 1984):

a) **Rock falls,** individual boulders or disrupted masses of rock that descend slopes by bounding, rolling or free fall

b) **Disrupted soil slides**, sheets of soil, a few decimeters to a few meters thick, that disintegrate during movement into chaotic jumbles of small blocks and individual soil grains

c) **Rock slides**, masses of rock fragments and blocks created during disordered movement sliding on planar or gently curved surfaces where joints, bedding planes, or other surfaces of discontinuity dip out of the slope.

d) **Rock avalanches**, landslides that integrate into streams of rock fragments, able to travel several kilometers on slopes of a few degrees, at velocities of hundreds of kilometers per hour, and

e) **Rapid soil flow,** streams of soil grains, usually but not always, mixed with water, flowing in a fluid-like fashion at high velocities. In some cases, rapid slows can travel several kilometers, on slopes of only few degrees, transporting significant amount of boulders (up to few hundred tons).

Keefer (1984) made a further distinction based on the character of the movement into:

a) **disrupted slides**: rock falls, rock slides, rock avalanches, soil falls, disrupted soil slides and soil avalanches

b) **coherent slides**: rock slumps, rock block slides, soil slumps, soil block slides and slow earth flows, and

c) **lateral spreads and flows**: soil lateral spreads, rapid soil flows and subaqueous landslides.

Afterwards based on other characteristics such as the internal disruption degree and the water content he improved his suggestions.

The same author categorized the landslides according to their material into two groups:

a) **coherent rocks**, and

b) **soil welded**, which sometimes contains organic material

a. The smallest earthquakes' magnitude that causes landslides

In order to find the cutoff magnitude able to trigger landslides, Keefer (1984) considered for his research a group of 300 earthquakes in a region of the U.S.A. He concluded that sixty-two (62) of these earthquakes present a magnitude M_L<4.0. However, only one earthquake (M_L =3.5) of this sixty-two (62) earthquakes had caused landslide. By further processing, he classified the formed type of landslides according to the magnitude of the seismic event :

1. M_L ~ 4.0: rock falls, rock slides, soil falls, disrupted soil slides
2. M_L ~4.5: soil slumps and soil block slides
3. M_L ~5.0: rock slumps, rock block slides, slow earth flows, soil lateral spreads, rapid soil flows and subaqueous landslides.
4. M_L ~6.0: rock avalanches.
5. M_L ~6.5: soil avalanches.
6. M_L > 6.5: rock slides, avalanches and debris flow on mountain slopes (Yamada et al., 2013).

b. Correlation of the earthquake magnitude and area affected by landslides

The areas, affected by landslides are a function of earthquake magnitude and its focal depth. Landslides triggered by seismic events of greater magnitude have the ability to propagate to broader areas (figure 1.10).

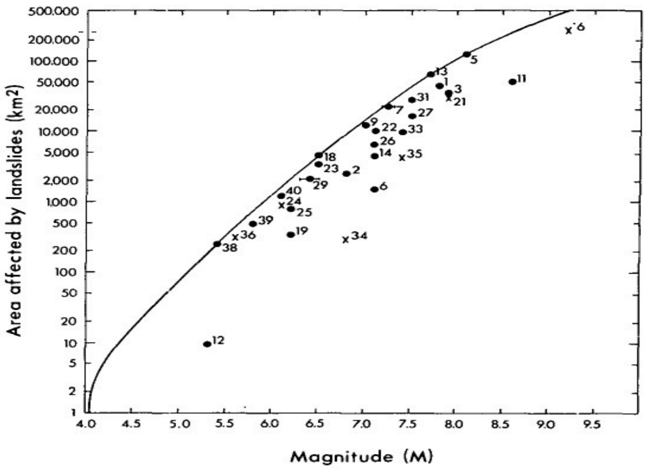

Figure (1.10) : The Area affected by landslides in relation with the magnitudes of earthquakes. The solid line indicates the upper bound enclosing the data (after Keefer, 1984).

c. Magnitude and maximum distance of landslides from the earthquake epicenter

Keefer (1984) made a further distinction of the types of landslides into three (3) greater categories based on the characteristics of the movement.

As shown in figure (1.11), the upper limit of rock falls is located above the limit of coherent slides, which either coincides or is above the limit of earth flow. The relationship between the upper limits indicates that rock falls can be caused by an earthquake of lower magnitude than coherent slides. On the other hand, earth flows are triggered only by seismic events of larger magnitudes (with respect to coherent slides).

Earthquakes with epicenters deeper than 30 km generally engender rock falls, while coherent slides form due to shallow seismic events. The depth, however, does not influence the epicentral distance of the Earth flows. In terms of topography, the upper bound of rock, falls above the upper bound of coherent slides, however both limits converge as the earthquakes' magnitude increases.

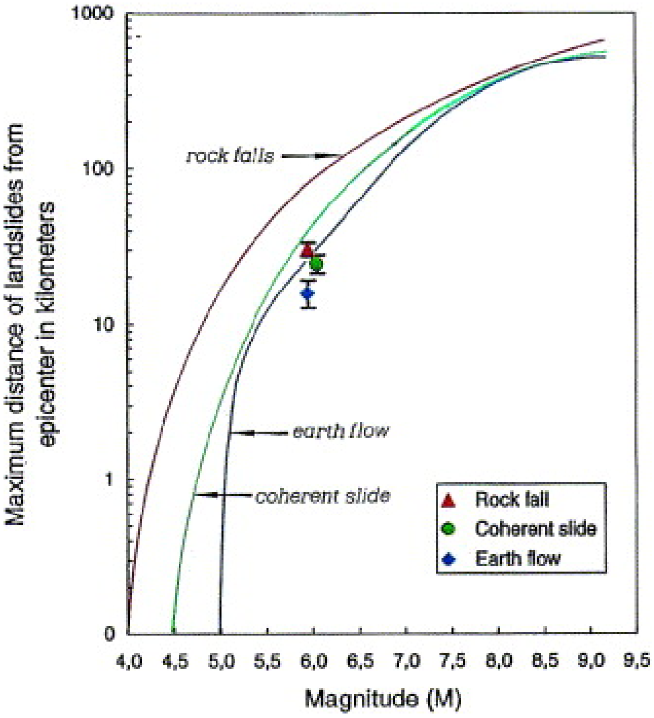

Figure (1.11): Maximum distance of landslides from epicenter in kilometers related to the earthquakes magnitude (Keefer, 1984;Esposito et al., 2000).

d. Relationship between magnitude and maximum landslide's distance from the fault.

Maximum distances of landslides from the nearest edges of fault rupture zone in relation to earthquake magnitudes are illustrated in figure(1.12).

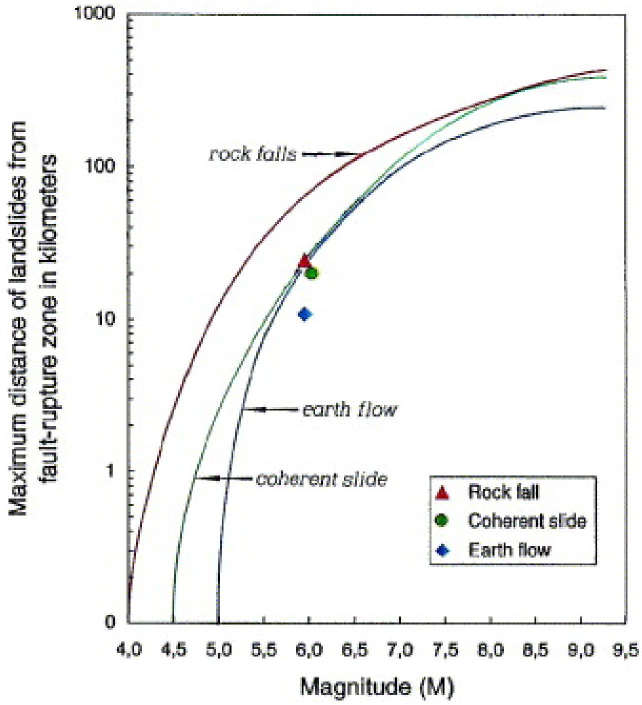

Figure (1.12): Maximum landslide's distance from the fault for different earthquake's magnitudes (Keefer, 1984;Esposito et al., 2000).

As long as seismic energy is not released at a single point but throughout a fault rupture, the maximum landslide distance from the fault seems to correlated better with the earthquakes' magnitude than the maximum epicentral distance.

In this regard, figure (1.12) complies with figure (1.11). Concluding, the needed magnitude to trigger earth flows is greater than the one needed to form rock falls or coherent slides. The lowest magnitude is M_L~ 4.0 for rock falls and M_L~ 4.5 for coherent slides.

e. Landslides and seismic shaking intensity

According to Keefer (1984), the most common used scale in the U.S.A. is Modified Mercalli (MMI), as proposed by Wood and Neumann in 1931 and revised by Richter, 1958. Modified Mercalli scale estimates the intensity of a seismic event at a specific location or over a specific area by considering its effects on people, objects, and buildings. In order to determine the minimum intensity values of seismic events associated with landslides, iso-seismal maps were compared to maps depicting landslides.

Comparison was made separately for the three categories of landslides, rock falls, coherent slides and earth flows and are shown in the following figure (1.12).

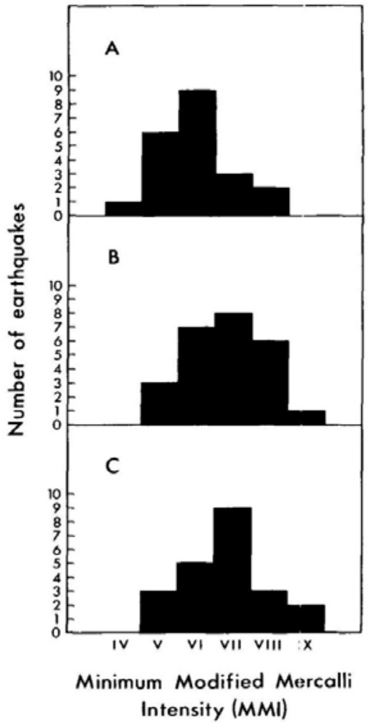

Figure (1.13) : Minimum value of Mercalli intensity at which landslides occurred in earthquakes. A: minimum intensities for the rock falls, B: minimum intensities for the coherent slides and C: minimum intensities for the earth flow (after Keefer, 1984).

The dominant minimum intensity value for rock falls is MMI VI. The minimum dominant intensity value for the other two categories is MMI VII (figure 1.13).

1.7 DISCRIMINATION BETWEEN EARTHQUAKES AND EXPLOSIONS

The discrimination between natural earthquakes and explosions is an issue that seismologists had to deal with the last decades. In this regard, three (3) seismic techniques were suggested by (Dahy and Abdrabou, 2012).

a) Waveform and mechanism of natural earthquakes and explosions.

The two events, shown in figure (1.14), feature the same characteristics concerning, size, seismic station, type of equipment and distance between the event and the recording station. However, the explosion waveform is dominated by P waves (the first arrival) and has no love waves, while earthquakes have large S and surface waves. Furthermore, explosions have an impulsive character, thus shorter process duration times with respect to earthquakes (Dahy and Abdrabou, 2012).

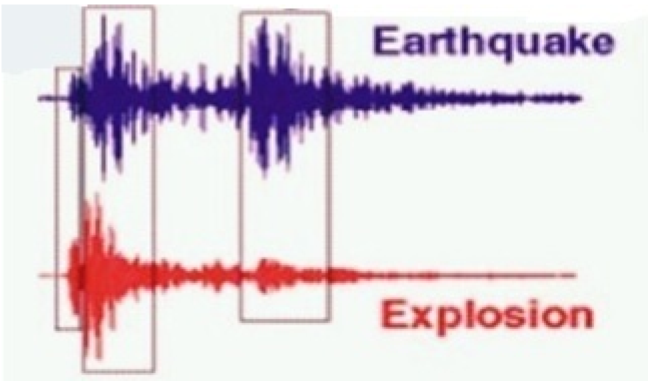

Figure (1.14) : Earthquake and explosion seismograms (after Dahy and Abdrabou, 2012).

The mechanism of an explosion appears to have a spherical symmetry and its radiation pattern is isotropic, meaning that:

i) is compressional in all directions,

ii) its amplitude is homogeneous and

iii) shear and love waves are not generated.

While Longitudinal waves of equal amplitudes would radiate in all directions in a theoretically homogeneous structure of the Earths' crust, in practice, this is not attainable, because of the inhomogeneous character of the crust. In section b of figure (1.15), the seismic source mechanism of a natural earthquake is shown. Earthquakes have a double couple character, with a quadripolar seismic radiation pattern of the generated P-waves, which depends on the fault geometry and ray direction, for body and surface waves (Dahy and Abdrabou, 2012).

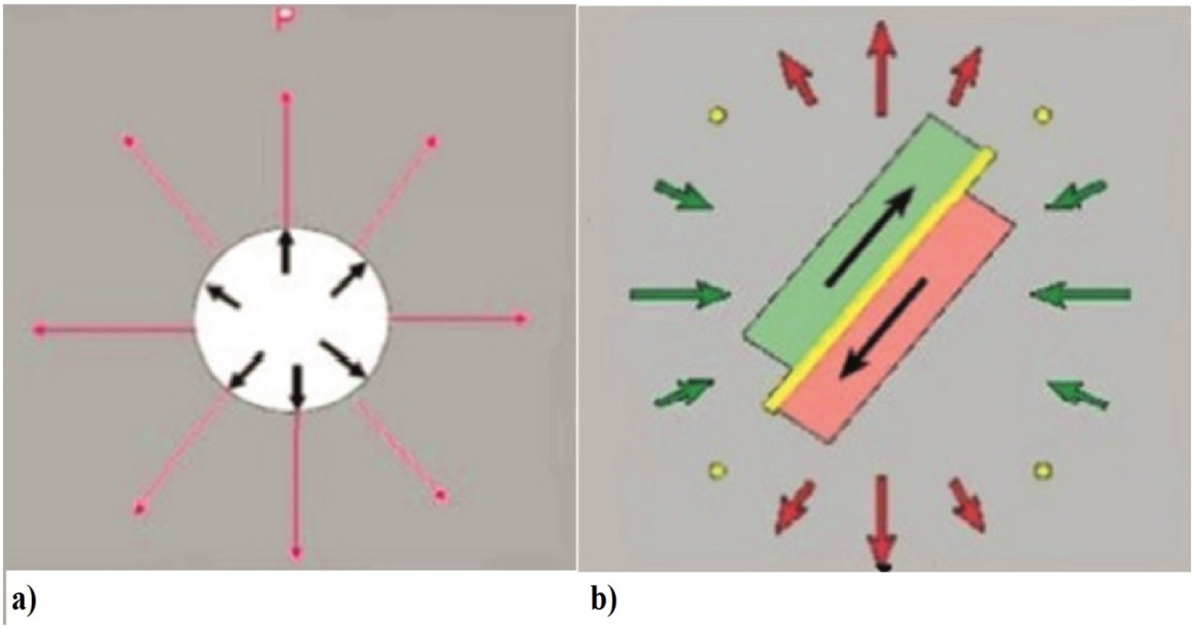

Figure (1.15) : Seismic source mechanisms of a) explosion and b) Earthquake (Dahy and Abdrabou, 2012)

Theoretical differences between the quarry blasts and an earthquake are summarized in the following table (1.3).

Table (1.3): Theoretical differences between explosion and earthquake (after Walter et al., 2006).

Explosion	**Earthquake**
Pressure pulse on a sphere	Shear slip on a plane
P-wave energy dominates	S-wave energy dominates
No Love waves	Strong Love waves
Constant Rayleigh and P-wave pattern	Rayleigh and P-wave radiation pattern
$m_b > M_s$	$m_b \sim M_s$
P/S >1	P/S <1
Isotropic	Double-couple

Figure (1.16), shows for instance, the waveforms of two events recorded in Novaya Zemlya. The blue waveforms refer to an earthquake while the red one to an explosion (Walter et al., 2006). The signal is filtered to a bandpass frequency of 1-2 Hz Figure (1.16a). Figure (1.16b) depicts the same recordings using a 6-8 Hz Bandpass filter this time. In figure (1.16b), the distinction between a seismic event and an explosion is not obvious. On the other hand, figure (1.16a) clearly shows that explosions are characterized by larger P/S amplitude ratios than earthquakes (Walter et al., 2006).

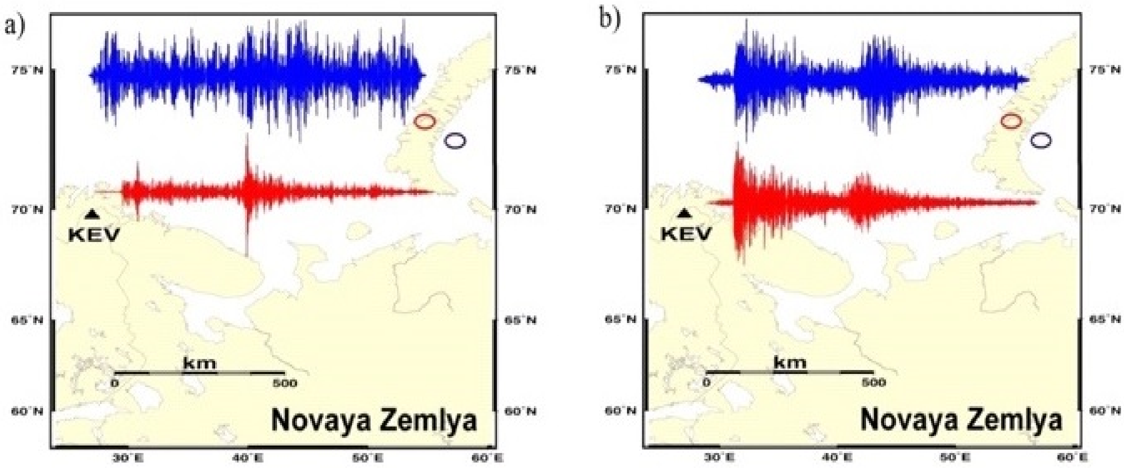

Figure (1.16) : a) 1-2 Hz and b) 6-8 Hz, Bandpass filtered seismograms of earthquake (blue) and explosion (red) pairs at the same site, Novaya Zemlya (after Walter et al., 2006).

b) Spectral analysis method

Based on Walter et al., (2006), distinction between earthquakes and quarry blasts is based on spectral analysis. Numerous studies for the discrimination between blasts and earthquakes are based on spectral characteristics' variation of the direct wave phases, such as P_n, P_g, L_g, R_g, etc., or on spectral ratios at different frequencies. Blasts and earthquakes have yielded different spectral amplitudes for the same direct wave phase at regional distances in many instances. The quarry blast seismograms spectra are poorer in high frequencies than seismograms of earthquakes with comparable magnitudes (figure 1.17), (Dahy and Abdrabou, 2012).

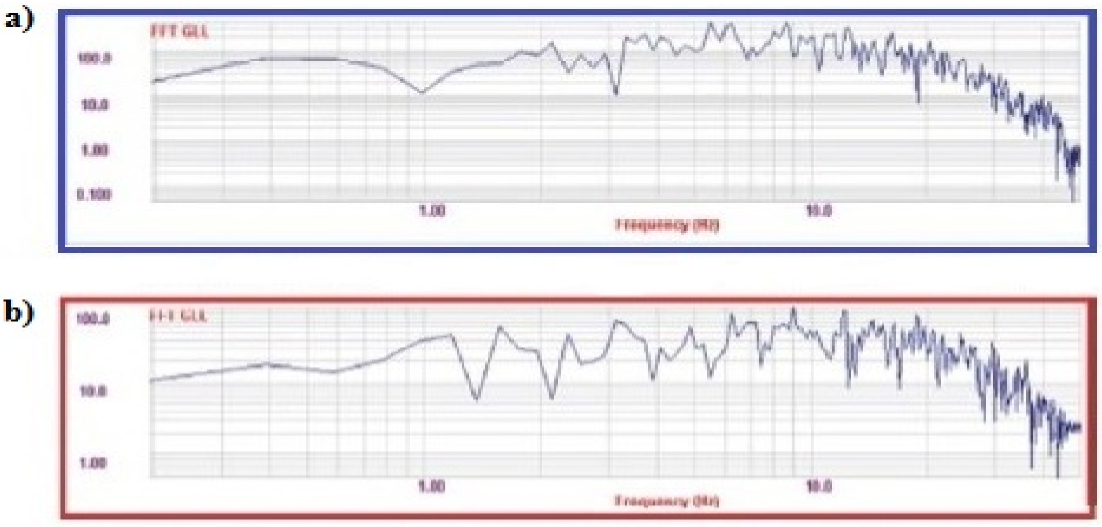

Figure (1.17) : Spectral analysis of natural earthquake (blue frame) and quarry blast (red frame) of the data for the research have been made from Dahy and Abdrabou, (2012) records of GLL station and dated on 01-11-2007 (after Dahy and Abdrabou, 2012).

For instance, based on the theory of the initial motion of the *P* wave, which determines whether the ray left the source in a compressional (upward first motion at a surface receiver) or dilatational quadrant (downward first motion) (Shearer, 2009), one can recognize the downward first motion of the blast waveform depicted in figure (1.17b)**.**

c) Body and surface Wave amplitudes method.

This method is based on the body, Primary wave (P-wave) and Secondary (S-wave) or surface wave amplitudes. Figure (1.18) shows the relation between body and surface waves. Quarry blasts appear to have P waves with larger magnitudes with respect to seismic events. This is not the case for S waves, which are of greater magnitude for seismic events. The study of Dahy and Abdrabou, 2012 also shows the tendency of the recorded explosion waveforms to move in a compressive manner at first.

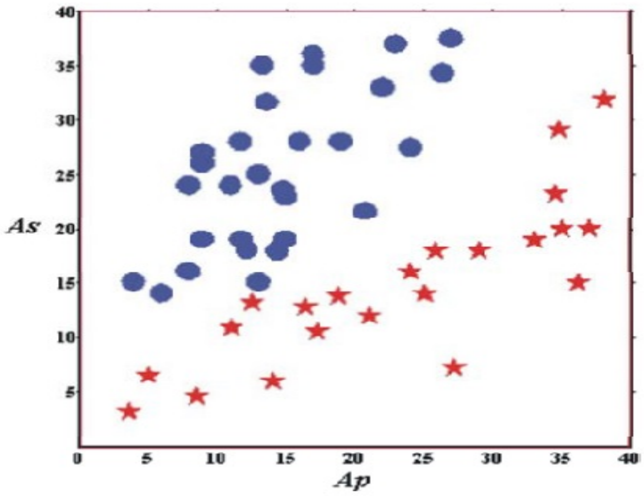

Figure (1.18) : Relation between Surface amplitude (A_s) and body amplitude (A_p). The blue cicles refer to earthquakes and the red stars refer to quarry blasts (after Dahy and Abdrabou, 2012).

Contrariwise, earthquakes' first motions are dilatational rather than compressive. Aside from the above conclusions, is underlined that events, identified as quarry blasts, occurred during daytimes and specific working days.

CHAPTER 2 - GEOLOGY AND TECTONICS

2.1 GEOLOGY

2.1.1 General Geological context of Greece

The Greek region, such as the entire Balkan peninsula, are part of the extensive Alpine Mountain ranges. The current configuration and geometry of this mountains is a result of the Atlantic ocean expansion, that started in Upper Jurassic, as a form of tectonic events.

The Northern prologation of Africa, better known as the oceanic plate of Eastern Mediterranean, is subducted beneath the continental lithosphere of Aegean along the Hellenic arc.

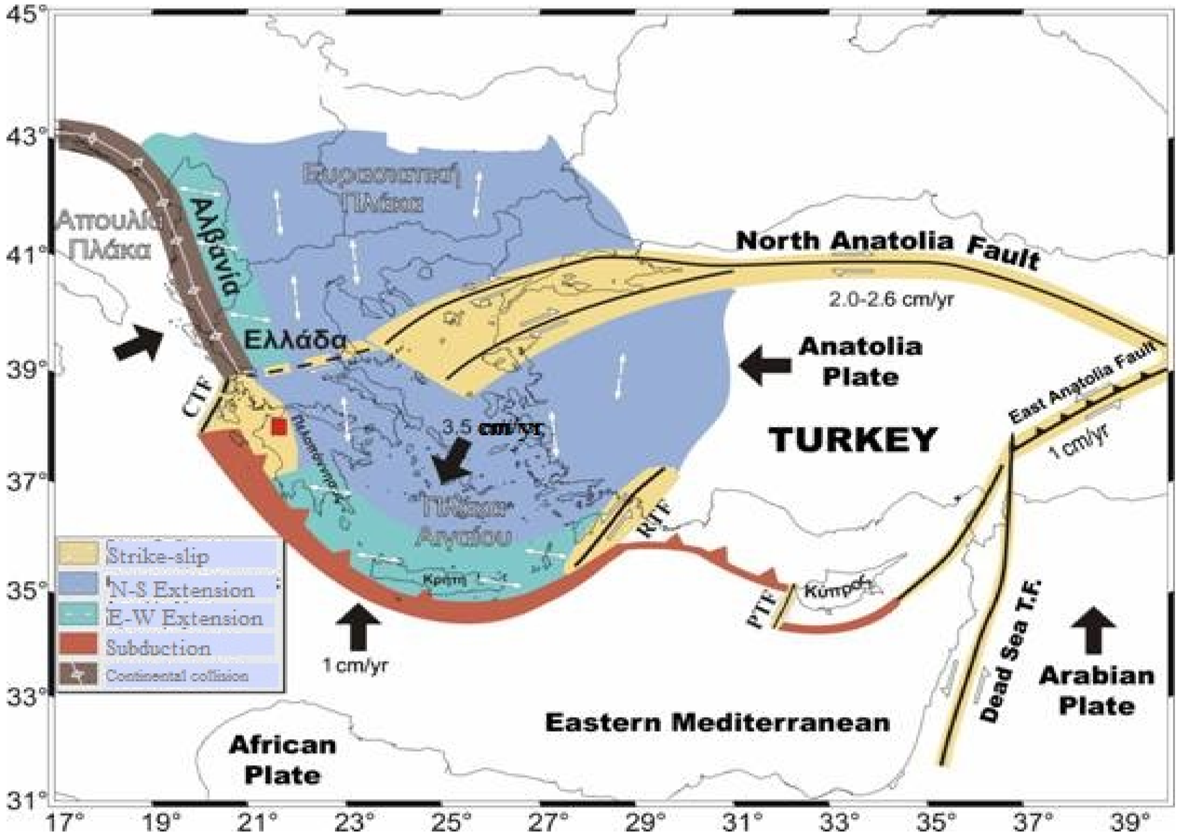

Figure 2.1: The main seismotectonic and geodynamic features of the Eastern Mediterranean (after Papazachos et al., 1998)

This deformation is the result of three main geodynamic causes (figure 2.1) :

a) the Northward movement of Africa, causing the plunge of the Eastern Mediterranean lithosphere beneath the Aegean region.

b) the Westward movement of the Anatolian plate, which is driven by the micro-plate Arabia, since the latter, moves to North.

c) the East-Northeast (ENE), collision between Apulia and coasts of the Greek Mainland North of the Kefalonia Transform Zone (KTZ).

An important feature of geological history of the Greek area was magmatism of Cenozoic period. The Post-Miocene magmatism is strongly related to the volcanic arc (Mountrakis, 1988&2005).

2.1.2 Geology of the broader area

Rocks of Pelagonian and sub-Pelagonian geotectonic zone characterize the geomorphology of the broader area concerning this study. The Pelagonian zone is located in the region of Eastern and Northern Thessaly, Western Macedonia, and continues North to Albania (Karab zone) and to the FYROM under the name of Goliza. The main feature of this zone concerns enrichment changes of the substratum and the pre-ofiolithic with younger deposits, consisting mainly of cones of weathering and contemporary fluvial deposits. The substratum lithology is characterized by rocks from Pelagonian zone, as well as from Alpine and pre-Alpine regions formed in Paleozoic, Mesozoic and Tertiary. On the Upper formation of the substratum, meta-Alpine formations, including molasse sediments of Mid-Hallenic and Pleio-Pleistocene deposits of the Servia-Kozani and Grevena basins, are present.

2.1.3 Geology of the examined area

The basin of Ptolemais is a lengthwise limnetic basin located at the North boarder of Eastern Mediterranean, 100 km West of Thessaloniki, and is part of a tectonic trench, which length is >120 km (figure 2.2). This trench extends from Monastery (former Yugoslav Republic of Macedonia, fYROM) to Elassona, South of Aliakmon river, has a NNW-SSE direction and is situated approximately 700 m above the sea level.

Mavropigi village belongs to Ptolemais basin and is located South-East at the edges of the St. Markos hill, 21 km NW of the city of Kozani, at an altitude of 740 m.

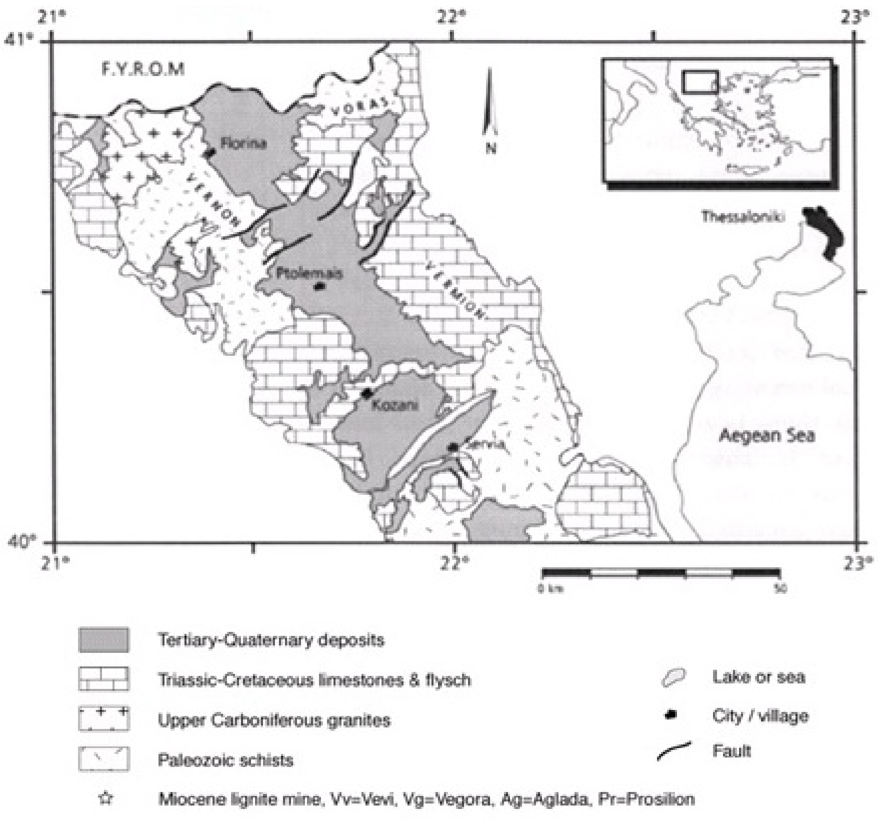

Figure 2.2: Simplified geological map of Florina - Ptolemais-Servia basin (after Igme;Steenbrink et al., 2000).

The lignitic layers accompanied by limnetic sediments constitute the formation of Ptolemais (Pavlides, 1985).

In the stratigraphic sequence of the Ptolemais basin can be distinguished three (3) different litho-stratigraphic units.

The underlying layers of lignite sediments together with the lower lignite layer constitute the lower member of the formation (or main field). At about 300 m thickness, two distinct lithological types of layers extending throughout the basin are encountered. The first type is the lithological horizon Neritina, which is a thin layer of gray marl and is located in the upper layers of the lower member. The second lithologic type is a thin layer of quartz sand of 10-30m thickness, which has a significant horizontal development and is located in the lower layers of the lower lignitic layer. Moving upwards, the intermediate member (Kardia) follows. This formation with a thickness of about 110m, consists of a rhythmic alternations of lignite layers and limnetic marl and is divided into Main (Kurio), Theodoxus and South. The layers of the upper surfacial member can be found in many regions of the basin. These have various texture, which consist of sands, clays, marls, loose conglomerates, sandstone grains and thin layers of limestone marl, lying under the lignite layers. The extensive marly limestone horizon with a thickness of a few centimeters to a few meters, is a relatively typical formation.

More specifically, Village of Mavropigi is built upon two main geological units(figure 2.3 & figure 2.4):

1.**Rocks of substratum**. The WSW part of the village is built on this formation. This consist of ash, recrystallized limestone of Mid.- Triassic – Lower- Liasio (T3-J5.k), settled in the crystalline background of dimarmarygiac schist of (sch) Palaeozoic.
2.**Formations of Proastio**. Includes mainly polygenetic thick conglomerates of fluvial origin of Lower Villafragkion. The majority of Mavropigi village is built on this formation. This geological formations are covered, in places, by small, thick, alluvial and collouvial deposits, cones of weathering deposits, soil mantle and anthropogenic layers.

Figure 2.3 : Geological map of Greece, Siatista sheet (Igme).

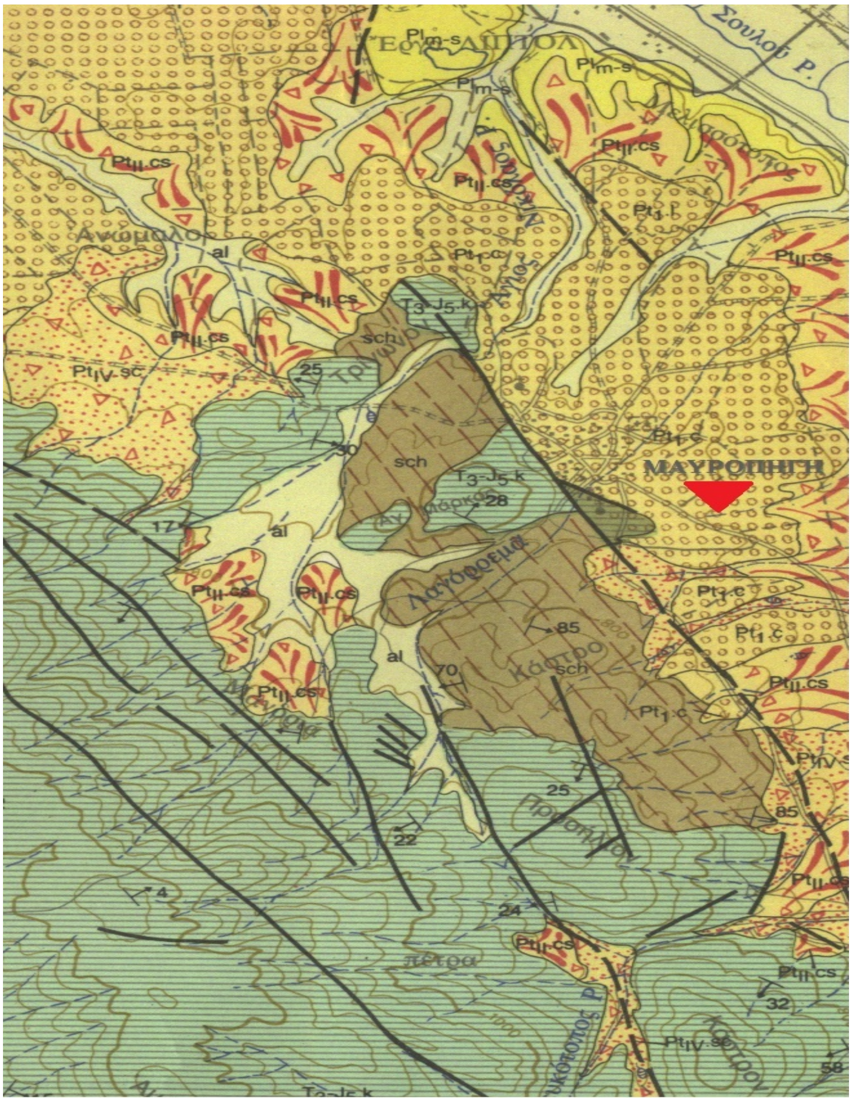

Figure (2.4) :Extract from the published geological map , Siatista sheet, Region of Mavropigi (Igme).

2.2 TECTONICS

2.2.1 Current tectonic situation of the Hellenic arc

The Aegean arc, is a complex of phenomena arising from the convergence of tectonic plates of Europe and Africa. Due to this convergence, sinking of the African plate beneath European plate occurs, the active margin of which is the Greek area . The sinking is believed to be amphitheatric. Hence, the name arch and Hellenic arc (figure 2.5). The yellow arrows, in figure 2.5, show the direction of the tensile field in

Upper Miocene - Pliocene while the red arrows the direction of the active tension. Black arrows show the direction of movement of the African plate and the direction of compressive stresses (Mountrakis, 1988&2005).

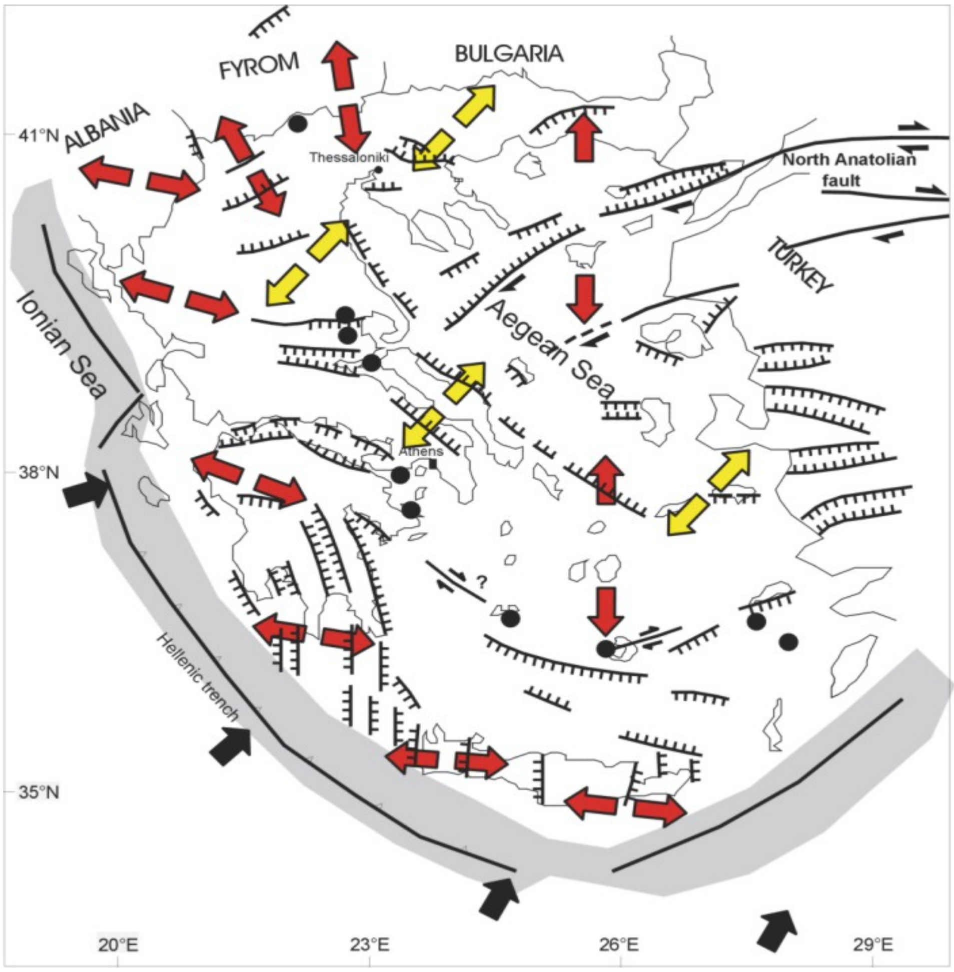

Figure 2.5: Main characteristics of active tectonics of the Greek arch and the broader Aegean region (Mountrakis, 2005).

2.2.2 Tectonics of the examined area

The trench was created by tectonic rift during the Neogene. During the Upper Miocene, tensile stresses with NNE-SSW direction prevailed, creating the main graben with NW and SE direction. During the Upper Pliocene and Quaternary, tensions with a NW-SE directions, departed towards splitting in individual basins, bounded by NE-SW faults. Thus, Florina, Amyntaio - Ptolemais, Kozani-Servia and Elassona basins were formed. The delimitation of the basin consists of two faults, which may be associated with tensional events (Pavlides and Mountrakis, 1987). The first episode, during the Upper Miocene, resulted in tension with basin orientation NE-SW. The second tensional event, during the quaternary, with NW-SE orientation, formed NE-SW faults, which now characterize numerous basins, including Florina, Ptolemais and Servia (Pavlides and Mountrakis, 1987).

Due to the tectonics and geomorphology of the region, the basin of Florina – Ptolemaidas is divided by cavities and bulges in many tension sub-basins of NE-SW directions, almost perpendicular to the direction of the great basin (Pavlides, 1985). The symmetrical position of the four lakes, situated in the area (Vegoritida, Petron, Zazari, Xeimaditis), depends on the tectonic as well. Some very important normal faults of NE-SW and 30 Km length, created the Quaternary sub-basin. (Pavlides and Mountrakis, 1987).

Major faults extending from NW-SE to NNW-SSE are difficult to be identified. Sediments on the surface of the basin mask this faults allowing their diagnosis only from boreholes in the ground or geophysical survey.

Contrarily, faults of NE-SW direction dominate in the topography and demonstrate typical geomorphological features of recent neotectonics or active faults. Last but not least, some NE-SW direction faults were recently activated from weak (Pavlides and Simeakis, 1988) and strong earthquakes (Mountrakis, 1988;Pavlides et al., 1995).

In the structure of the region the following tectonic lines dominate:

The rift Achladas-Skopou Papadias, located on the West side of the Vorras mountain, near the Greek-Yugoslavian border. This normal fault, has a NE-SW direction and exceeds in length the 10Km. The Kellis - Agios Athanasios normal fault, located on the Southwest side of the Vorras mountain, approximately 12Km long and a NE-SW direction.

The major tectonic line Petron - Xynou Nerou –Aetos – Nympheon, more than 30 Km long, with 30^0 N orientation, sinking to SE. The great fault of Vegoritis, 20 Km long, with orientation 40^0 N, which immerses to SE and passes with direction of 40^o N, through the villages of Agios Spiridon, Agios Panteleimon and Vegora.

Chimaditis – Anargyroi fault is located near the homonymous lake. This is a normal fault with a NE-SW direction and submerged to NW, more than 10 Km long (Pavlides, 1985).

Finally, the group of parallel normal faults of Vermio - Komnina and Ptolemais – Proastio basins, which extend over 10 Km (Pavlides and Mountrakis, 1987). The faults which affect the Neogene - Quaternary sediments of the basin coincide or have similar direction to the faults that affect the pre - Neogene rocks, but mainly the Mesozoic limestone, which is situated in the margins of the basin . Some normal faults affect the Mesozoic limestone, Palaeozoic metamorphic rocks on the margins of the basin and continue in sediments of the basin. These effects are also persivable in the sediments of the basin. This were, initially, created in the pre-Neogene period (Mountrakis, 1982&1984) and possibly disabled by Neotectonic deformations.

CHAPTER 3 – SEISMICITY

3.1 STUDY OF THE REGIONAL SEISMICITY

In early July 2010 a ground rupture on the North side of Mavropigi Village was discovered. The investigation of the feature was assigned to the Institute of Geology & Mineral Exploration (IGME) by Kozanis' Prefecture. The outcome of the investigation (issued on 10/8/10) proposed its monitoring. On the 1st September of the same year a second ground rupture, almost parallel to first one, was observed, about 100 meters from the boundary of Mavropigi mine. These two lines of deformation behave slightly differently but are considered to operate simultaneously and have the same origin. The study includes the area bounded by 40.10^{o} - 40.80 ^{o} N (latitude) and 21.40 ^{o} - 22.30 ^{o} E (longitude).

In order to assess the earthquake hazard of the area, seismic events reported in literature or recorded instrumentally in the area was examined.

Figure (3.1) illustrates the map of the broader area, and the epicenters of earthquakes with magnitude M> 2.0 (regardless of completeness), that occurred in the study area from 1695 to 2010. In this map, epicenters are denoted with different symbols, according to the earthquake magnitudes.

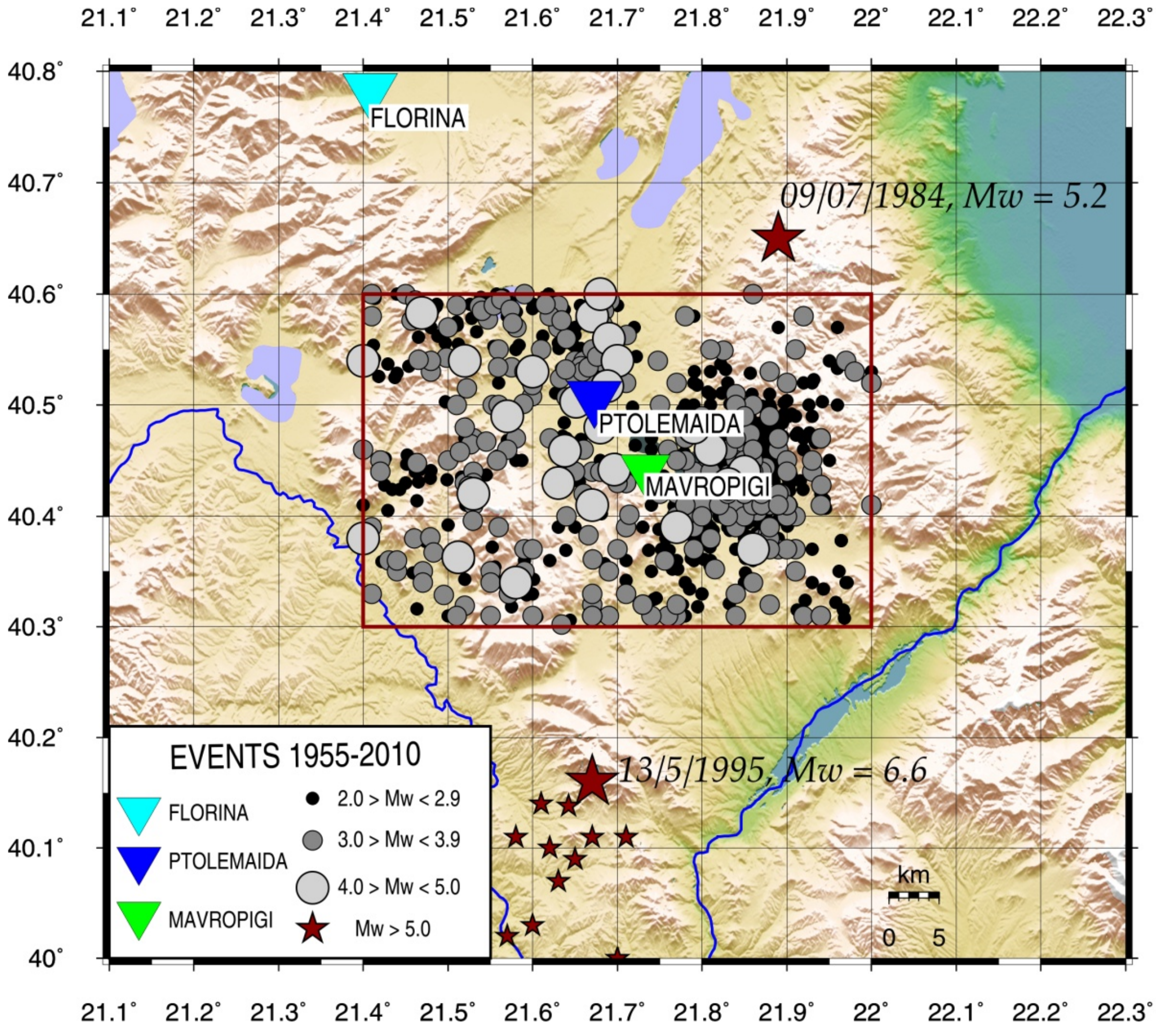

Figure 3.1 Map of the epicenters of all earthquakes with magnitude M > 2.0 that occurred in the study area since 1695. The positions of the various towns and villages of the area are distinguished, as well. The two notably earthquakes, which pointed out with the big stars are discussed below, in the main text.

The region of interest presents three (3) main faults, as shown in Figure (3.2):

(1) Vegora –Vegoritida fault. With a N 40^0 E direction, dips to SE passing the Agios Spiridon, Agios Panteleimon and Vegora villages and its length is about 20 Km long. This is a typically normal fault.

(2) Nymfaion-Petron fault. The great tectonic line Petron - Xynou Neron- Aetou-Nymphaeum with a N 30^0 E direction and SE sinking, longer than 30 km, and a shifter character

(3) Proastion-Asvestopetra fault. The middle of the fault's length is approximately 7 Km distaned from the center of the village.

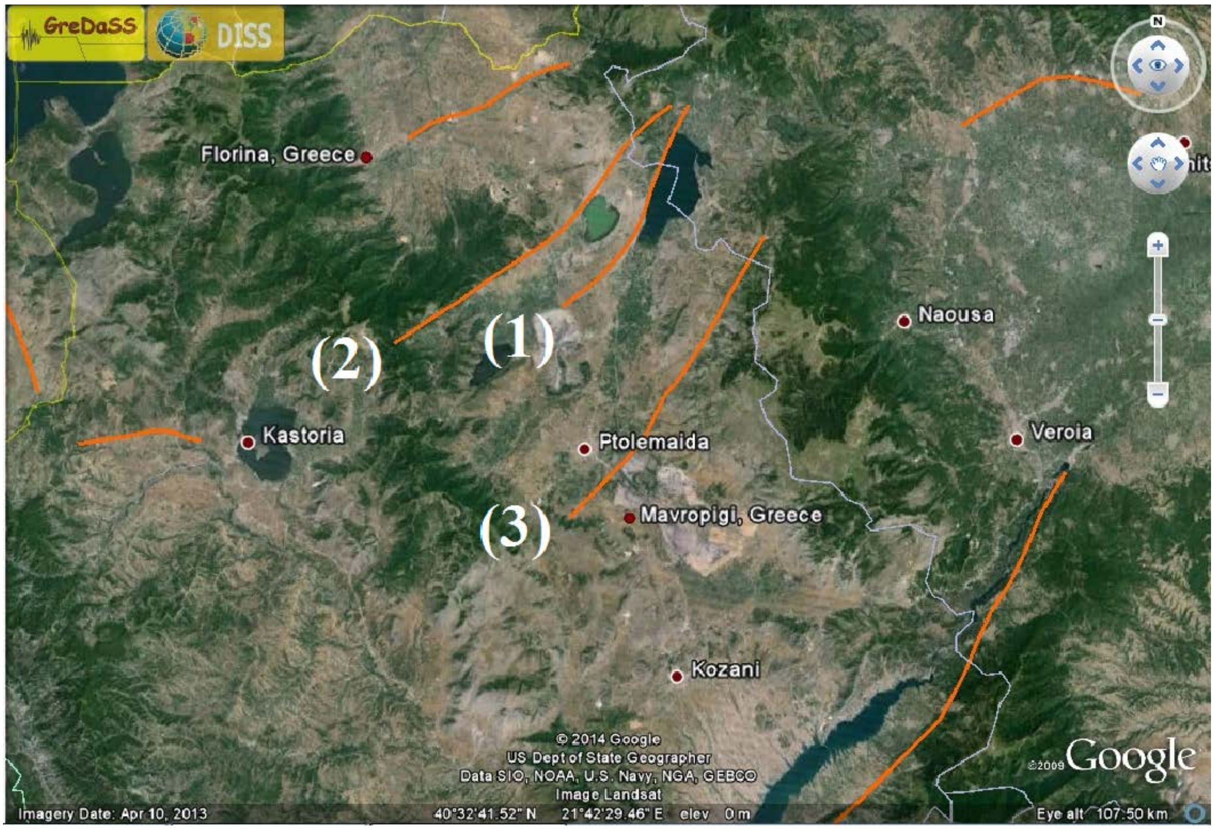

Figure 3.2 : The three main faults of the region. (1) Vegora-Vegoritida fault, (2) Nymfaion-Petrwn fault and (3) Proastion-Asvestopetra fault. Faults are illustrated in Google Earth (Google, 2010) based on the GreDaSS (after Caputo and Pavlides, Pavlides et al., 2010;Caputo et al., 2012)

Despite their capability to accumulate adequate amounts of energy to trigger seismic vibrations, there is no evidence of such events happening in the past (Tsapanos et al., 2011). The aforementioned accumulated energy is directly related to the dimension of the fault according to Wells and Coppersmith, (1994) and Pavlides and Caputo, 2004.

According to the Greek Seismic Code, 2000 (as modified F.E.K. B' 1154/12-8-2003, Case No. D17a/115/9/FN275) the study area is characterized as a zone of low-moderate seismicity. The expected seismic acceleration, with a 10% probability of exceedance in the next 50 years is a = 0.16g, is 16% of the acceleration of gravity (Zone I).

In this region, earthquakes, are shallow, (Figure 3.3) with an average focal depth of 9 Km, while the big majority presents depths up to 20 Km (small to medium sized earthquakes). The number of earthquakes depicted in Figure (3.3) is 797, and of sizes M> 2.0.

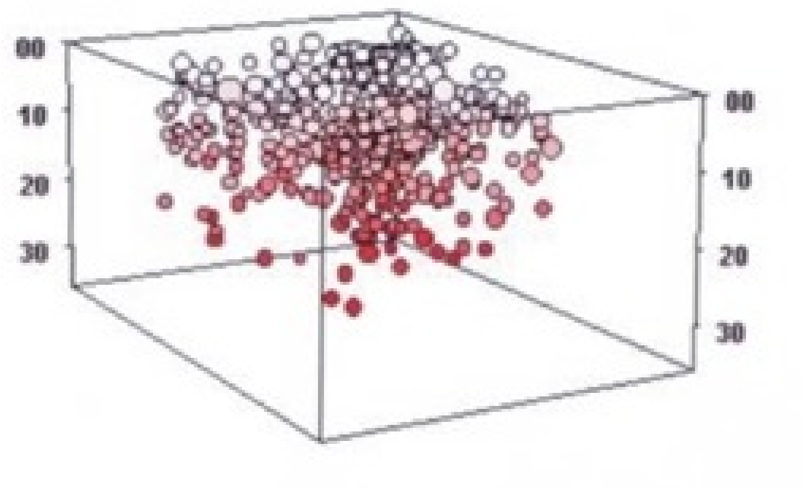

Figure 3.3 Three-dimensional representation of the earthquakes focal depths in the area. Average focal depth of 9 Km. The majority of the earthquake occurs to a depth of 20 Km (after Tsapanos et al., 2011).

67% of these earthquakes, have magnitudes from 2.0 to 3.0, 29%, have magnitudes between 3.0 and 3.9, while only the 3.9% are medium-size earthquakes (4.0 to 5.0) (Tsapanos et al., 2011).

Only one earthquake with Mw=5.2 was recorded in the region, in 1984. This event did not cause any damages in Mavropigi because of the large distance between its epicenter and the village. Moreover, one seismic event of magnitude M=6.6, located 32 Km away from Mavropigi, was recorded in 1995. Its ground acceleration was measured to be a<0.16g, in fully accordance with the acceleration given by the Seismic Code for this region (Tsapanos et al., 2011). These two epicenters are shown in Figure 3.1.

3.2 DATA PROCESSING – METHOD OF GUTENBERG-RICHTER

The data used in the present was extracted from the data bank of the seismological station of the Aristotle University of Thessaloniki.

Numerous studies on measures of quantitative seismicity are currently available for earthquake hazard assessment **(**Galanopoulos and Delibasis, 1972, Makropoulos and Burton, 1984, Papazachos, 1990, Tsapanos and Burton, 1991, Hatzidimitriou et al., 1994, Tsapanos and Papazachos, 1998, Tsapanos, 2001a, Tsapanos, 2001b, Bayrak et al., 2008, Öztürk et al., 2008 and Bayliss and Burton, 2013 among others).

According to Gutenberg and Richter, (1944) law, the cumulative number of earthquakes, N, with magnitudes larger than or equal to M, located at a certain place and taking place at a certain time t, is given by the following equation :

$$\mathrm{Log}N = a_t - bM \qquad (1)$$

where a_t and b are parameters. The b parameter, depends on tectonic characteristics of the region (Allen et al., 1965;Hatzidimitriou et al., 1985;Wang, 1988;Tsapanos, 1990) and decreases when stress increases (Scholz, 1968). Low values of b are related to a low degree of heterogeneity, large strain rate, large deformation velocity and large faults (Manakou and Tsapanos, 2000). On the other hand, the a_t parameter, depends on the seismicity of the region, on the area covered by the epicenters and the time interval t, during which the earthquake occurred. Usually, $a_{t,}$ is reduced to a period of one (1) year by applying the relation

$$a_1 = a_t - \log t \qquad (2)$$

where t is the time interval.

The mean return period T_m (in years) of earthquakes, having a magnitude M or greater, is given by

$$T_m = \frac{10^{bM}}{10^a} \qquad (3)$$

The probability P_t, of an event to become an earthquake of magnitude M or greater at time t, assuming Poisson time distribution, is given by the relationship

$$P_t = 1 - e^{\left(-10^{a-bM}\right)} \cdot t \qquad (4)$$

The most likely maximum magnitude, M_t, during a specific time period, t, is given by

$$M_t = \frac{a + \ell ogt}{b} \qquad (5)$$

Equations (3, 4 and 5) are used for the computation of quantitative seismicity of the area. The catalog of earthquakes used for the analysis of the seismicity should be complete, in order to obtain reliable results. Applying the statistical law of Gutenberg and Richter, (1944) for the data set in Figure (3.1), the magnitude distribution of earthquakes with magnitude equal to or larger than 2.0 is obtained and depicted in Figure 3.4.

Setting Mavropigi as the origin of a locus with radius equal to the distance between the village and the middle of Vegora-Vegoritida fault (30Km), the candidate earthquakes towards investigation were identified (all located within the radius). Note that the selected distance corresponds to seismic events of magnitude M=6.5, as found in literature (Papazachos and Papazachou, 1997; Pavlides and Caputo, 2004).

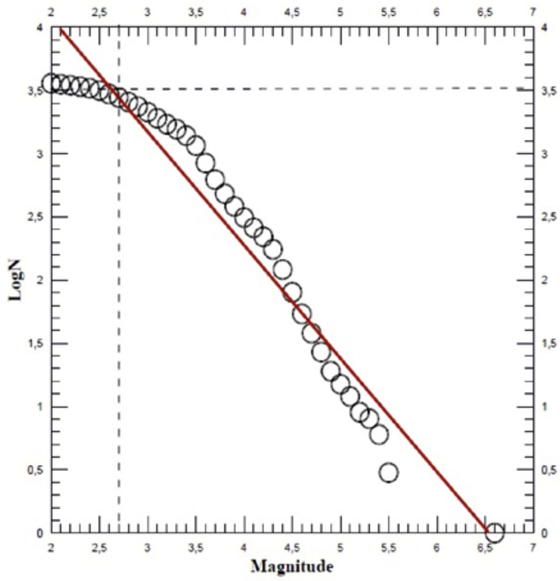

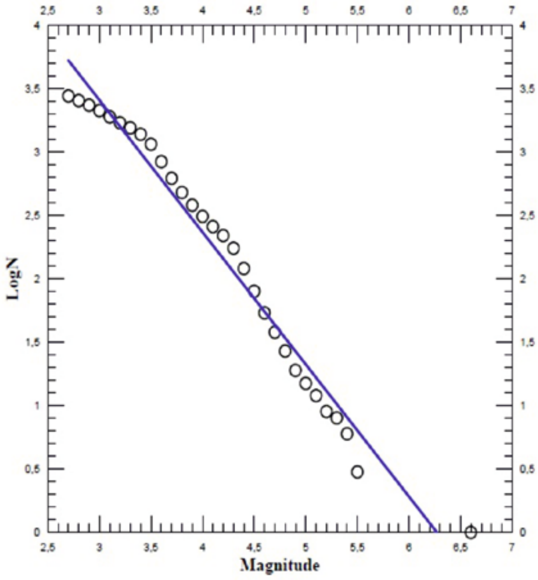

Figure 3.4 : Implementation of the statistical law magnitude distribution in the area for the full sample earthquakes of Figure (3.1). Figure 3.5 : Implementation of the statistical law magnitude distribution in the area for the full sample earthquakes of Figure (3.1).

The red line in Figure (3.5) represents the data linear fit (open circles). Note that the fit is not optimal.

In order for the data processing to be possible, and towards getting valuable results, their completeness was first established. As a first step, the total observation time was divided in smaller sub-periods. The intervals showing consistent data were : 1) 1966-2010 M $\geq$ 4.5 , 2) 1973-2010 M $\geq$ 4.1, 3) from 1996 to 2010 M$\geq$3.5 and 4) 2003-2010 M $\geq$ 2.7 (Tsapanos et al., 2011).

Subsequently, was made a data reduction (cases 1, 2, 3 and 4) in the period from 1800 to 2010 (κ = 210 years). Considering that earthquakes follow a normal distribution with time and V is the number of earthquakes of magnitude M, occurring over a period of K_i years, then the "reduced" number of earthquakes V_κ, is given by :

$$V_\kappa = V\frac{K}{K_i} \qquad i = 1,2,3,4 \qquad (6)$$

where K is the total time of available data, 210 years in our case. From this relation we obtain the "reduced" number of earthquakes, according to the completeness of the sample above. Then data was mapped (Figure 3.5) based on its completeness. According to the above, the data has completeness for magnitudes M$\geq$2.7. The blue line in Figure (3.5) represents the adjustment of the theoretical straight in our data (open circles).

Thereby, for the region under study and complete data sets, the parameters $\mathbf{a_t}$ and **b** were calculated, with $\mathbf{a_t}$ **= 6.09** and **b = -0.95.** Then using equation (2) $\mathbf{a_1}$ was found equal to **3.75** (Tsapanos et al., 2011).

Next the seismic metric of the examined area was computed. By applying relation (3), the mean return period of earthquakes with specific magnitudes, are computed. The obtained results are shown in Table (3.1). Figure (3.6) shows the mean return period of earthquakes (in years) for magnitudes from 2.7 to 6.5.

Table 3.1. Mean return periods for earthquakes greater than or equal to 3.0, 3.5, 4.0, 4.5, 5.0, 6.0 and 6.5 (Tsapanos et al., 2011).

Magnitude	**3.0**	**3.5**	**4.0**	**4.5**	**5.0**	**6.0**	**6.5**
Recurrence period in years	**0.1**	**0.4**	**1.1**	**3.3**	**10.0**	**90.0**	**267.0**

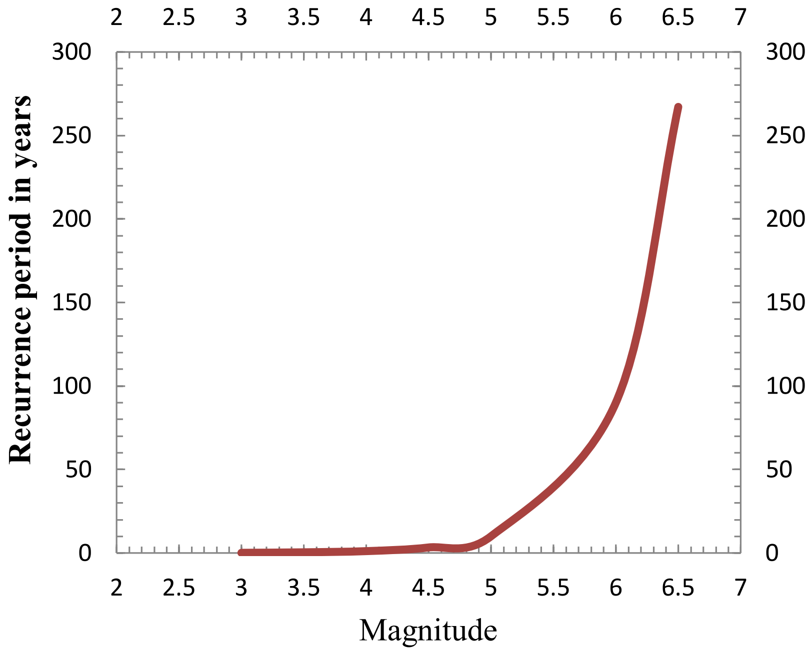

Figure 3.6 Reccurence period of earthquakes in the region of Mavropigi.

Moreover, using equation (4), the probability (Pt) for an earthquake of magnitude greater than or equal to M (3.0, 3.5, 4.0, 4.5, 5.0, 6.0 and 6.5), for a period of 1, 10, 25, 50 75 and 100 years, to occur was calculated. The results are shown in Table (3.2). Note that the mean return period for seismic events of magnitude M=6.5 was found equal to 268 years, in good agreement with the results from Tsapanos, (2005) for the entire Western Macedonia (272 years).

Table 3.2 Probabilities for earthquakes generation with magnitudes greater than or equal to 3.0, 3.5, 4.0, 4.5, 5.0, 6.0 and 6.5 for different periods (in years) (Tsapanos et al., 2011).

Magnitude	P1	P10	P25	P50	P75	P100
3.0	1.000	1.000	1.000	1.000	1.000	1.000
3.5	0.930	1.000	1.000	1.000	1.000	1.000
4.0	0.590	1.000	1.000	1.000	1.000	1.000
4.5	0.258	0.949	0.998	1.000	1.000	1.000
5.0	0.095	0.632	0.918	0.993	0.999	1.000
6.0	0.004	0.011	0.164	0.267	0.301	0.395
6.5	0.0003	0.0008	0.012	0.018	0.034	0.293

Table (3.2)shows that the probability for an earthquake of magnitude M> 6.0 to occur during a period of 100 years is about 40%, while an earthquake with magnitude M> 6.5 (the maximum expected magnitude for the examined area) and for the same time period the probability is of about 30%.

One additional usefully figure within the scope of this work, is the most probable maximum magnitude M_t during a specific period of time (in years). M_t was calculated using equation (5) and the obtained results are summarized in Table (3.3).

Table 3.3 : The most probable maximum magnitude M_t for a time period of 1, 10, 25, 50, 75, 100 and 500 years

Years	**1**	**10**	**25**	**50**	**75**	**100**	**500**
Magnitude	**3.9**	**5.0**	**5.4**	**5.7**	**5.9**	**6.1**	**6.6**

For a period of 100 years, the most probable magnitude to occur was found to be 6.1. This value is in a good agreement with the mean return period for earthquakes with magnitude $M \geq 6.0$ as shown in Table (3.1) and is equal to 90 years. The most probable maximum magnitude computed over 500 years is 6.6, almost identical to the maximum earthquake magnitude ($M = 6.5$), which theoretically can occur according to the potential of the Proastion-Asvestopetra fault (Tsapanos et al., 2011).

CHAPTER 4 - SEISMIC EVENTS RECORDING

4.1 INTRODUCTION

Within a research program concerning the ground effects in the vicinity of the village of Mavropigi, a temporal seismological network was installed in the broader area. The scope of the study is to identify whether the ground effects are products of the local seismicity of the area or on the mining activity, which is currently in operation. This portable seismological network consisted of five (5) stations and operated for four months. During this period, ninety tree (93) weak vibrations were recorded at very short distances from the installed instruments. In this section, a complete analysis of these records and resulted conclusions are presented.

4.2 INSTALLATION AND OPERATION OF THE SEISMOLOGICAL NETWORK

Digital seismological stations (Reftek 72A07) with broadband seismometers (Gural CMG40T), were installed near the area of Mavropigi. The seismographs were equipped with a Global Positioning System (GPS) in order to produce position and time of high accuracy. Very distinct readings of local earthquakes, achieved by setting a sample rate of 125 samples / second, simplified epicenter estimations. Additionally, earthquakes with epicenters outside the area of interest were recorded as well.

Figure (4.1a) depicts the local stations of the portable seismological network situated in Mavropigi (Google Earth, Google, 2010). Figure (4.1a) shows also the presence of an open pit in operation on the Northern side of Mavropigi, in a short distance from the area of installation. Note that changes in the mine topology occurred since 2010. The distance between the seismological stations is short and ranges approximately from 200 to 1500 meters. This short distance permits the recording of the very weak vibrations in a sufficient number of seismological stations enabling the accurate determination of the focal coordinates (Tsapanos et al., 2011).

Figure (4.1b), shows the broader area of Mavropigi. The yellow squares represent the five seismic stations . Three of them (with code names PAND, DHMS and CHAI) were installed inside the village, two (code names ANAN and APOT) in the surrounding area outside the village and the remaining three (FNA, KZN and PENT) belong to Hellenic Unified Seismological Network (HUSN).

a)

Figure (4.1a) (Google, 2010) Map of the broader region of Mavropigi, Ptolemaida. The five portable seismic stations and also the three stations (FNA, PENT and KZN) of the Hellenic Unified Seismological Network (HUSN) are depicted with black-white squares.

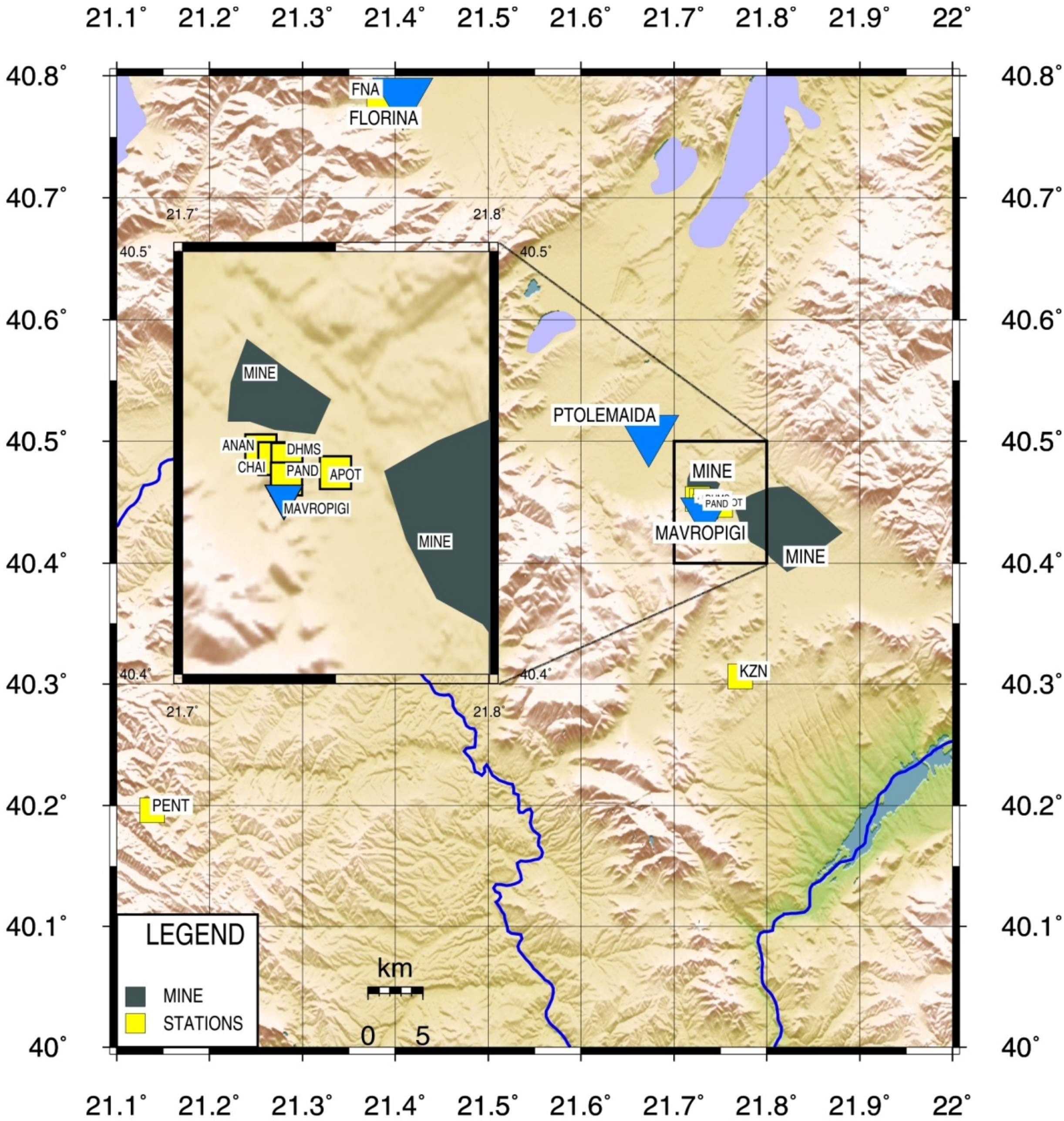

b)

Figure (4.1b) Map of the broader region of Mavropigi, Ptolemaida. The five portable seismic stations and also the three stations (FNA, PENT and KZN) of the Hellenic Unified Seismological Network (HUSN) are depicted with yellow squares. The mine is distinct in the North of Mavropigi. Kardia mine is located Eastern of the village (GMT software, Wessel and Smith, 2006).

Table (4.1) presents the coordinates of the seismological stations.

Table (4.1) :Coordinates of the stations, which were used in the seismic events location of the present study.

Name	Latitude (^{0}N)	Longitude (^{0}E)
ANAN	40^0 27.17’	21^0 40.45’
APOT	40 ^{0}26.86’	21^0 40.44’
CHAI	40^0 27.06’	21^0 40.45’
DHMS	40^0 27.05’	21^0 40.45’
PAND	40^0 26.77’	21^0 40.44’
KZN	$40^0$18.40’	21^0 46.25’
PENT	40^0 11.75’	21^0 08.30’
FNA	40^0 47.05’	21^0 22.95’

Figure (4.2) illustrates one of the installed seismograph which operated under the code name ANAN. From right to left, the seismometer, the battery, the system log (digitizer and disk data storage) are depicted. On the very left, the computer, which was used for the setup of the seismograph is also shown (Tsapanos et al., 2011).

Figure (4.2) Picture of the installation of the seismological station with codename ANAN. It is illustrated from right to left, the seismometer, the battery, the digitizer, the disk storage of data and the computer (after Tsapanos et al., 2011).

In Figure (4.3), the GPS antenna used for the accurate determination of time and location, is shown in the upper left side of the chimney.

Figure (4.3) The arrow at the top (on the left) of the chimney indicates the GPS antenna signal receiver for the exact positioning and time recording in the station ANAN (Tsapanos et al., 2011).

In some cases, the installation of a solar panel connected to a battery was necessary in order to supply electric power to the stations (Figure 4.4).

Figure (4.4) Solar panel for supplying the seismological station codenamed ANAN (Tsapanos et al., 2011).

4.3 SEISMIC DATA ANALYSIS

4.3.1 First Model characterized by High velocities

The catalogue of the seismic data derived from the recordings of the five (5) non-permanent seismographs' (PAND, DHMS, CHAI, ANAN and APOT) installed in Mavropigi and the near vicinity, is given in (Appendix I). These recordings were compared with the catalogues of the National Unified Seismological Network for the period from 29/1/2011 up to 11/5/2011. The catalogue of these earthquakes is listed in Appendix II. Using the data sets from both the NUSN and the local network, the phases of the arrival times for both P waves and S waves (where possible) were computed. This file of phases was used to determine the coordinates of the epicenters (location). HYPOINVERSE (Klein, 2002), running on a Linux environment was used in this regard. During this process, arose the necessity to identify a model of velocities, which could improve the accuracy in epicenters estimation.

During the first data processing attempt, various velocity models of the Earth crust (Hatzfeld et al., 1996, Rigo et al., 1996 and also Panagiotopoulos and Papazachos, 1985) were assumed. The high velocities model proposed by Rigo et al., 1996 , gave the smallest errors.

Table (4.2) : High velocities model.

Velocity, Vp (km/sec)	**Depth (km)**
4.80	0.0
5.20	4.0
5.80	7.2
6.10	8.2
6.30	10.4
6.50	15.0
7.00	30.0

The derived epicenters from the data in Table (4.2) is given in Appendix III. Figure (4.5) shows a map depicting the distribution of the epicenters of recorded seismic events. A large number of epicenters seems to be located in the Eastern edge of Kardia mine, East of Mavropigi.

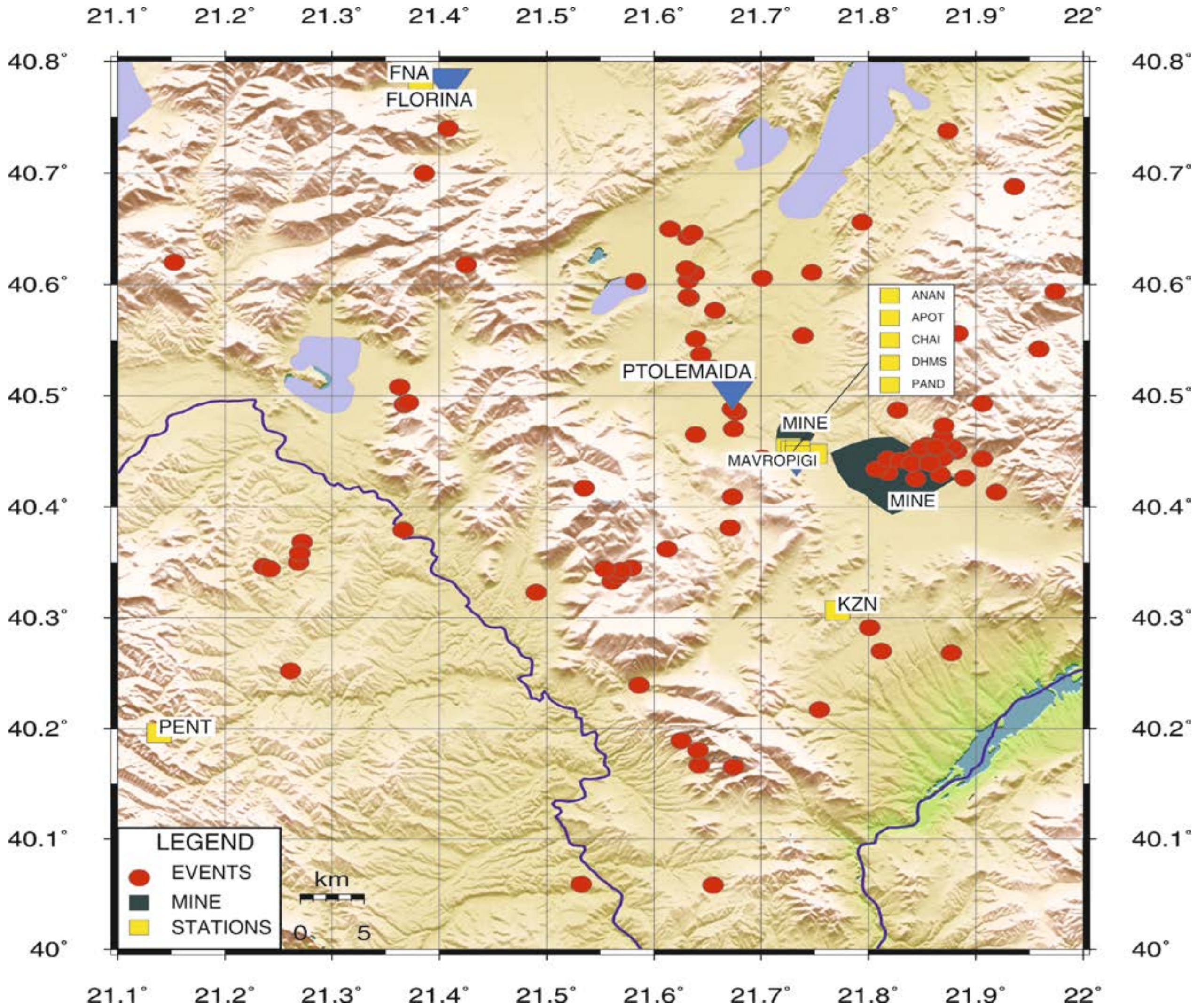

Figure (4.5) : Epicenters of the High velocity model.

For the high velocities model, focal mechanism of seismic events were estimated using FPFIT-FPPLOT-FPPAGE (Reasenberg and Oppenheimer, 1985). Results are listed in Appendix V. In this regard, the Vp/Vs ratio, was calculated as per Wadati computational method. Figure (4.6) shows its main value, which is equal to 1.78, in agreement with other found in literature (1.77 and 1.83) (Rigo et al., 1996).

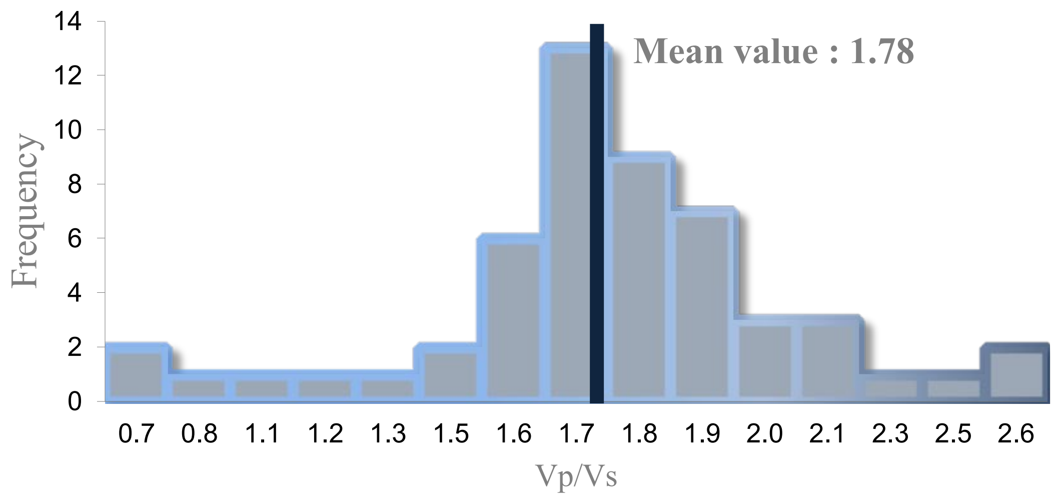

Figure (4.6) : The histogram shows the velocities ratio, Vp/Vs, relative to the frequency. The ratio's Mean value calculated to be 1.78.

<u>Errors in high velocity model</u>

Error values for the high velocities model, such as the Root Mean Square of the travel time residuals (RMS), the error in epicenter (ERH) and the error in the depth (ERZ) were calculated. The mean values of the errors, as shown in Figure (4.7 a, b and c), are **0.28** for the mean RMS value, **14.1** for the mean ERH value and **18.6** for the mean ERZ value.

a)

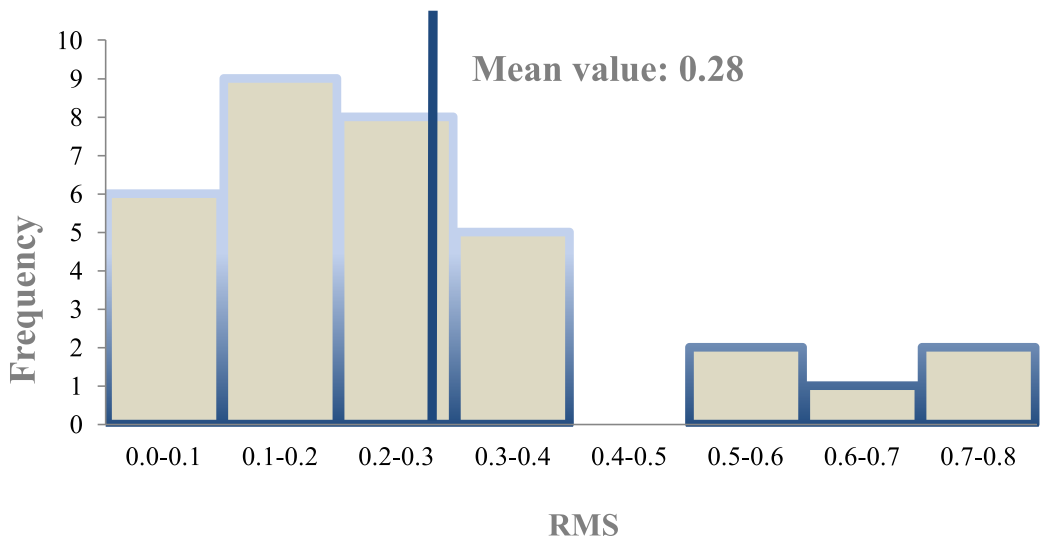

b)

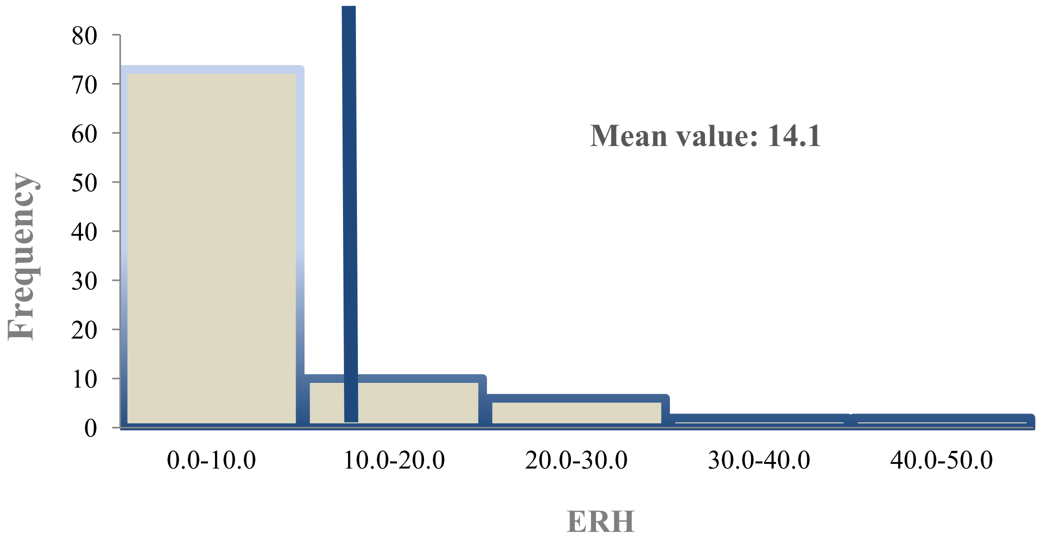

c)

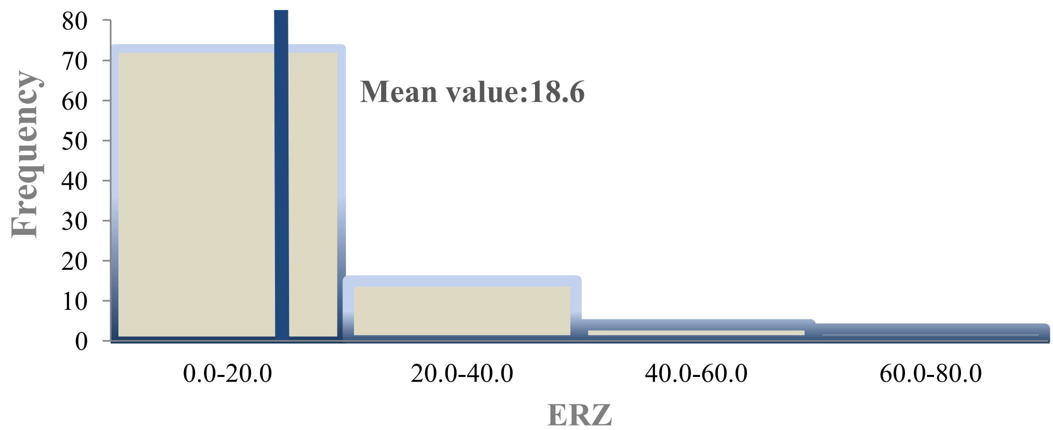

Figures 4.7 : Histograms of the errors for the high velocity model a) RMS, b) ERH and c) ERZ.

4.3.2 Second Model characterized by Low velocities

A further improvement of this model was possible by assuming variable velocities especially for the surface layers. Low velocities gave better results (grouping of the epicenters and smaller errors). As mentioned before, the stations of the local seismological network, where the vibrations were recorded, were placed in small intervals the one from the other, since the seismic rays propagate only in the layers near the surface. For that reason and taking into account the geophysical studies that took place in the region during the program, the high velocity model was modified. In this regard, and for the first 1000 meters, layers allowing low velocity propagation of the P-waves were added, resulting into a new “low velocity” model, shown in Table (4.3). This is a model of 10 layers over a half space. Time residuals for each seismological station were calculated to correct any model uncertainties and lateral variations of the structure, following a procedure proposed by Karakostas et al., (2012 & 2014). Applying the Wadati method the Vp/Vs ratio was calculated equal to 1.85 (Kalogirou et al., 2014).

Table (4.3) : Low velocities model.

Velocity(km/sec)	**Depth (km)**
0.4	0.1
0.5	0.2
1.2	0.3
3.0	0.7
5.2	4.0
5.8	7.2
6.1	8.2
6.3	10.4
6.5	15.0
7.0	30.0

Figure (4.8) illustrates the distribution of the seismic events location resulted from the low velocity model. A great number of epicenters (Appendix IV) seems to be located in the Kardia mine area, as well as Eastern of Mavropigi. However, this time, the epicenters are concentrated in the whole area of Kardia mine and not only on the Eastern edge.

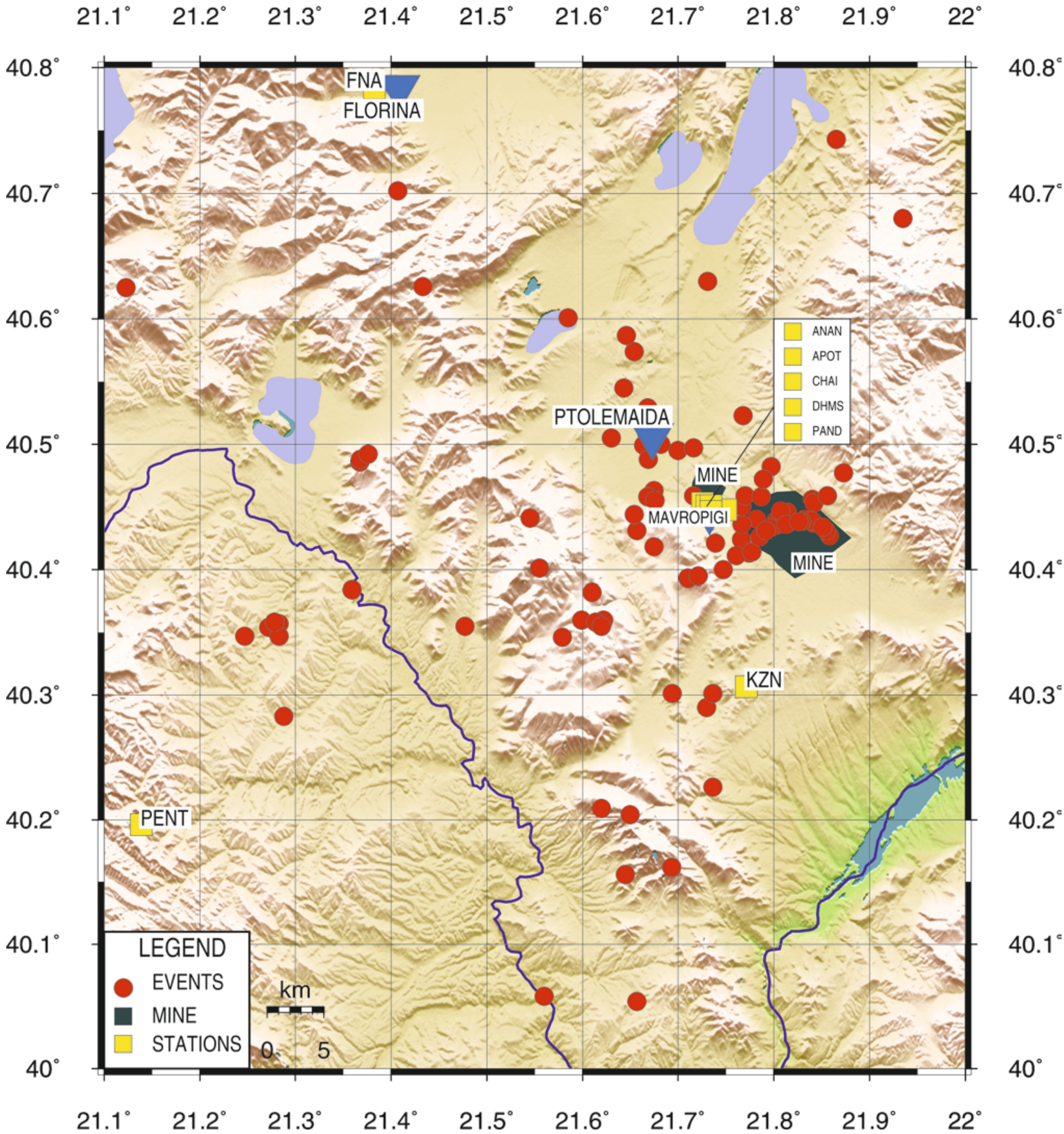

Figure (4.8) : Epicenters of the Low velocity model.

Errors in low velocity model

Errors for the new low velocity model were computed as well. The mean values of the errors are:

- **RMS** = **0.23**,
- **ERH** = **11.4** and
- **ERZ** = **11.8**.

The results are shown in Figure (4.9 a, b and c)**.**

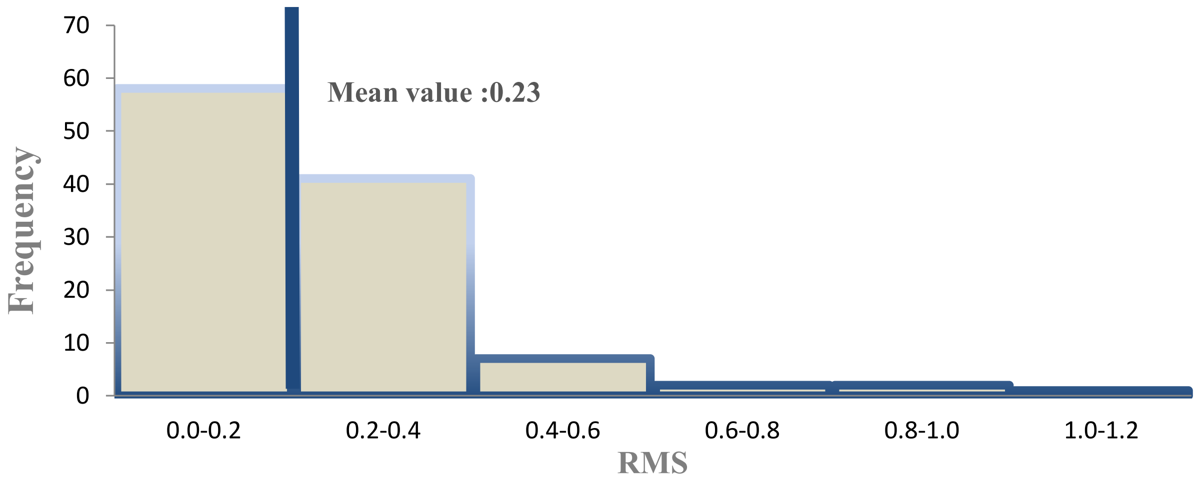

a)

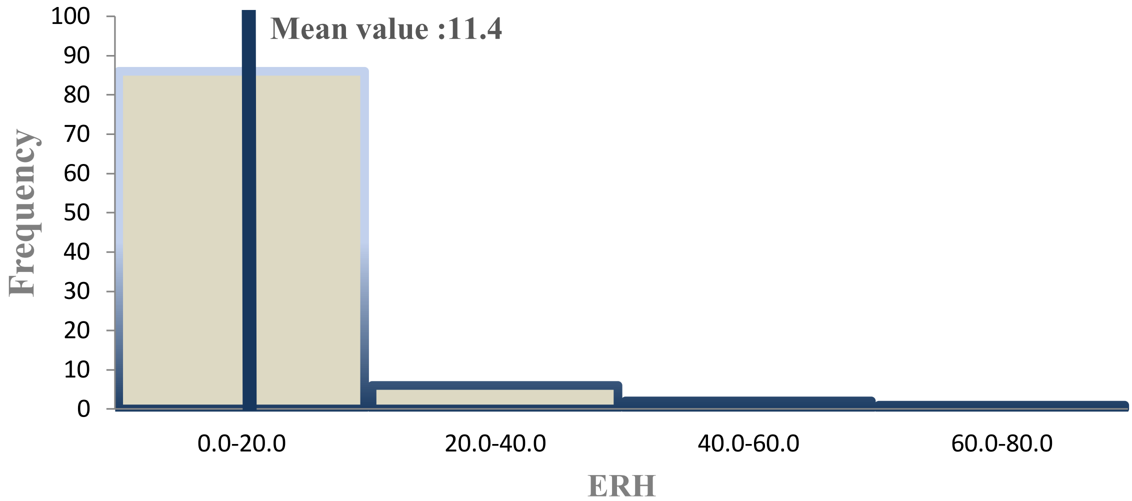

b)

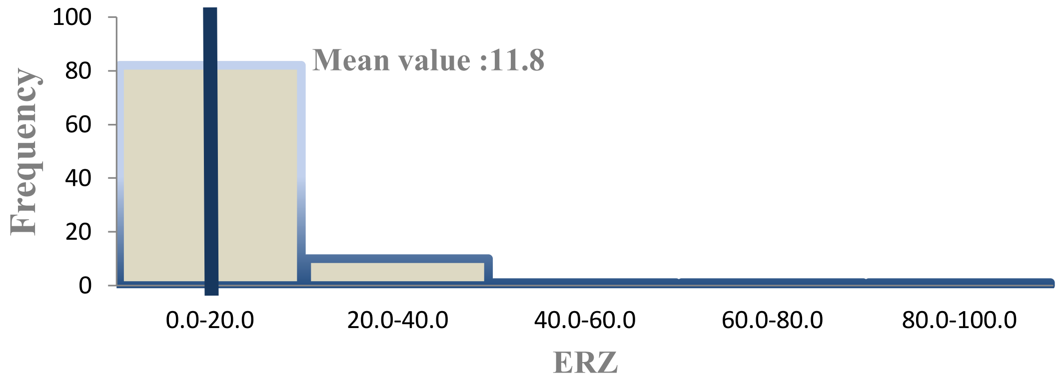

c)

Figure (4.9) : Histograms of the errors for the Low velocity model a) RMS, b) ERH and c) ERZ.

Data processing using the two models, revealed substantial differences between the two, especially with regard to :

- depth distribution
- in origin time and
- the epicentral location.

4.3.3 Comparison between the two models

The high velocity model presents a mean value of **9.69 Km** concerning depth, while the Low velocity model has a mean value of **7.7 Km**, Figure (4.10a and b). Moreover, the difference in depth between the two models is presented in Figure (4.10c).

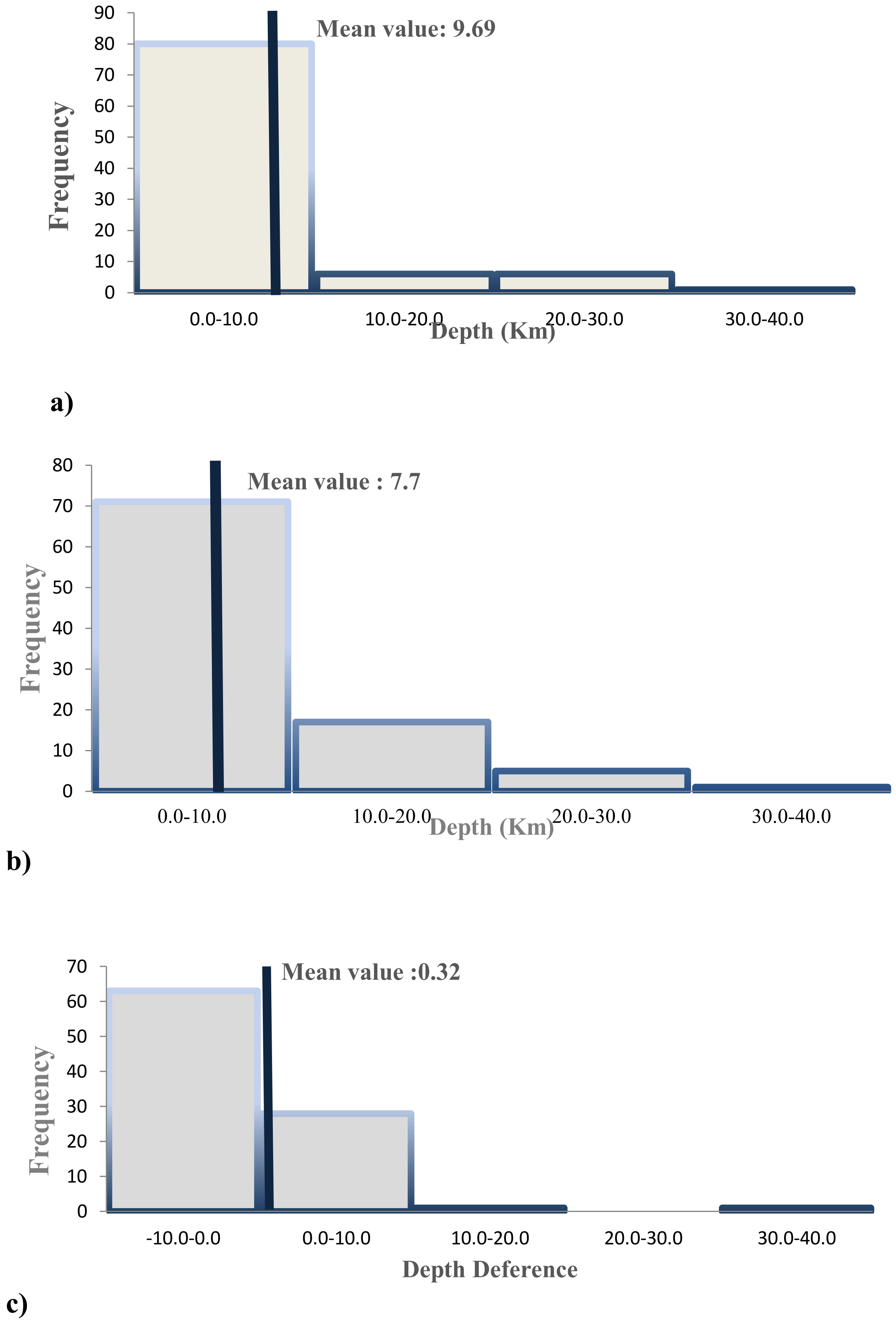

Figure (4.10) : Depth distribution of the a) high Velocity Model and b) the Low Velocities Model and c) Distribution of the difference in depths between the two models.

In addition, differences in origin time (in sec), and in epicenters (in Km) were computed. The calculated mean values for these cases are **1.4** (Figure 4.11) and **9.1** (Figure 4.12) respectively.

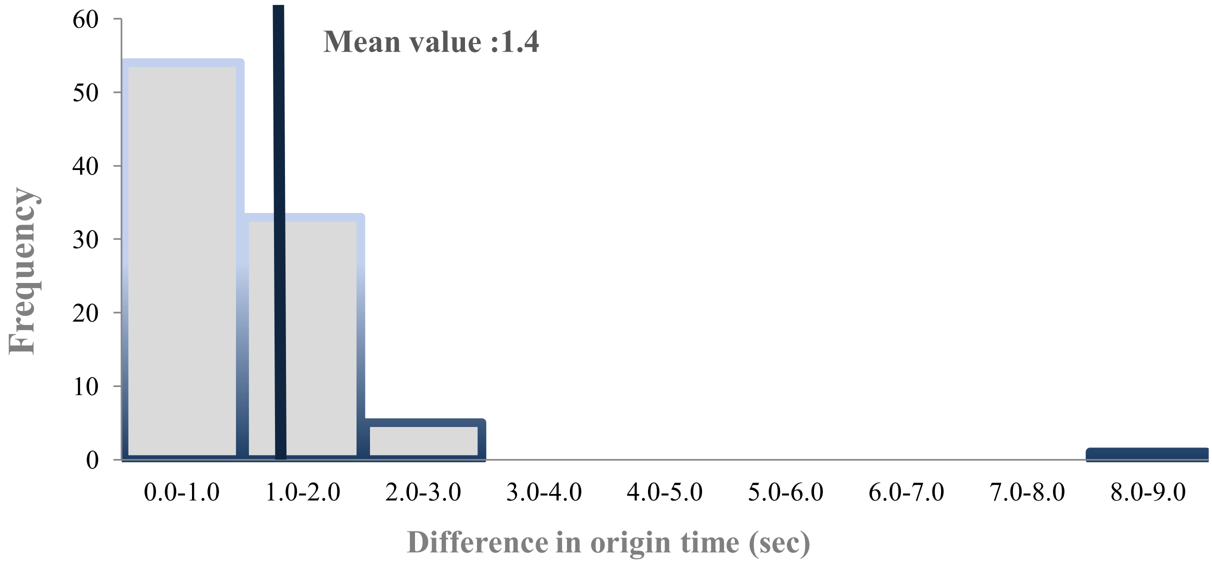

Figure (4.11) : Distribution of the difference in origin times between the two models.

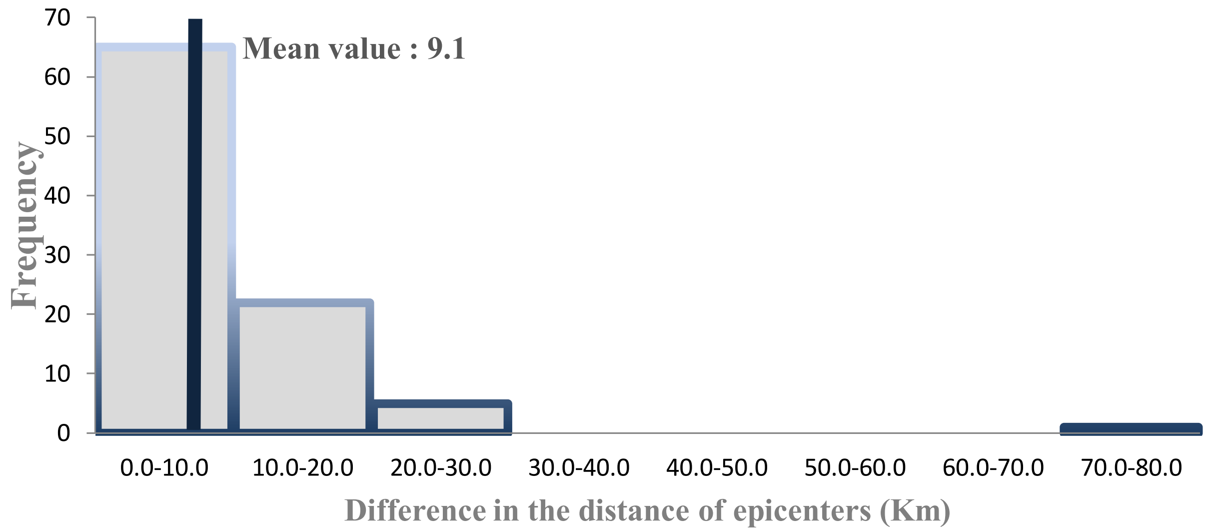

Figure (4.12) : Histogram of the difference in the distance of epicenters between the two Models.

Considering the above diagrams comparing the two models and the spatial distribution of the epicenters, as shown in Figure (4.5) for the High velocities Model and Figure (4.8) for the Low velocities Model appears to be the more reliable between the two, hence the more suitable to describe any correlation between the focal mechanism of some earthquakes and the tectonic region.

4.3.4 Correlation of low velocities focal mechanisms with tectonics

Focal mechanism estimation for the low velocities model (Appendix VI) was then undertaken. In this regard, further data processing was needed in order to identify events with clear records. Thus, events of many low magnitudes and small number of phases recorded, were discarded. It is noticed here that the local seismic network was located NW of the Mavropigi mine. Where, both natural earthquakes and explosions (taking place inside the mine) were recorded. The need to distinguish between the two events was thus fundamental. Reliable results were foresight, as mentioned above, by selecting data sets which clearly allowed the calculation of the focal mechanisms (Figure 4.13).

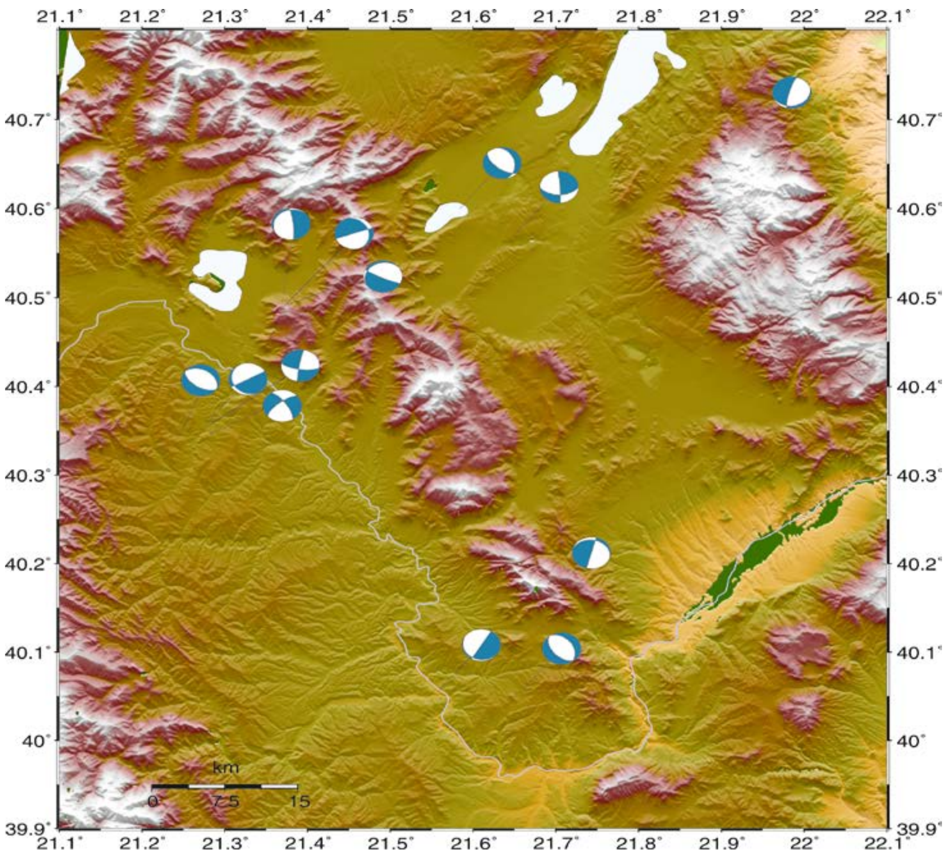

Figure (4.13): Earthquake focal mechanisms in the surrounding area of Mavropigi.

The predominance of extension with respect to compression is visible. This follows the study results concerning the tectonic regime of the area, however, one should note the scars amount of data available for the estimation of the focal mechanism.

4.4 WAVEFORM CHARACTERISTICS

4.4.1 Local earthquakes waveforms

At this point is important to illustrate a waveform as recorded by the local seismological network. In Figure (4.14a) a small local earthquake (s-p ~ 3 sec) is shown. The arrival time of the S waves (taking in mind the horizontal components) is 288 sec. The Fast Fourier Transform applied to this waveform (4.14b), for the initial and the late part of the waveform, appears to have the same corner frequency of about 30 Hz (Kalogirou et al., 2014).

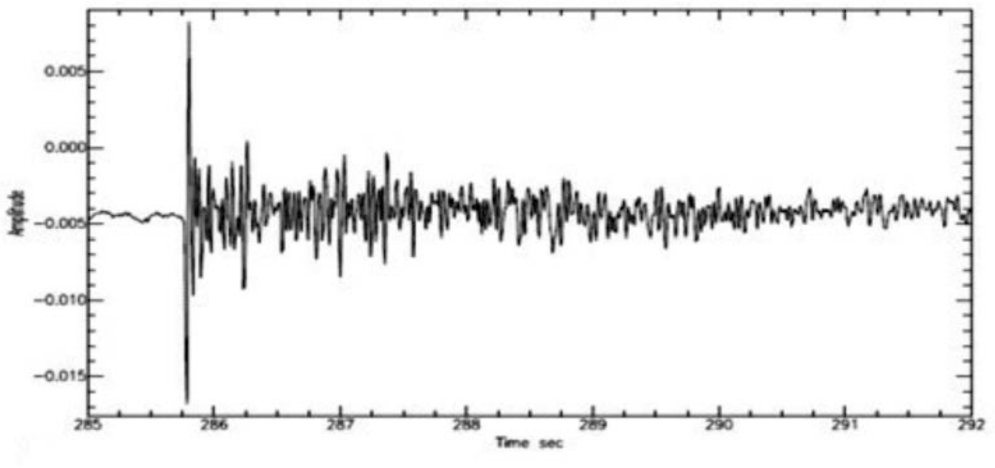

a)

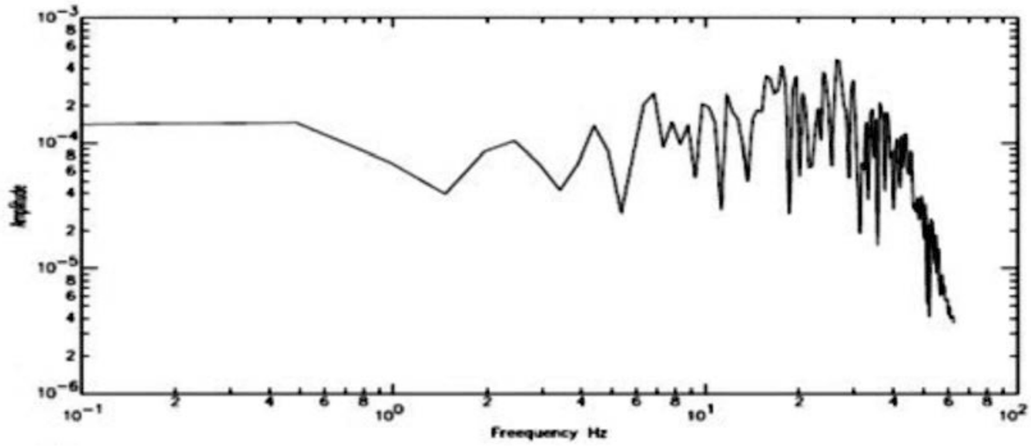

b)

Figure (4. 14) : (a) A small local earthquake (waveform) Amplitude related to the Time (sec).– (b) The Fast Fourier Transform for the initial or the late part of the waveform (Amplitude related to Frequency (Hz)) (after Kalogirou et al., 2014).

Moreover, in Figure (4.15) are illustrated, indicatively, some of the non filtered earthquake waveforms, which were recorded during the four months period. Indications in the upper side of the window are related to the path folder, the date (e.g. 20110306) of data collection and the date and time of the earthquakes as well. The same seismic events were also recorded from the permanent seismological network. In Appendix VII are presented some more earthquake waveforms.

1. **110203_0926, 2.4**

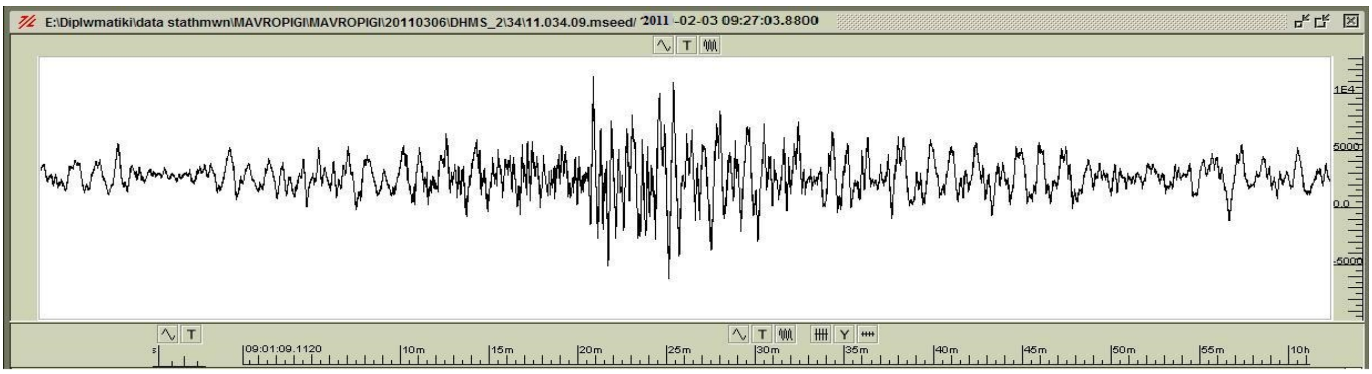

2. 110203_0934, 2.6

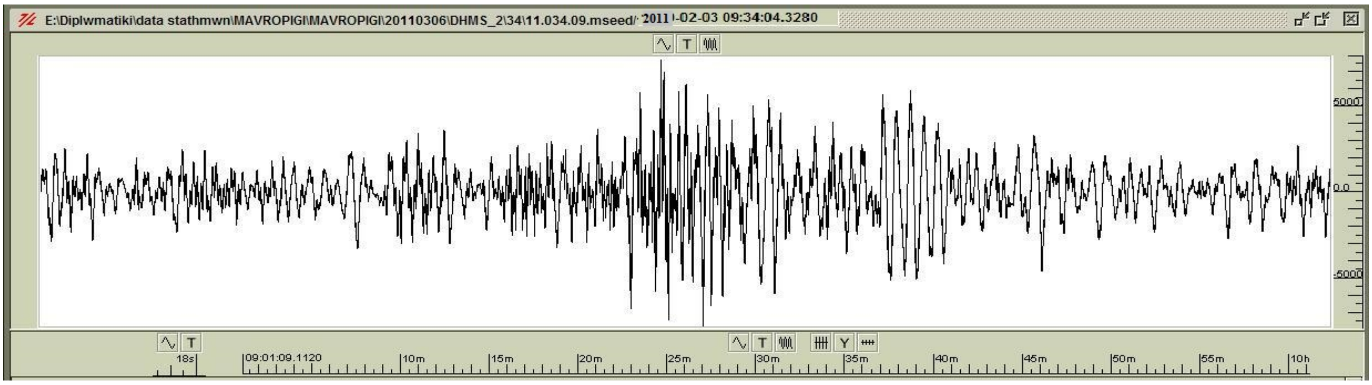

3. 110204_1713, 2.5

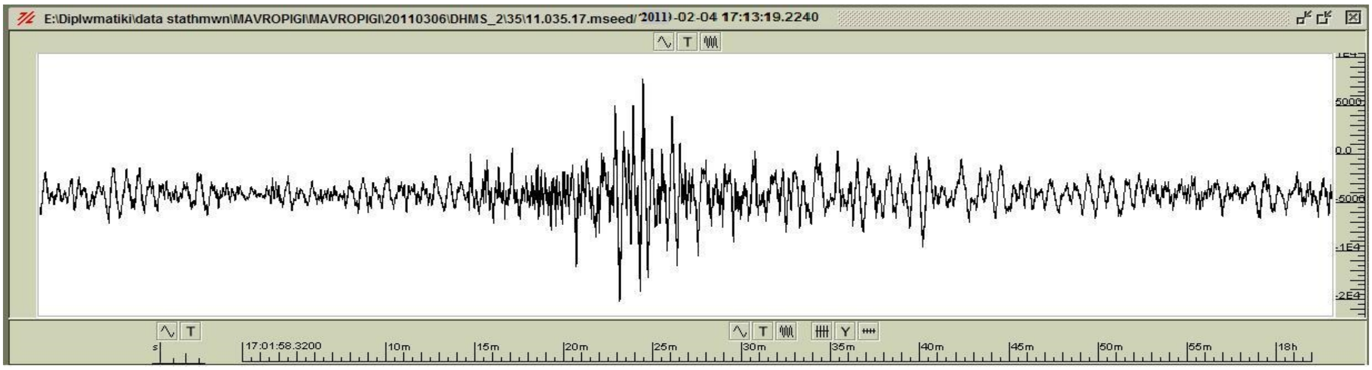

4. 110424_1226, 2.9

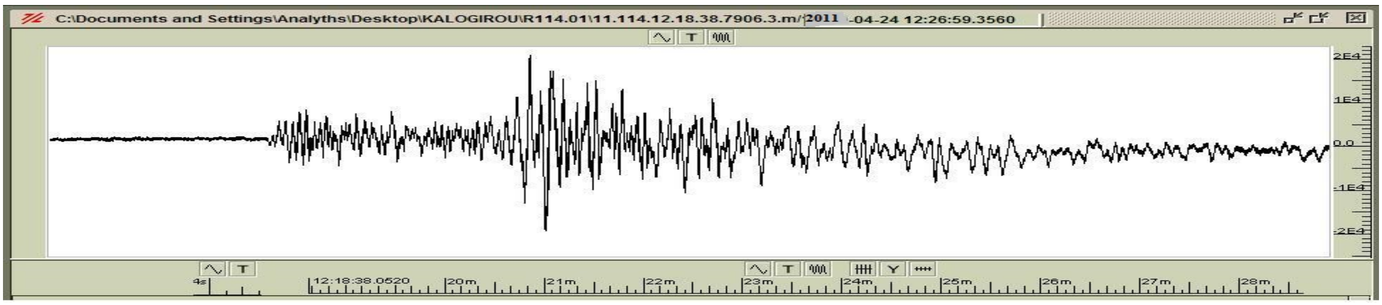

Figure (4.15): Earthquake waveforms that recorded during the fourth months period from the installing local seismological network.

Finally, taking into account magnitudes and recorded phases of every seismic event, an estimation of the relationship between the two is made Figure (4.16).

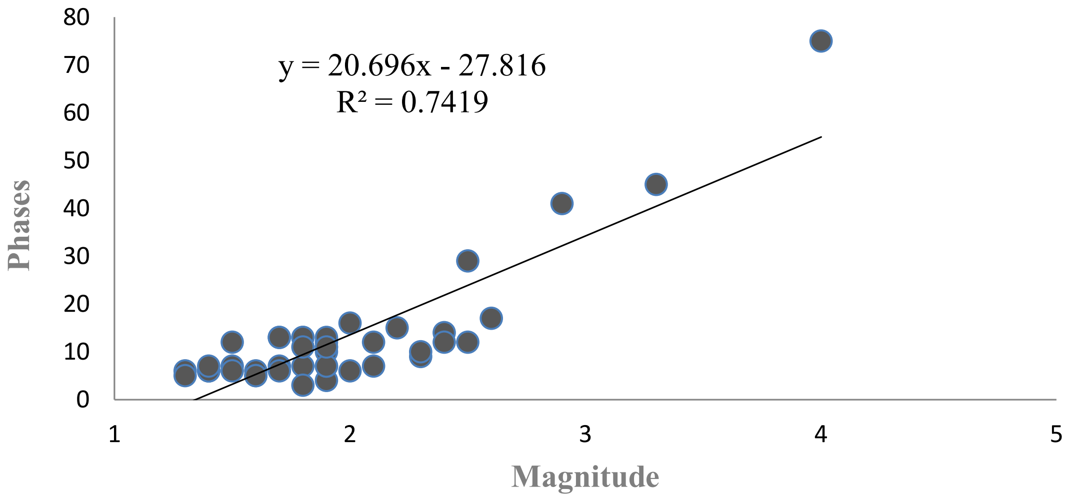

Figure (4.16): The relation between the seismic events magnitude and the recorded phases.

For magnitudes up to M=2.0 the number of phases ranges from 5 to 16. Larger magnitudes, up to 2.9 present a number of phases between 7 and 17. Finally, for events with magnitudes larger than 2.9 the number of phases exceed the 40 records. Thus one can conclude that the number of phases increases with the magnitude. The equation that describes the relationship between magnitude (M) and recorded phases (Ph) is : $Ph = 20.7 \cdot M - 27.8$. The R-squared value has a relatively small value due to the fact that the largest pair of values occur in earthquakes with magnitude $M \leq 2.5$.

4.4.2 Explosion waveforms

In addition, as aforementioned, for the earthquake waveform and for comparison reasons the vertical component of a ground tremor recorded at one of the local seismological stations is presented. The time is measured in seconds after the beginning of a ten (10) minutes file and amplitudes show velocity in m/sec. This waveform, which is representative of several other recordings, start with higher frequencies while after some seconds longer periods are dominant. (Figure 4.17a). The body waves at the beginning of the signal are followed by surface waves. Figure (4.17b) shows the spectrum of the first part of the recording (251.8-253 sec). Corner frequency was found to be about 30 Hz. Then, for higher frequencies, continuous attenuation of the amplitude signal is observed. Figure (4.17c) shows the spectrum of the second part of this recording (255-286.2). The amplitude attenuation starts slowly roughly at 3Hz to reach higher values around 30 Hz. This is comparable to the body waves of an earthquake, especially in terms of corner frequency ~30 Hz (Figure 4.14b) (Kalogirou et al., 2014).

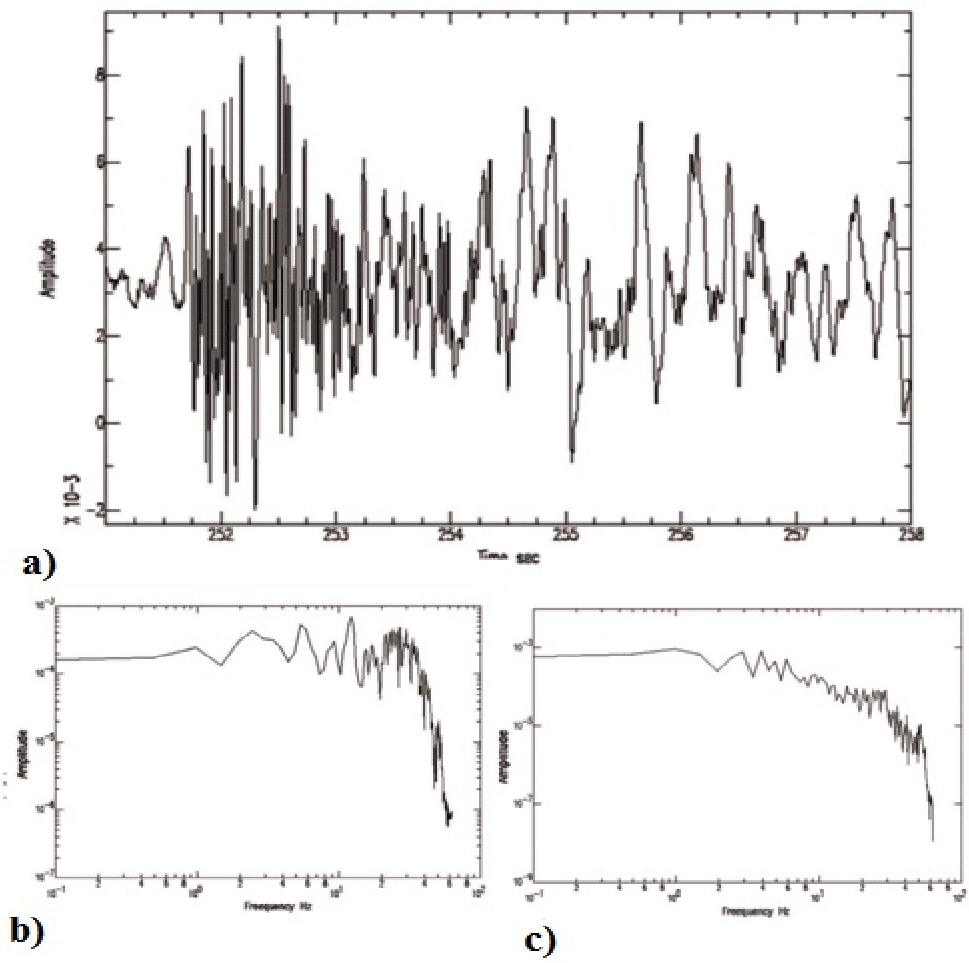

Figure (4.17) : (a) Waveform of an explosion vertical component with body waves at the beginning followed by surface waves – (b). Fourier Transform of the first part of the waveform (body waves) with corner frequency to ~30 Hz – (c) The same process is also applied for the next part of the waveform, where both body and surface waves that have been arrived, is characterised by a corner frequency in the interval 4 Hz - 30 Hz (after Kalogirou et al., 2014).

As for the earthquakes waveforms, some of the explosion waveforms are presented (Figure 4.18). More waveforms are given in Appendix VIII.

1. 120324_0911

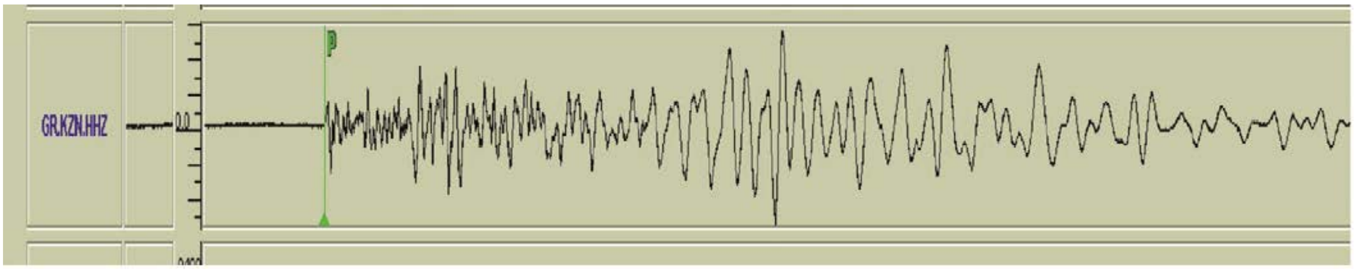

2. 110208_1221

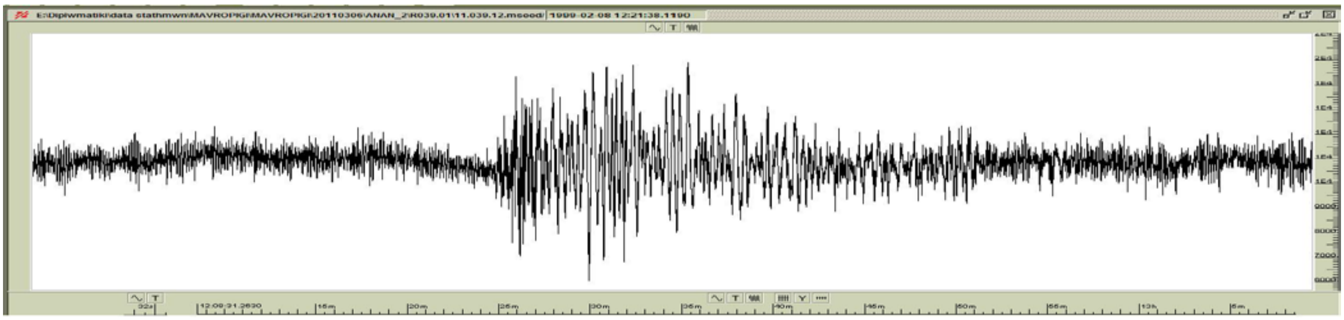

3. 110210_1229

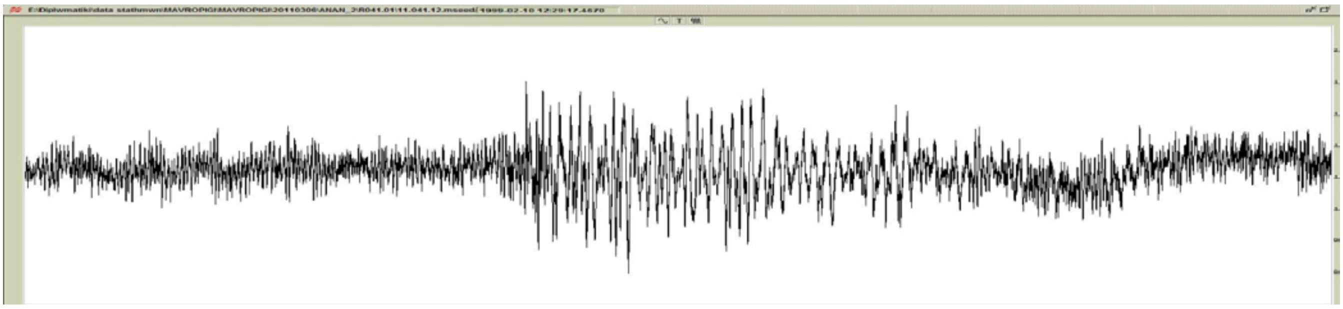

4. 110215_1225

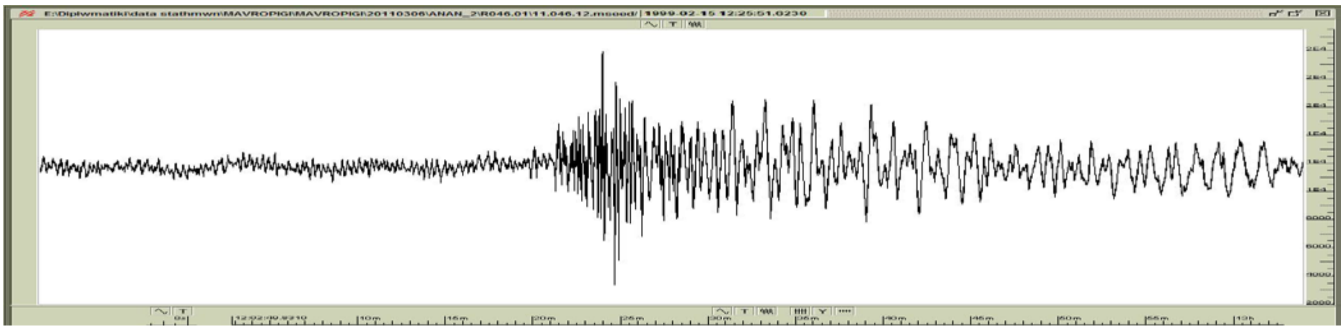

5. **110418_1215**

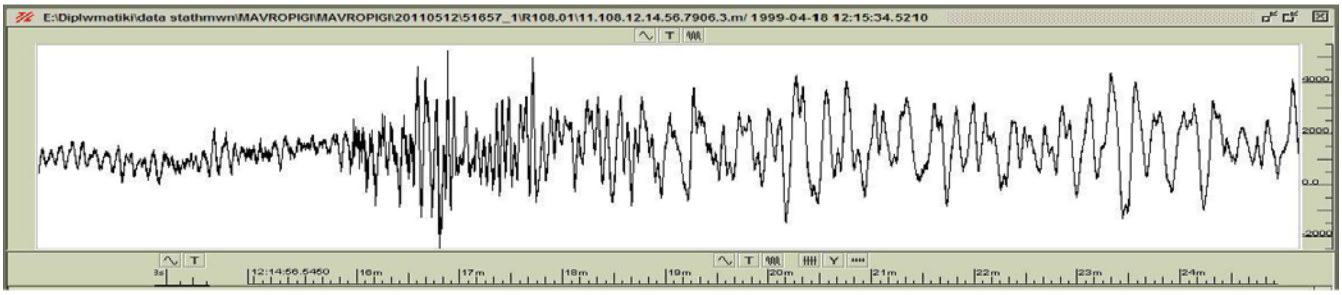

Figure (4.18): Explosion waveforms that recorded during the fourth months period from the installing local seismological network.

Figure (4.18 -1.) shows an explosion waveform recorded on March 24th 2012 from the permanent network (HUSN) of Kozanis' seismological station (KZN). The next three (3) charts are shown explosion waveforms as recorded by the local seismic network during the four (4) months of installation. Note that the signals are not filtered.

4.5 - EXPLOSION DATA PRODUSED FROM THE PPC

Evaluation of the recorded waveforms highlighted the differences between natural earthquakes and blasts.

Thus, in order to better classify the recorded waveforms, a full list of explosion that took place from 01/02/2011 to 11/05/2011 was provided by the PPC. 215 explosions happened during the time interval. Comparison between blast and seismic events showed that the majority of blasts were detonated inside the Kardia mine, while only few earthquakes of smaller magnitudes took place there. Blasts took place from 11 to 12 and from 13 to 14 (Local time zone) (Figure 4.19), described in the data provided by the PPC. Note that the time shift from winter to summer was taken into account.

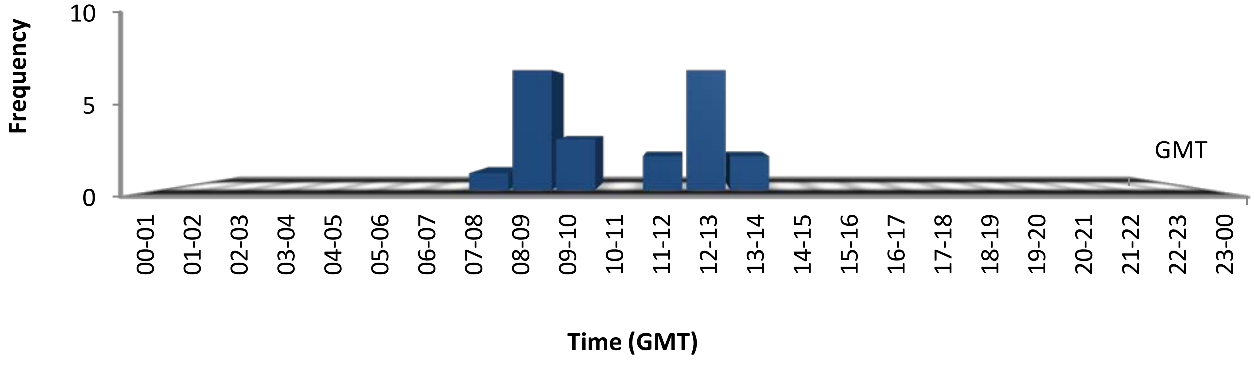

Figure (4.19) : The Time that have taken place the seismic events, whose epicenters occur in Kardia mine, using both the GMT zone.

Figure (Figure 4.20) depicts the depth distribution for the two models. The low velocities model gives better results in shallow depths (0 to 3 Km), especially between 0 and 1 Km.

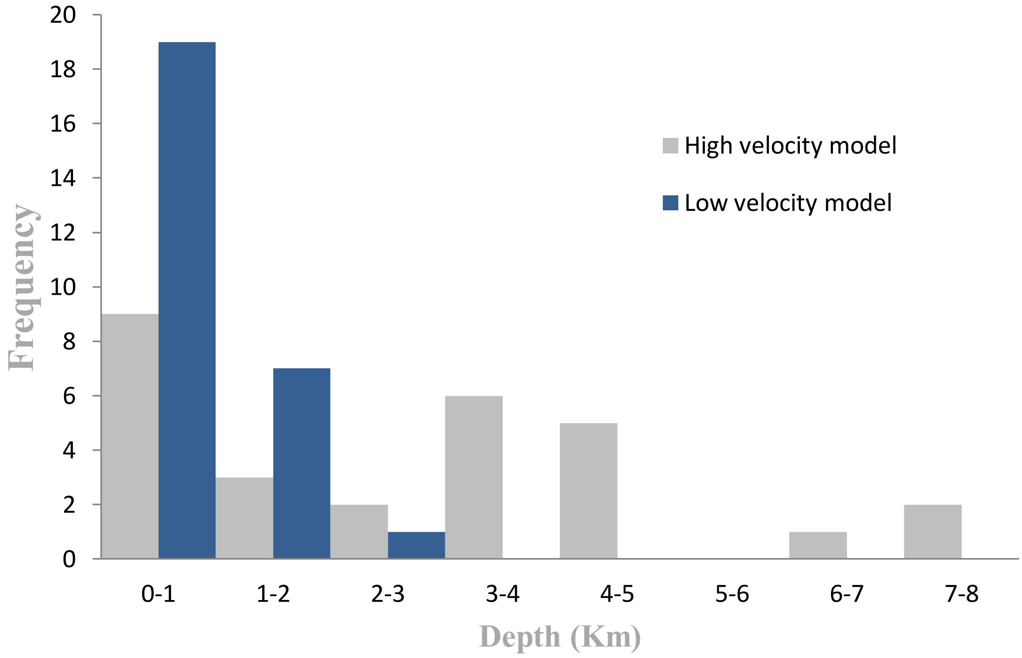

Figure (4.20) :Depth distribution for the two models.

CHAPTER 5 - GEOTECHNICAL INVESTIGATION OF THE AREA

The tectonic layout of the region and the fieldwork observations showed that the region is prone to landslides towards the direction of the mine. The geotechnical study of the area, carried out by the Aristotle University research team (School of Geology) and in particularly by the Assistant Professor V. Marinos, demonstrated this trend as well. Since July 20th 2011 the research team expressed fears for landslide in Mavropigi mine, based mainly on two factors:

- Field observations, showing the fault extension
- new surface ruptures developed in the surrounding area

A closer look to the under investigation area, revealed the need to study the existing induced displacements and ground failures around the PPC mining area in Ptolemais basin in Western Macedonia, Greece. Around these pits, occasional deformations occurred, which disappeared after a distance of 200-250 m. However, significant ruptures with both horizontal and vertical displacements were observed 600 m westwards from the open pit, where the village of Mavropigi is located (Kalogirou et al., 2014). By narrowing the area of research, a fault extending from North into the limestones and continuing until the village of Mavropigi, can be observed. Alongside this fault other ruptures occured as well, in the Neogene basin. Crack on the upper surface which continue to significant depths, are associated with the rupture, as shown by the geological survey carried out during the research. In this regard, a model to illustrate cracks were developed. The results are shown in Figure (5.1) with the ruptures marked in red and the fault in black. The limit of the lignite exploitation is depicted on the right hand side as reference.

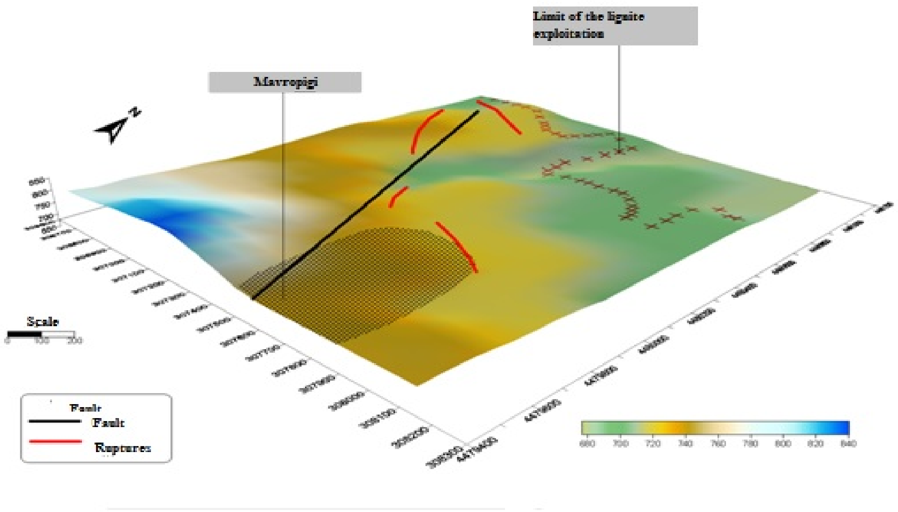

Figure (5.1) : Sharpen rupture imprinting in the narrow region of Mavropigi (after Tsapanos et al., 2011- compiled by V. Marinos).

Figure (5.2) illustrates the fault that “cut” the stony walkway. The pictures were taken in December 2010, when the rupture was firstly located. The lower right hand side picture shows the rupture that reaches the open pit of the mine, which is shown in the background.

Figure (5.2) : Pictures of the region northwards of Mavropigi that have been taken on December, 2010 .

As aforementioned the settlement of Mavropigi is built upon two main geological units (Figure 2.5):

1.**Rocks of substratum**. WSW part of the village is built on this formation. These consist of ash, recrystallized limestone of Mid.- Triassic – Lower- Liasio (T3-J5.k), which settled in the crystalline background of dimarmarygiac schist of (sch) Palaeozoic.
2.**Formations of Proastio**. Includes mainly polygenetic thick conglomerates of fluvial origin of Lower Villafragkion. On this formation the majority of Mavropigi village is constructed.

This geological formations are covered by small and generally thick alluvial and colluvial deposits, scree cones, side scree, soil mantle and anthropogenic layers. Details of the geology and tectonics of the area are given in chapter 2.1.3-Geology of the examined area.

The contact between those two main geological units is tectonic. As depicted on the map (Figure2.5), a NNW-SSE fault separates them. The fault can be characterized as normal, with an ENE tilt and belongs to the older generation of faults affecting the basin of Ptolemais. This is one of the faults that formed the original basin of Ptolemais and caused the creation of the lake of Vegoritis and the deposition of lignite marls.

Alteration of the initial field stress caused phenomena such as excessive stress relieve, ground rupture and large displacements. The stress field changed, after the excavation, the geological characteristics of the site. More specifically, the groundwater and the new mechanical properties formed discrete geological units. These units involve the Quaternary deposits, the weathered and sound marl, the bedding and the fault zones (Figure 5.3). Both in situ and research studies prove the above hypothesis.

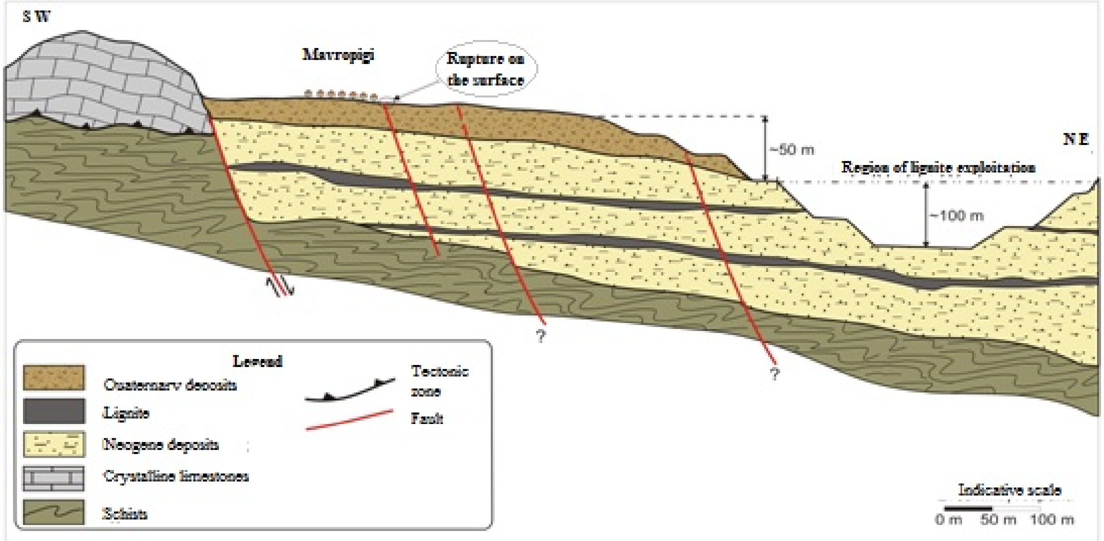

Figure (5.3) : Specified geological intersection from Mavropigi to the extraction site (after Tsapanos et al., 2011-compiled by V. Marinos).

The Neogene marly deposits lie on a bedrock of schists and limestones. A thin cover of recent Quaternary deposits of reddish clays also exists. The sliding phenomena, within the marl formation, concern both the weathered and the non-weathered zone. Bedding planes with a sub-horizontal geometry towards the main basin and the open pit are also present. The faults in the area have a NNW-SSE and NE-SW direction. These faults, parallel to the excavation of the pit, have a substantial role to the overall stability of the area and the mechanism of failure due to their mechanical characteristics. The exact location of these faults was retrieved through a geophysical survey (Kalogirou et al., 2014).

Regarding the hydrogeogical conditions, groundwater is within limestones, while some confined groundwater can be found in the marly deposits, around 30 m depth. Groundwater flow is towards the open pit, while the water table is lowered after every excavation step. The groundwater level of the ground surface varies from 28,48 m (drilling MA2) to 111,67 m (drilling MA10). These drillings can be found in the map of Figure (5.4) (Tsapanos et al., 2011).

Geotechnical analysis of the horizontal movement of the soil upstream of the excavation, towards the village of Mavropigi, was done by means of simulation. Excavation analysis is done in four (4) stages. A groundwater and an aquifer, either a piezometric or a constantly humbled (method abasement of the water) surface and the depth of 80m within the Neogene deposits, was assumed after each stage of excavation (the excavation starts always from the bottom).

Nevertheless, the effect of the aquifer seems to be cumulative rather than provocative.

In order to prove the trend of the landslides to extend towards the mine, Prof. V. Marinos, considered a variety of factors. For example, the excavation depth was assumed to be 160 m, the dip of excavation cuts 45^0-70^0 angle, the dip of natural ground (towards the village) $4,5^0$, the friction angle for Quaternary deposits $\varphi = 20^0$, 33^0 for Neogenic deposits, 34^0 for limestones, while the fault zone friction angle is $\varphi = 18^0$.

Two different profiles (A-A' and B-B'), depending on the distance between the excavation from Mavropigi and the ruptures, were analysed. These profiles are clearly in Figure (5.4).

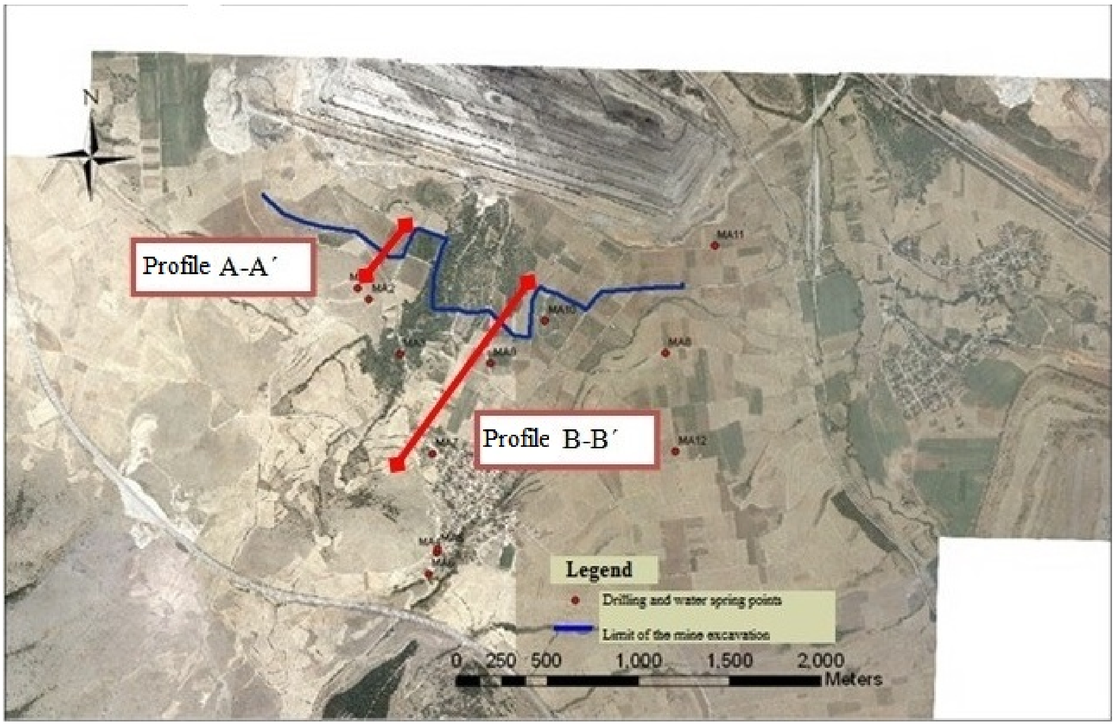

Figure (5.4) : Positions of the profiles A-A' and B-B'. Blue line indicates the bounds of the open pit of the mine, red dots indicate drillings. (after Tsapanos et al., 2011- compiled by V. Marinos).

The first A-A’ profile refers to the Northward area of Mavropigi. The excavation is in a short distance (approximately 100 m from the open pit) from the two major ruptures and near the site, where the phenomenon of ruptures started.

The second analysis concerns the B-B’ profile. The excavation is located approximately 600m from Mavropigi and the observed rupture while extends up to the village of Mavropigi.

Both profiles present surface cracks due to the mining activities, as suggested by the research team.

Profile A-A’

This profile refers to the Northern portion of the study area where the excavation limit is very close to fault zones. The A-A’ profile has the following characteristics:

• Left (West) limit of rigid rock (limestone)

• Existence of a fault within the limestones at 1000m depth

• Existence of rupture that contacts the limestones with Neogene deposits within 300m depth

• Aquifer within the Neogene formations at 80m depth

Analysis of this profile resulted in (Figure 5.5) and is summarized below.

• During the gradual excavation of lignite, horizontal displacements up to 300m away from the excavation were formed

• These shifts increase considerably after the fault zone. This displacement in the range of 10cm and increases towards the boundary of the mine excavation. The existence of the groundwater increases slightly that moving (from 10cm to 12cm).

• Development of major tensile ruptures on the surface in the position of the fault (Figures 5.1 and 5.4).

• This area, considering the correlation between excavations and fault formations, was the point where the first ruptures formed.

• The analysis has not revealed any excavation slopes failure, as actually observed, and the safety factor's value was calculated 1.25.

• Should be noted that these results do not show dramatic change without considering the fault zones. In contrast, movements increased slightly, when the aquifer effects added to the analysis (Tsapanos et al., 2011).

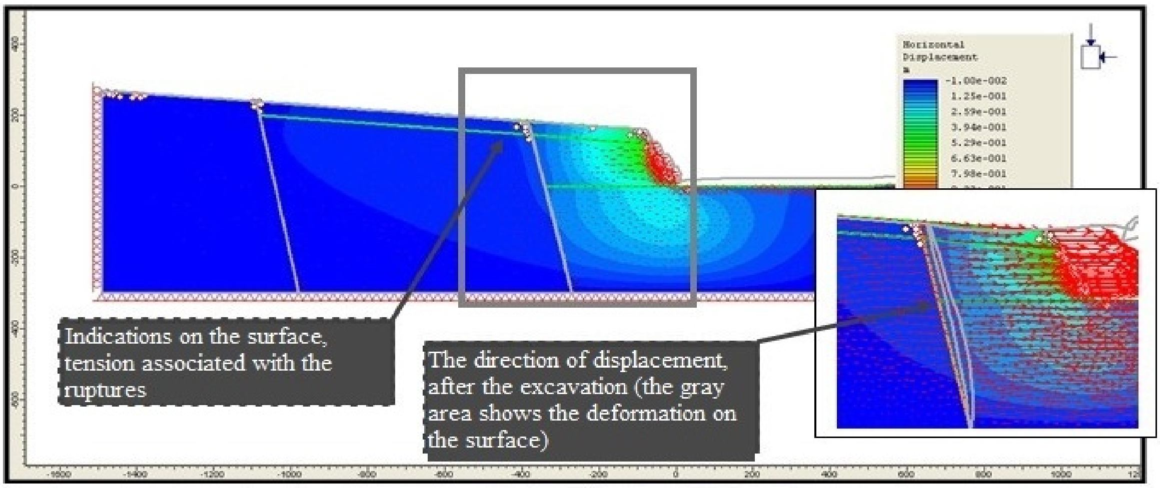

Figure (5.5) : Results of finite data analysis, profile A-A' (after Tsapanos et al., 2011-compiled by V. Marinos).

<u>Profile B-B'</u>

This profile refers to the central part of the study area, where the limit of the excavation is directly related to Mavropigi.

The B – B' profile has the following characteristics:

• Left (West) limit of rigid rock (limestone)

• Existence of ruptures brings together the limestones with the Neogene deposits at 1000m

• Existence of a fault within the Neogene deposits within 600m

• Aquifer occur in Neogene formations at 80m depth.

This analysis revealed the following conclusions (Figure 5.6):

• During the gradual excavation of lignite resulting horizontal displacements up to 600m away from the excavation. These shifts clearly therefore reach the village because of the gradual excavation.

• These displacements are considerably increased after the fault zone as shown by the surfaces displacement in Figure (5.5). This displacement is of the range of 10-15cm at this point.

• Development of shear ruptures in the region, after the rupture to the excavation indicates compression in this region.

• The analysis has not shown excavation slopes failure, as actually observed, and the calculated safety factor of 1.15.

• It should be noted that these results do not show dramatic change without considering the fault zones. In contrast, movements increased slightly, when is added to the analysis the aquifer, as well.

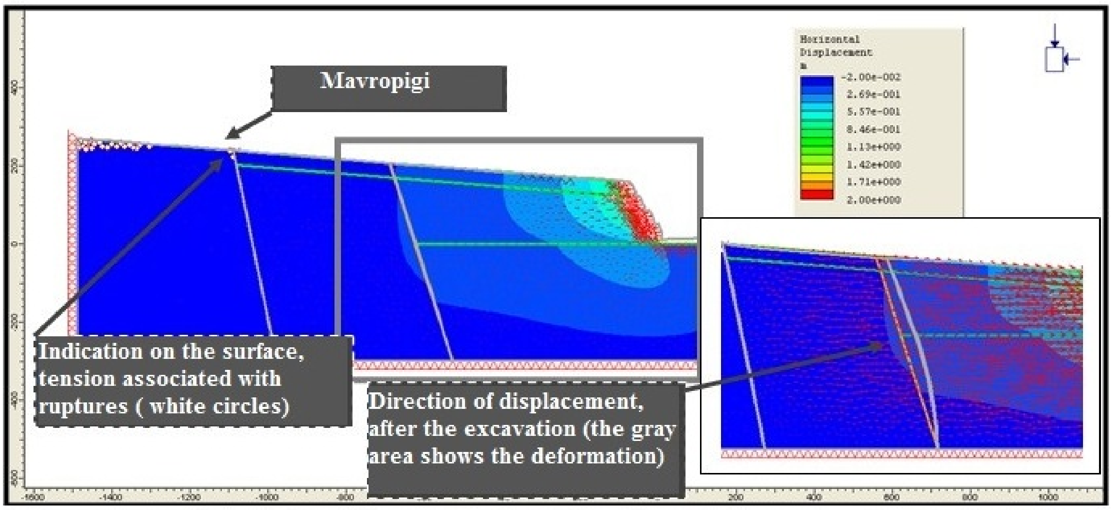

Figure (5.6) : Results of finite data analysis, profile B-B' (after Tsapanos et al., 2011-compiled by V. Marinos).

Summarizing, the results from the analyses showed that the displacements and local slide failures are clearly connected with the exploitation of the open pit lignite mine (Figure 5.6). These displacements are not limited to the excavation surface (decades of m) but may exceed in distance the 600 m, where the village of Mavropigi is located.

This is an ongoing phenomenon. The displacement first started in 2010, few mm to 20 cm (around the fault zones), as is shown in Figure (5.2) but is constantly increasing. Nowadays has reached a few meters while its length is of several hundred meters. Note that pictures in Figure (5.7) were taken on May 2012.

Figure (5.7) : Pictures of the same region as in Figure (6.2), that have been taken on May 2012, almost two years after.

On October 28th 2011, a landslide inside the mine open pit occurred. Figure (5.8) shows this feature, as resulted from mine exploitation activities phenomenon.

Figure 5.8 : Pictures from landslide.

In this case, damages to the buildings lead to a relocation plan for the all village.

Figure 5.9 : Damages in house walls and house basis in Mavropigi residences.

Figure (5.9) shows extensively those damages.

DISCUSSION AND CONCLUSIONS

The present study investigates and analyses the induced displacements and slide failures around the open excavations of a PPC lignite mine in Ptolemais basin, near the village of Mavropigi (Northern Greece). Significant ruptures and displacements, horizontal and vertical as well, rather than deformations, were observed 600m Westward from the open pit, where the village of Mavropigi is located. These phenomena caused extended damages in a number of houses in the village hence the relocation of the village has been decided.

Geological, Seismological and geotechnical survey of the field indicated that the village of Mavropigi is located on a NW-SE trending normal fault, dipping towards NE, which is one of the neotectonic faults that shaped the Ptolemais basin (Kalogirou et al., 2014). This survey evidenced that:

- Even though, similar in strike, surface fissures and the existing neotectonic fault, is not directly associated. Excluding the last from any involvement in the fissure formation process (ground fissures appearance),
- The aforementioned ground fissures moved in a slightly different way, though it was considered their collective behavior. This assumption was based on their common origin.
- The seismicity of the examined region is low. Consequently, the ground fissures cannot be associated with seismicity.
- The earthquake magnitudes that occurred in the surrounding area are mostly weak, with an average depth of 9 km and epicenters close to Mavropigi.
- For the events' location process, there was used at first, a High velocities model which is based on the widely used Rigo et al. (1996) model.
- Afterwards, there was the need for giving emphasis on layers near the surface. These layers characterized by low velocities, as derived from the geophysical prospecting in the study area. Thus, used the low velocities model.
- This model seemed more convenient for the needs of the investigation, due to the shift of the epicenters that occurred on the map after model application.

- Careful inspection the records revealed that some recordings start with higher frequencies and after some seconds longer periods become dominant.
- Fast Fourier Transform application shows that corner frequency in the first part of these recordings attain a value of 30 Hz, while the next waveform part characterized by corner frequency values from 4 to 30 Hz.
- Carefully inspection on the records revealed that the observed events close to Mavropigi, are rather explosions, inside the Kardia mine, than earthquakes. The help of the PPC is considerable and based on the information provided, it was verified that these events are blasts, and they account for almost 1/3 of the total recorded events.
- Geotechnical analysis results showed a clear connection between the open pit excavations and the ground movements. These displacements are not limited close to the excavation surface (decades of m) but extend as far as 600 m, where the village is located.
- The underground water movement is towards the mine excavation.
- The results of the analysis show clearly the tension of the soil for movement after excavation. Consequence of that might be the landslides that happen until today (Figure 6.1).
- Displacements phenomenon is ongoing since the main displacement started on 2010 with few mm to 40 cm (around the fault zones) but has been constantly increasing and has recently reached few meters at the surface.
- The movements do not concern only the narrow area of excavation (tens of meters) but exceed 600m where found and the settlement of Mavropigi.
- These displacements increased significantly after fault zones in that area and can reach 10-15cm in these zones. These displacements are larger towards the limit of excavation.
- The surface ruptures resulting from significant compressions near the excavation area and tensions further behind that. These tensions are mostly occurred in fault surfaces.
- The rupture surfaces help this development of displacements but do not cause them.

Figure (6.1) : The 14th January of 2014 landslide in the mine open-pit.

The landslide that has taken place inside the mine on 14th January of 2014 is an evidence that this is an ongoing phenomenon (Figure 6.1).

ABSTRACT

During the July 2010 a ground fissure was observed in the field, near the village of Mavropigi, in its NW side. Various interpretations about the phenomenon were proposed by the local authorities. At the beginning of September 2010, another ground fissure close and almost parallel to the previous one and very close to the limits of the lignite exploitation by the Public Power Corporation (PPC), appeared. The lignite deposits are found in Neogene sediments, consisting of alternation of clayey and marly layers. The geotectonic survey indicated that the aforementioned fissures moved in a slightly different way, though it was considered that they both operated together based on the same causative.

In order to investigate if these tectonic phenomena are results of seismic activity in the region, five digital seismometers installed inside and around the village of Mavropigi. They were in operation for about five months. The obtained results compared with the records received by the national network of seismographs in order to inspect if the shocks are local or not. Afterwards, the ninety local events separated for further processing. Firstly, a map of seismicity with the epicenters of the ninety events produced. A first inspection in the map showed that almost all the events formed a group near the lignite mine which is in Southeast direction of Mavropigi.

The seismological investigation revealed that the seismicity of the region characterized as low. There were used two different velocity models for the epicenters' location, one characterized by high velocities and the second that characterized by low velocities. The second considered to be more accurate because of the lower error values. Using the low velocities model, constructed a map of the epicenters of the recorded seismic events and observed that most of the data form a group within Kardia mine, in the South-East of Mavropigi. Afterwards, an extensive observation in the waveforms of these seismic events found that have explosion characteristics rather than these of earthquakes.

It turned out that these seismic events are directly related to the mining activity (e.g. blasts) in the mines of P.P.C., which located in the region, South-East of Mavropigi.

ΠΕΡΙΛΗΨΗ

Στις αρχές Ιουλίου του 2010 παρουσιάσθηκε μία εδαφική διάρρηξη στη βορειοδυτική μεριά του Δ.Δ. Μαυροπηγής. Η δημοσιότητα που δόθηκε στο φαινόμενο από τους κατοίκους υποχρέωσε την τότε Νομαρχία Κοζάνης να αναθέσει στο ΙΓΜΕ την μελέτη του φαινομένου. Το πόρισμα του ΙΓΜΕ εξεδόθη στις 10/08/2010 που μεταξύ άλλων πρότεινε την παρακολούθηση του φαινομένου Στις 01/09/2010 παρατηρήθηκε και δεύτερη εδαφική διάρρηξη η οποία βρίσκονταν σε πολύ κοντινή απόσταση (και σχεδόν παράλληλη με την πρώτη) από το όριο του ορυχείου της Μαυροπηγής (100 m περίπου). Οι δύο γραμμές παραμόρφωσης συμπεριφέρονται με ελαφρώς διαφορετικό τρόπο, αλλά θεωρείται ότι λειτουργούν ταυτόχρονα και λόγω του ίδιου αιτίου.

Στα πλαίσια της διερεύνησης του φαινομένου και στη υπόθεση ότι υπάρχει σεισμικότητα στη περιοχή εγκαταστάθηκε και λειτούργησε ένα μικρο-δίκτυο από πέντε ψηφιακούς σεισμογράφους στην περιοχή γύρω και μέσα στη Μαυροπηγή. Το δίκτυο αυτό λειτούργησε για περίπου πέντε μήνες. Τα δεδομένα που πάρθηκαν από αυτό το μικρο-δίκτυο συγκρίθηκαν με τις καταγραφές του εθνικού δικτύου σεισμογράφων για να καταταγούν αυτοί οι σεισμοί αν ήταν τοπικοί ή όχι..

Από την σεισμολογική έρευνα προέκυψε ότι η σεισμικότητα της περιοχής χαρακτηρίζεται χαμηλή. Χρησιμοποιήθηκαν δύο διαφορετικά μοντέλα ταχυτήτων, το ένα χαρακτηρίζεται από υψηλές ταχύτητες, ενώ το δεύτερο χαρακτηρίζεται από χαμηλές ταχύτητες. Το δεύτερο μοντέλο θεωρήθηκε πιο ακριβές λόγω των χαμηλότερων σφαλμάτων. Χρησιμοποιώντας το δεύτερο μοντέλο, κατασκευάσθηκε ένας χάρτης με τα επίκεντρα των καταγραφέντων σεισμικών γεγονότων και παρατηρήθηκε ότι τα περισσότερα δεδομένα σχηματίζουν μία ομάδα μέσα στα ορυχεία της Καρδιάς, στα νοτιοανατολικά της Μαυροπηγής. Στη συνέχεια, έγινε εκτενής παρατήρηση στις κυματομορφές αυτών των σεισμικών γεγονότων και βρέθηκε ότι αυτές έχουν χαρακτηριστικά εκρήξεων.

Αποδείχθηκε ότι τα σεισμικά αυτά γεγονότα έχουν άμεση σχέση με τη μεταλλευτική δραστηριότητα στα ορυχεία της Δ.Ε.Η. που βρίσκονται στην περιοχή, Νοτιο-Ανατολικά της Μαυροπηγής.

REFERENCES

AGU, A.G.S. (2008). "Blogosphere."

Allen, C.R., Amand, P., Richter, C.F. and Nordquist, J.M. (1965). "Relation between seismicity and geological structure in the Southern California region." Bull. Seism. Soc. Am. **55**: 752-797.

Andropoulos, B. , Rozos, D. and Hadzinakos, I. (1991). "Subsidence phenomena in the industrial area of Thessaloniki, Greece, paper presented at Proceedings of the 4th International Symposium on Land Subsidence, Houston, TX, USA."

B.G.S, B.G.S. "How does BGS classify landslides?" Landslides at BGS, from https://www.bgs.ac.uk/landslides/how_does_BGS_classify_landslides.html.

Bayliss, T. and Burton, P.W. (2013). "Natural Hazards." Seismic hazard across Bulgaria and neighbouring areas: regional and site-specific maximum credible magnitudes and earthquake perceptibility(68): 271–319.

Bayrak, Y., Öztürk, S., Koravos, G.C., Leventakis, G.A. and Tsapanos, T.M. (2008). "Seismicity assessment for the different regions in and around Tyrkey based on instrumental data:Gumbel first asymptotic distribution and Gutenberg-Richter cumulative frequency law." NHESS(8): 1090-1022.

Burford, R.O. and Harsh, P.W. (1980). "Slip on the San Andreas fault in central California from alignement array surveys." Bulletin of the Seismological Society of America **70**: 1233-1261.

Caputo, R., Chatzipetros, A., Pavlides, S. and Sboras, S. (2012). "The Greek Database of Seismogenic Sources (GreDaSS): state-of-the-art for northern Greece." Ann. Geophys. **55** (5): 859-894.

Caputo, R. and Pavlides, S. (07/02/2014). "GreDaSS (Greek Database of Seismogenic Sources)." from http://gredass.unife.it/.

Cruden, D.M. and Varnes, D.J. (1996). Landslides and processes in Turner, A.K. and Schuster, R.L. Landslides : Investigations and mitigation Washington D.C., Transportation Research Board Special Report 36-75.

Dahy, S.A. and Abdrabou, G.E. (2012). "Spectral Studies of Quarry Blasts and Earthquakes in Eastern Cairo, Egypt." Research Journal of Earth Sciences **4**(2): 56-62.

Esposito, E., Porfido, S., Simonelli, A., Mastrolorenzo, G. and Iaccarino, G. (2000). "Landslides and other surface effects induced by the 1997." Engineering Geology **58**: 353-376.

Galanopoulos, A.G. and Delibasis, K. (1972). Map of maximum observed intensities in Greece (period 1800-1970). Athens.

Google (2010). Google Earth, (Computer software).

Goulty, N.R. and Gilman, R. (1978). "Repeated creep events on the SanAndreas fault near Parkfield, California, recorded by a strainmeter array." Journal oh Geophysical Research **83**: 5415-5419.

Gutenberg, B. and Richter, C.F. (1944). "Frequency of earthquakes in California. ." Bull. Seism. Soc. Am. **34**: 185-188.

Harp, E.L. and Jibson, R.W. (1996). "Landslides triggered by the 1994, Northridge, California earthquake." Bulletin of the Seismological Society of America **86**(1B): S319–S332

Harp, E.L., Jibson, R.W., Kayen, R.E., Keefer, D.K., Sherrod, B.L., Carver, G.A., D., C.B., Moss, R.E.S. and Sitar, N. (2003). "Landslides and liquefaction triggered by the M7_9 Denali fault earthquake of 3 november 2002." GSA TODAY(August).

Hatzfeld, D., Kementzetzidou, D., Karakostas, V., Ziazia, M., Nothard, S., Deschamps, A., Karakaisis, G., Papadimitriou, P., Scordilis, M., Smith, R., Voulgaris, N., Kiratzi, S., Makropoulos, K., Bouin, M.-P. and Bernard, P. (1996). " The Galaxidi earthquake of November 18, 1992 :A possible asperity within the normal fault system of the Gulf of Corinth (Greece). ." Bull. Seismol.Soc. Am. **86**: 1987-1991.

Hatzidimitriou, P.M. , Karakaisis, G.F. and Papazachos, B.C. (1994). Seismicity of the Aegean sea and surrounding area. Proc. XXIVGen. Ass. Eur. Seism. Comm, Athens

Hatzidimitriou, P.M., Papadimitriou, E.E., Mountrakis, D.M. and Papazachos, B.C. (1985). "The seismic parameter b of the frequency-magnitude relation and its association with the geological zones in the area of Greece." Tectonophysics **120**: 141-151.

Highland, L.M. and Bobrowsky, P. (2008). The Landslide Handbook— A Guide to Understanding Landslides. Reston, Virginia, U.S. Geological Survey.

Holzer, T.L. (1979). "Elastic expansion of the lithospere caused by groundwater depletion." Journal oh Geophysical Research **84**(B9): 4689-4698.

Holzer, T.L. (1984a). "Ground failure induced by groundwater withdrawal from unconsolidated sediments." Geological Society of American.

Holzer, T.L. (1984b). "Man-induced land subsidence." Geological Society of American, Boulder, CO.

Holzer, T.L. (1986). "Ground failure caused by groundwater withdrawal from unconsolidated sediments." United States, IAHS Publication **151**.

Holzer, T.L. and Clark, M.M. (1993). "Sand boils without earthquakes." Geology **21**(10): 873-876.

Holzer, T.L. and Gabrysch, R.K. (1987). "Effect of water- level recoveries on fault creep." Ground water, Houston, Texas (USA) **25**(4): 392-397.

Holzer, T.L. and Pampeyan, E.H. (1981). "Earth fissures and localized differential subsidence." Water Resources Research **17**(1): 223-227.

Hungr, O. , Leroueil, S. and Picarelli, L. (2014). "The Varnes classification of landslide types, an update." Landslides **11**(2): 167–194.

IGME. " Institute of Geology & Mineral Exploration." from http://portal.igme.gr/portal/page?_pageid=33,56803&_dad=portal&_schema=PORTAL.

Kalogirou, E., Tsapanos, T., Karakostas, V., Marinos, V. and Chatzipetros, A. (2014). "Ground Fissures in the area of Mavropigi village (N. Greece): Seismotectonics or Mining activity?" ACTA Geophysica **62**(6): 1387-1412.

Karakostas, V. , Karagianni, E. and Paradisopoulou, P. (2012). "Space-time analysis, faulting and triggering of the 2010 earthquake doublet in western Corinth gulf" Nat.Haz. **63**(2): 1181-1202.

Karakostas, V. , Papadimitriou, E. and Gospodinov, D. (2014). "Modeling the 2013 North Aegean (Greece) seismic sequence: geometrical and frictional constraints, and aftershock probabilities, ." Geophys. J. Int. .

Keefer, D.K. (1984). "Landslides caused by earthquakes." Geological Society of American Bulletin **95**: 406-421.

King, H. (2006). "Landslide Triggering Mechanisms." From http://www.geologyeducation.com/blackboard/lan/triggers.htm.

Klein, F.W. (2002). User's guide to HYPOINVERSE-2000, a FORTRAN program to solve for Earthquake Locations and Magnitudes U. S. Geol. Surv. **:** Open-file Rept., 02-171, .

Kovach, R.L., Nur, A., Wesson, R.L. and Robinson, R. (1975). "Water-level fructuations and earthquakes on the San Andreas zone." Geology **3**: 437-440.

Lekkas, E. (1999, 2014). from http://www.elekkas.gr/menu11h/sc-photos/g1999/chi-chi99.html.

Makropoulos, K.C. and Burton, P.W. (1984). "Greek tectonics and seismicity." Tectonophysics(106): 275–304.

Manakou, M.V. and Tsapanos, T.M. (2000). "Seismicity and seismic hazard parameters evaluation in the island of Crete and the surrounding area inferred from mixed data files." Tectonophysics **321**: 157-178.

Mountrakis, D. (1982). "Emplacement of the Kastoria ophiolite on the western edge of the Internal Hellenides." Ofioliti **7**(N. 213): 397-406.

Mountrakis, D. (1984). " Structural evolution of the Pelagonian zone in Northwestern Macedonia." Journal of the Geological Society of London **17**(581-590).

Mountrakis, D. (1988). A concise tectonic evolution of the broader Hellenic region.

Mountrakis, D. (2005). Tertiary and quaternary tectonics in Aegean area. Developments in Volcanology. Vougioukalakis, Michael Fytikas and Georges E. **7:** 1-10.

Muir-Wood, R. and King, G.C.P. (1993). "Hydrological signatures of earthquake strain." Journal oh Geophysical Research **98**(B12).

Öztürk, S., Bayrak, Y., Cinar, H., Koravos, G.C. and Tsapanos, T.M. (2008). "A quantitative of earthquake hazard parameters computed from Gumbel I method for different regions in and around Turkey. ." Nat. Hazards(47): 471-495.

Panagiotopoulos, D. and Papazachos, B. (1985). "Travel times of Pn -waves in the Aegean and surrounding area." Geophys. J. R. astr. SOC. **80**: 165-176.

Papazachos, B. and Papazachou, C. (1997). The earthquakes of Greece. Thessaloniki, Ziti.

Papazachos, B.C. (1990). "Seismicity of the Aegean and the surrounding area." Tectonophysics(178): 287–308.

Papazachos, B.C., Papadimitriou, E.E., Kiratzi, A.A., Papazachos, C.B. and Louvari, E.K. (1998). "Fault plane solutions in the Aegean sea and the surrounding area and their tectonic implications " Bolletino di Geofisica Teorica ed Applicata **39**(199-218).

Pavlides, S. (1985). Neotectonic evolution of Florina- Vegoritis-Ptolemais basin. , Aristotle University of Thessaloniki. **Phd**.

Pavlides, S. (2007). Geo-Research work for the investigation of surface fissures in the municipal district of Peraia, Thessaloniki. Final Report of Geological Research.

Pavlides, S. and Caputo, R. (2004). "Magnitude versus faults' surface parameters: quantitative relationships from the Aegean Region." Tectonophysics **380**: 159 – 188.

Pavlides, S., Caputo, R., Sboras, S., Chatzipetros, A., Papathanasiou, G. and Valkaniotis, S. (2010). "The Greek Catalogue of Active Faults and Database of Seismogenic Sources." Bull. Geol. Soc. Greece **43** (1): 486-494.

Pavlides, S. and Mountrakis, D. (1987). "Extensional tectonics of northwestern Macedonia, Greece, since the late Miocene." Journal of Structural Geology **9**(4): 385-392.

Pavlides, S. and Simeakis, K. (1988). "Neotectonics and active tectonics ίη low seismicity areas of Greece: Vegoritis (NW Macedonia) and Melos isl complex (Cyclades)." Annales Gιologiques Des Pays Hellιniques **XXXIII**: 161-176.

Pavlides, S., Zouros, N.C., Chatzipetros, A.A., Kostopoulos, D.S. and Mountrakis, D.M. (1995). "The 13 May 1995 western Macedonia, Greece (Kozani-Grevena) earthquake, preliminary results." Terra Nova **7**: 544-549.

Reasenberg, P. and Oppenheimer, D.H. (1985). FPFIT, FPPLOT and FPPAGE. Fortran computer programs for calculating and displaying earthquake fault-plane solutions. Open-File Report, 85-739, U.S. Geological Survey**:** 109 p. ;128 cm.

Richter, C.F. (1958). Elementary Seismology. San Francisco, W. H. Freeman and Co.

Rigo, A., Lyon-Caen, H., Armijo, R., Deschamps, A., Hatzfeld, D., Makropoulos, K., Papadimitriou, P. and Kassaras, I. (1996). "A microseismic study in the western part of the Gulf of Corinth (Greece): Implications for large-scale normal faulting mechanisms." Geophys. J. Int. **126**: 663-688.

Sassa, K. (1999). Landslides of the world, Kyoto University press.

Scholz, C.H. (1968). "The frequency-magnitude relation of microfracturing in rock and its relation to earthquakes." Bull. Seism. Soc. Am. **58**: 399-415.

Shearer, P.M. (2009). Introduction to Seismology, CAMBRIDGE UNIVERSITY PRESS.

Soulios, G. (2009). Project study of the phenomenon of surface ground fissures in the region of Anargyroi village of the Municipality of Florina

Steenbrink, J., Van Vugt, N., Kloosterboer-van Hoeve, M.L. and Hilgen, F.J. (2000). "Refinement of the Messinian APTS from sedimentary cycle patterns in the lacustrine Lava section (Servia Basin, NW Greece)." Earth and Planetary Science Letters **181**: 161-173.

Stiros, S.C. (2001). "Subsidence of the Thessaloniki (northern Greece) coastal plain, 1960-1999." Engineering Geology **61**(4): 243-256.

Tsapanos, T., Pavlides, S., Voudouris, K., Panagiotopoulos, D., Karakostas, V., Tsourlos, P., Vargemezis, G., Marinos, V., Chatzopetros, A., Stabolidis, A., Fikos, I., Mattas, C., Lialiampis, I., Dimoudi, E., Koravos, G., Delogkos, E., Michailidou, A., Karamanos, C. and Olasoglou, E. (2011). Final report of the research of surface fissures phenomenon in the broader area of Mavropigi, municipality of Ptolemaida. Thessaloniki, Aristotle University of Thessaloniki.

Tsapanos, T.M. (1990). "b-Values of two tectonic parts in the circum-Pacific belt." Pure Appl.Geophys. **134**: 229-242.

Tsapanos, T.M. (2001a). "Earthquake hazard parameters estimated in Crete island and the adjacent area." Pageoph(158): 1691–1718.

Tsapanos, T.M. (2001b). "Evaluation of the seismic hazard parameters for selected regions of the world: the maximum regional magnitude." Ann. di Geofisica(44): 69-79.

Tsapanos, T.M. (2006). Geological and Seismological research of the fault in Lagyna Village of Municipality of Lagkadas.

Tsapanos, T.M. and Burton, P.W. (1991). "Seismic hazard evaluation for specific seismic regions of the world." Tectonophysics(194): 153-169.

Tsapanos, T.M. and Papazachos, B.C. (1998). "Geographical and vertical variation of the Earth's seismicity. ." Journ. of Seismology(2): 183-192.

Tsapanos, T.M. (2005). "Seismicity and seismic hazard of the Western Macedonia, Greece " Bull. Geol. Soc. Gr. **XXXVII**: 232-244.

USGS. (March 06, 2013). "Historic earthquakes." from http://earthquake.usgs.gov/earthquakes/world/historical.php/.

Varnes, D.J. (1978). Slope movement types and processes in Schuster, R.L. and Krizek, R.J. Washington D.C., National Research council.

Walter, W.R., E., M., Pasyanos, M.E., D.B., H., Gok, R. and S.R., F. (2006). EMPIRICAL OBSERVATIONS OF EARTHQUAKE-EXPLOSION DISCRIMINATION USING P/S RATIOS AND IMPLICATIONS FOR THE SOURCES OF EXPLOSION S-WAVES. 29th Monitoring Research Review: Ground-Based Nuclear Explosion Monitoring Technologies, Lawrence Livermore National Laboratory.

Wang, J.H. (1988). "b- Values of shallow earthquakes in Taiwan " Bull. Seism. Soc. Am. **78**: 1243-1254.

Wells, L.D. and Coppersmith, J.K. (1994). "New Empirical Relationships among Magnitude, Rupture Length, Rupture Width, Rupture Area, and Surface Displacement " Bulletin of the Seismological Society of America **84**(4): 974-1002.

Wessel, P. and Smith, H.F., W. (2006). The Generic Mapping Tools, A Map-Making Tutorial, School of Ocean and Earth Science and Technology University of Hawaii at Manoa and Laboratory for Satellite Altimetry NOAA/NESDIS/NODC**:** Generic Mapping Tools Graphics.

Yamada, M. , Wang, G. and Mukai, K. (2013). The Classification and Features of Earthquake-Induced Landslides in the World. Earthquake-Induced Landslides. Ugai, K., Yagi, H., Wakai, A. Berlin, Heidelberg, Springer

Yin, Y. , Wang, F. and Sun, P. (2008). "Landslide Hazards triggered by the 12 May 2008 Wenchuan Earthquake, Sichuan, China." Landslides:the Journal of International onsortium on Landslides.

Zouros, N. , Pavlides, S.B. and Chatzipetros, A. (1994). "Recent movement on the Larissa plain neotectonic faults (Thessaly, c. Greece). Water level fluctuationor tectonic creep? paper presented at Proceedings of the XXIV General Assembly of the European Seismological Commission."

Appendix I : Catalogue of the recorded events in Mavropigi for the period from 29/1/2011 to 11/5/11.

Date		Time	Lat	Lon									
2011	0129	31038.8	40.529	21.830	0.21	0	6	353	11.30	0.89	72.70	20.10	D
2011	0202	84458.8	40.432	21.757	0.15	0	6	356	02.50	0.69	24.60	00.50	D
2011	0203	43734.0	40.406	21.615	0.12	0	8	355	10.70	0.08	14.00	01.60	D
2011	0203	92659.5	40.389	21.517	0.11	0	8	358	19.10	0.08	14.00	01.20	D
2011	0203	93404.8	40.544	21.541	0.09	0	7	359	18.60	0.06	13.50	00.90	D
2011	0204	171313.5	40.590	21.841	0.14	0	7	357	17.90	0.09	14.60	01.60	D
2011	0205	30536.3	40.433	21.716	0.01	0	6	334	02.10	1.03	62.60	08.20	D
2011	0208	73958.7	40.432	21.715	0.01	0	6	336	02.20	1.31	84.70	11.20	D
2011	0208	122135.1	40.431	21.712	0.01	0	7	338	02.60	0.41	27.30	03.60	D
2011	0210	90659.2	40.425	21.666	0.08	0	7	351	05.90	0.04	12.90	01.10	D
2011	0210	122915.2	40.481	21.656	0.17	0	4	357	06.60	0.20	20.70	02.30	D
2011	0212	91115.0	40.444	21.725	0.01	0	6	288	00.80	0.36	04.50	00.50	D
2011	0212	122019.5	40.365	21.730	0.20	0	4	357	09.00	0.10	14.60	04.00	D
2011	0213	75121.9	40.436	21.718	0.01	0	6	330	01.80	1.11	57.60	07.60	D
2011	0213	90615.1	40.466	21.799	0.17	0	6	351	06.00	0.07	13.90	01.50	D
2011	0213	171307.6	40.434	21.717	0.01	0	8	332	02.00	1.02	50.50	06.70	D
2011	0214	90320.8	40.471	21.795	0.59	0	7	351	05.60	0.20	15.30	13.70	D
2011	0215	122549.1	40.423	21.723	0.05	0	7	344	02.70	0.10	02.90	00.20	D
2011	0215	183328.4	40.336	21.657	0.01	0	6	356	13.90	0.47	41.20	03.70	D
2011	0215	235122.1	40.433	21.715	0.01	0	6	334	02.10	1.18	70.70	09.30	D
2011	0216	120326.1	40.453	21.697	0.21	0	4	351	02.80	0.01	11.50	05.00	D
2011	0216	140238.7	40.451	21.718	0.26	0	6	338	01.00	0.07	12.50	05.40	D
2011	0218	124444.8	40.448	21.727	0.31	0	6	288	00.40	0.03	00.60	11.30	D
2011	0227	21501.4	40.478	21.720	0.01	0	4	354	03.10	0.79	19.10	03.50	D
2011	0306	122501.6	40.447	21.763	0.13	0	5	346	01.10	0.04	12.60	02.10	D
2011	0306	160821.9	40.542	21.653	0.06	0	6	359	11.60	0.05	13.20	01.20	D
2011	0311	162127.8	40.471	21.664	0.00	0	9	355	05.60	0.24	23.20	02.10	D
2011	0314	91115.1	40.444	21.566	0.04	0	6	359	13.60	0.10	14.80	01.30	D
2011	0315	123343.8	40.525	21.618	0.05	0	6	359	12.10	0.14	17.10	01.50	D

2011	0318	14115.2	40.454	21.639	0.20	0	8	355	07.30	1.21	95.40	26.40	D
2011	0318	172501.8	40.463	21.739	0.47	0	6	327	01.50	0.04	01.40	12.00	D
2011	0320	91530.8	40.489	21.769	0.01	0	8	337	04.80	0.36	28.30	02.50	D
2011	0321	122259.1	40.517	21.751	0.00	0	7	344	07.40	0.16	17.50	01.60	D
2011	0327	80420.8	40.483	21.727	0.00	0	5	338	03.60	0.20	20.60	01.80	D
2011	0327	80700.3	40.571	21.708	0.05	0	6	359	13.50	0.31	28.80	02.60	D
2011	0327	80958.7	40.470	21.811	0.00	0	8	352	05.80	0.19	20.30	01.80	D
2011	0402	80923.4	40.571	21.688	0.02	0	6	358	13.80	0.17	18.70	01.70	D
2011	0402	113010.1	40.433	21.721	0.01	0	8	324	01.80	1.25	44.00	05.80	D
2011	0407	73443.2	40.466	21.749	0.01	0	6	303	02.00	0.34	06.40	00.80	D
2011	0407	132522.9	40.441	21.722	0.01	0	6	312	01.10	0.53	13.40	01.70	D
2011	0408	130754.8	40.303	21.751	1.02	0	7	353	16.00	0.03	05.60	12.70	D
2011	0409	80114.4	40.432	21.714	0.01	0	7	322	02.30	0.23	02.50	00.20	D
2011	0410	81642.9	40.429	21.714	0.01	0	9	325	02.60	0.57	05.00	00.60	D
2011	0413	132200.7	40.504	21.787	0.00	0	10	344	07.00	0.40	34.10	03.00	D
2011	0414	81018.8	40.396	21.668	0.00	0	5	353	07.90	0.32	29.20	02.60	D
2011	0415	80439.9	40.428	21.664	0.00	0	7	349	05.90	0.29	26.70	02.40	D
2011	0415	143105.5	40.562	21.541	0.56	0	8	358	19.80	0.05	11.30	07.00	D
2011	0416	80753.4	40.499	21.782	0.01	0	10	343	06.30	0.40	33.50	03.00	D
2011	0416	112836.0	40.389	21.611	0.25	0	5	355	12.10	0.07	13.40	03.70	D
2011	0417	80811.7	40.498	21.776	0.01	0	10	341	06.00	0.35	29.10	02.60	D
2011	0417	110846.6	40.465	21.810	0.13	0	7	350	05.50	0.08	14.00	01.60	D
2011	0417	193413.2	40.503	21.730	0.02	0	9	340	05.60	0.05	12.00	01.10	D
2011	0418	121532.8	40.489	21.760	0.01	0	9	334	04.70	0.27	20.10	01.80	D
2011	0419	81629.7	40.424	21.685	0.00	0	8	342	04.70	0.13	15.50	01.40	D
2011	0419	82306.7	40.717	21.351	0.06	0	10	359	43.20	0.15	17.70	01.20	D
2011	0420	82958.8	40.494	21.768	0.01	0	9	339	05.40	0.31	25.90	02.30	D
2011	0420	113347.3	40.439	21.719	0.01	0	8	322	01.50	0.38	12.60	01.60	D
2011	0420	215523.9	40.499	21.792	0.00	0	6	353	07.20	0.06	13.50	01.20	D
2011	0421	30924.3	40.494	21.503	0.10	0	10	358	19.40	0.17	19.00	01.70	D
2011	0421	112009.4	40.492	21.730	0.01	0	8	335	04.30	0.15	15.00	01.30	D
2011	0422	155806.7	40.555	21.592	0.03	0	6	358	16.10	0.11	15.60	01.40	D
2011	0423	114155.5	40.485	21.763	0.01	0	10	333	04.30	0.29	20.80	01.80	D

2011	0424	122658.5	40.428	21.712	0.01	0	10	327	02.80	1.59	13.20	01.30	D
2011	0425	80522.9	40.534	21.810	0.02	0	5	350	10.80	0.04	12.90	01.10	D
2011	0425	84212.9	40.422	21.359	0.12	0	6	358	31.30	0.14	17.00	01.50	D
2011	0427	35430.0	40.488	21.713	0.20	0	7	352	04.00	0.10	14.90	01.70	D
2011	0427	80533.2	40.419	21.685	0.03	0	7	342	05.10	0.07	13.10	01.20	D
2011	0427	131521.1	40.475	21.765	0.01	0	7	330	03.30	0.14	13.90	01.20	D
2011	0428	81259.1	40.501	21.773	0.01	0	7	342	06.30	0.51	42.20	03.70	D
2011	0428	113559.3	40.308	21.721	0.16	0	5	358	15.40	0.10	14.80	01.70	D
2011	0430	111528.8	40.399	21.695	0.14	0	7	347	06.20	0.07	13.70	01.50	D
2011	0501	73633.3	40.490	21.728	0.01	0	4	341	04.30	0.41	35.40	03.20	D
2011	0501	81724.3	40.459	21.745	0.19	0	7	287	01.30	0.08	02.20	00.30	C
2011	0503	113055.4	40.455	21.754	0.01	0	5	304	00.90	0.23	08.30	01.20	D
2011	0503	132311.6	40.456	21.751	0.00	0	5	290	00.90	0.10	04.00	00.60	D
2011	0504	60632.6	40.472	21.562	0.13	0	8	358	14.40	0.08	14.00	01.60	D
2011	0504	233443.5	40.497	21.688	0.40	0	5	358	06.20	0.31	21.80	19.00	D
2011	0505	01333.7	40.500	21.791	0.18	0	5	355	07.30	0.18	19.20	02.20	D
2011	0505	101818.7	40.509	21.767	0.00	0	7	346	07.00	0.33	29.80	02.70	D
2011	0507	13544.7	40.570	21.427	0.12	0	7	359	28.90	0.09	14.30	01.30	D
2011	0507	15159.2	40.504	21.727	0.01	0	5	345	05.90	0.83	69.30	06.20	D
2011	0507	21136.9	40.581	21.463	0.10	0	8	358	26.80	0.09	14.50	01.30	D
2011	0507	34830.1	40.549	21.427	0.13	0	7	359	27.90	0.06	13.50	01.20	D
2011	0507	93144.7	40.479	21.764	0.00	0	6	336	03.70	0.18	17.10	01.50	D
2011	0574	152029.4	40.588	21.678	2.69	0	7	355	15.90	0.09	09.00	11.40	D
2011	0508	80739.9	40.514	21.742	0.38	0	4	345	07.00	0.02	09.40	08.40	D
2011	0510	04839.3	40.568	21.434	0.02	0	8	359	28.30	0.06	13.50	00.90	D
2011	0510	195850.3	40.428	21.700	0.39	0	4	342	03.50	0.16	13.50	14.30	D
2011	0511	120548.9	40.328	21.698	0.29	0	7	353	13.50	0.09	14.00	03.90	D

Appendix II : Earthquake catalogue of the stations of Aristotle University of Thessaloniki and the Institute of Geodynamics of National Observatory of Athens for the period from 29/01/2011 to 11/05/2011.

Date	Time	Lat	Lon				Date	Time	Lat	Lon			
20110129	130933.2	40.19	21.68	13	2.7	ath							
20110203	092659.8	40.482	21.404	5.3	2.4	the							
20110203	093405.1	40.494	21.412	8	2.6	the	20110203	093404.1	40.5	21.42	21	2.4	ath
20110204	034844.8	40.18	21.67	16	1.2	ath							
20110204	171313.5	40.484	21.402	12.2	2.5	the	20110204	171312.7	40.51	21.43	20	2.2	ath
20110205	144059.3	40.49	21.39	25	1.5	ath							
20110208	073953.5	40.172	21.638	10.8	2.3	the	20110208	073953.7	40.17	21.64	11	1.9	ath
20110208	122135.3	40.418	21.878	0	1.8	the	20110208	122134.3	40.44	21.87	0	1.7	ath
20110209	210647.3	40.17	21.67	13	1.1	ath							
20110212	122020.6	40.456	21.866	11.5	1.9	the							
20110212	142816.5	40.238	21.726	14.6	1.7	the	20110212	142816.8	40.21	21.7	6	1.7	ath
20110213	075118.4	40.24	21.72	10	1.6	ath							
20110213	171303.3	40.25	21.85	19	1.5	ath							
20110214	090321.	40.42	21.86	15	1.8	ath							
20110214	142848.3	40.33	21.83	15	1.3	ath							
20110215	122549.3	40.447	21.882	0	2	the							
20110215	183327.1	40.19	21.68	15	1.4	ath							

20110215	235116.6	40.18	21.68	16	1.3	ath							
20110218	214236.2	40.09	21.6	25	1.9	ath							
20110219	091419.4	40.45	21.67	21	1.7	ath							
20110220	045003.1	40.08	21.77	0	1.6	ath							
20110220	061413.1	40.069	21.776	2.1	2.3	the	20110220	061412.8	40.1	21.77	19	2	ath
20110220	122055.5	40.44	21.84	0	1.3	ath							
20110225	090523.2	40.34	21.86	27	1.7	ath							
20110301	090605	40.43	21.86	7	1.7	ath							
20110301	114226.5	40.367	21.955	18.9	1.6	the	20110301	114227.6	40.45	21.87	0	1.4	ath
20110302	122247.2	40.43	21.88	0	1.8	ath							
20110304	135301.7	40.31	21.75	7	1.3	ath							
20110305	053538.5	40.3	21.76	18	1.6	ath							
20110306	160821.3	40.58	21.6	17	1.3	ath							
20110307	090433	40.41	21.82	10	1.6	ath							
20110311	162128	40.567	21.622	10.7	2.1	the	20110311	162127.5	40.57	21.62	18	2.1	ath
20110315	123345.2	40.42	21.87	11	1.9	ath							
20110315	222640.7	40.24	21.84	4	1.3	ath							
20110319	090555.2	40.41	21.76	13	1.3	ath							
20110320	091530.9	40.41	21.86	13	2	ath							
20110321	122259.8	40.42	21.89	15	1.7	ath							

20110323	200200.1	40.17	21.68	9	1	ath							
20110403	031038	40.02	21.53	19	1.1	ath							
20110404	075819.2	40.112	21.38	0	2.2	the	20110404	075817.9	40.11	21.34	18	2.3	ath
20110404	151554.3	40.099	21.326	20.7	2.6	the	20110404	151554.1	40.09	21.35	18	2.4	ath
20110404	173541.5	40.04	21.5	11	2.1	ath							
20110405	091729.5	40.021	21.469	12.5	2	the	20110405	091728.7	40	21.44	19	1.9	ath
20110405	120817.1	40.43	21.86	26	1.7	ath							
20110406	030217	40.27	21.92	10	1	ath							
20110406	113441.8	40.26	21.88	9	1.4	ath							
20110408	130757	40.429	21.871	0	1.9	the							
20110409	035355.5	40.002	21.411	11.9	1.3	the							
20110410	081642.5	40.409	21.86	8.4	1.9	the							
20110412	081314.2	40.39	21.88	11	1.9	ath							
20110413	132201	40.38	21.92	15	2.1	ath							
20110415	080440.5	40.43	21.85	0	1.5	ath							
20110416	080754.4	40.444	21.843	1.7	1.8	the							
20110417	080812.2	40.439	21.854	10.4	1.8	the	20110417	080812	40.42	21.86	10	1.6	ath
20110420	001952.5	40.18	21.65	12	1	ath							
20110420	082959.5	40.393	21.874	8.2	1.9	the							
20110421	030923.9	40.176	21.684	13.7	1.5	the	20110421	030924	40.18	21.68	14	1.4	ath

20110421	112010	40.429	21.848	1.6	1.9	the							
20110421	233725.6	40.08	21.59	14	1.1	ath							
20110422	155805.2	40.35	21.44	23	1.6	ath							
20110424	122651.8	40.064	21.664	0	2.9	the	20110424	122651.2	40.07	21.66	18	2.7	ath
20110425	080524.3	40.395	21.866	11.4	1.7	the	20110425	080524.4	40.41	21.89	10	1.7	ath
20110427	131054.4	40.18	21.65	11	1.1	ath							
20110428	081300.4	40.4	21.8	8	1.4	ath							
20110429	064208.7	40.601	21.455	16.5	2.1	the	20110429	064208.2	40.6	21.44	22	1.9	ath
20110430	080324.3	40.42	21.9	0	1.6	ath							
20110430	111529.1	40.42	21.9	0	1.4	ath							
20110501	073633	40.42	21.88	1	1.6	ath							
20110501	081722.6	40.44	21.89	0	1.5	ath							
20110503	132310.8	40.42	21.901	1.5	1.7	the							
20110503	150740.3	40.162	21.663	2.5	1.8	the	20110503	150740.1	40.16	21.66	11	1.7	ath
20110504	060632.6	40.598	21.619	0.5	2.2	the	20110504	060631.6	40.6	21.6	25	1.9	ath
20110507	013544.9	40.371	21.338	13.6	4	the	20110507	013543.5	40.36	21.32	26	3.9	ath
20110507	015154.5	40.367	21.317	13.3	1.9	the	20110507	015153.3	40.38	21.31	25	1.6	ath
20110507	021137	40.364	21.338	10.7	2.5	the	20110507	021135.8	40.38	21.35	25	2.4	ath
20110507	034830.3	40.38	21.337	9.6	3.3	the	20110507	034829.2	40.37	21.31	27	3.1	ath
20110507	063928.7	40.361	21.306	18.9	1.8	the							

20110507	093145	40.424	21.895	8.9	2.3	the							
20110507	152029	40.23	21.84	3	1.4	ath							
20110508	080739	40.39	21.88	19	1.7	ath							
20110510	004838.4	40.082	21.535	12.4	2.4	the	20110510	004838.3	40.08	21.56	16	2	ath
20110510	133958.1	40.14	21.71	16	1.5	ath							
20110511	120551.2	40.414	21.871	0	1.9	the							

Appendix III : Epicenters derived from the *High velocities model*.

Date	Time (HHMM SS.FF)	Lat	Lon											
110129	0310 39.43	40.551	21.639	06.96	0	05	360	11.60	0.79	67.10	55.1	D	-	0
110202	0844 58.76	40.380	21.670	02.24	0	06	360	07.30	0.67	57.20	49.1	D	-	0
110203	0437 33.83	40.603	21.631	07.23	0	07	359	17.10	0.05	12.10	13.1	D	-	0
110203	0926 59.34	40.492	21.366	09.31	0	21	109	26.40	0.37	00.80	2.9	C		0
110203	0934 04.37	40.507	21.363	18.70	0	23	114	27.10	0.37	00.70	2.3	C		0
110204	1713 13.13	40.493	21.370	05.93	0	20	108	26.10	0.27	00.60	2.2	C	#	0
110205	0305 32.19	40.269	21.811	18.20	0	10	292	05.40	0.05	01.50	0.6	C		0
110208	0739 53.21	40.167	21.642	05.93	0	13	180	19.00	0.14	00.60	0.9	B		0
110208	1221 33.56	40.450	21.862	00.02	0	18	087	15.90	0.29	00.80	1.2	C	#	0
110210	0906 58.91	40.443	21.839	00.02	0	09	286	14.00	0.10	01.60	1.3	C	#	0
110210	1229 15.40	40.430	21.818	00.00	0	05	276	12.40	0.02	02.50	1.2	D	#	0
110212	0911 13.30	40.362	21.611	07.04	0	06	273	10.70	0.06	06.90	10.4	D	-	0
110212	1220 19.52	40.439	21.851	01.83	0	18	083	15.10	0.36	00.80	1.1	C		0
110213	0751 17.38	40.217	21.753	12.38	0	09	260	10.00	0.05	01.50	2.2	C		0
110213	0906 05.23	40.739	21.408	06.68	0	06	345	69.80	0.35	16.20	23.5	D	-	0
110213	1713 02.82	40.268	21.877	20.40	0	10	299	10.00	0.00	00.07	1.6	C		0
110214	0903 20.68	40.434	21.806	00.01	0	11	235	11.30	0.20	01.00	0.8	C	#	0
110215	1225 48.05	40.454	21.862	00.03	0	19	086	15.90	0.55	01.20	2.4	D	#	0
110215	1833 27.10	40.188	21.625	05.20	0	11	229	18.00	0.11	03.10	2.7	D		0
110215	2351 16.95	40.179	21.641	09.58	0	10	235	17.90	0.07	01.30	3.8	C	#	0
110216	1203 26.82	40.485	21.676	01.21	0	05	360	38.00	7.00	13.90	10.4	D	-	0
110216	1402 38.38	40.443	21.700	05.98	0	06	228	23.30	6.00	10.10	3.5	D	-	0
110217	1434 14.48	40.408	21.672	02.48	0	04	360	04.20	4.00	13.00	8.4	D	-	0
110218	1244 44.76	40.465	21.638	00.90	0	07	330	03.40	6.00	04.70	10	D	-	0
110227	0214 53.46	40.251	21.260	38.59	0	10	159	12.10	0.20	01.30	2.4	C	#	0
110228	0910 33.30	40.643	21.631	07.08	0	06	360	21.70	0.15	17.40	15.6	D	-	0
110302	1222 44.67	40.645	21.635	07.00	0	06	360	21.80	0.07	11.70	9.9	D		0

110306	0314 45.45	40.687	21.935	08.15	0	15	112	34.30	0.25	00.80	4.1	C		0
110306	1225 00.63	40.442	21.818	00.23	0	08	279	12.30	0.28	03.70	2.3	D		0
110306	1608 21.60	40.605	21.701	16.99	0	10	302	17.20	0.04	01.10	1	C		0
110311	1621 27.48	40.577	21.657	9. 17	0	18	107	13.90	0.18	00.60	1.5	B		0
110314	0911 15.95	40.610	21.747	00.01	0	08	331	18.60	0.33	26.40	15	D	-	0
110315	1233 43.45	40.556	21.882	01.22	0	07	358	21.10	0.11	12.50	1.3	D		0
110318	0141 17.04	40.469	21.674	00.14	0	07	360	01.90	0.87	73.40	66	D		0
110318	1725 01.75	40.487	21.672	03.69	0	06	360	03.90	0.02	12.60	4.3	D	-	0
110320	0915 28.58	40.656	21.794	09.08	0	10	271	24.80	0.90	09.90	16.4	D	#	0
110321	1222 58.80	40.426	21.889	00.02	0	12	296	18.40	0.44	03.10	2.7	D	#	0
110327	0804 19.63	40.527	21.837	00.02	0	07	358	16.30	0.12	12.70	1.4	D	-	0
110327	0806 59.91	40.650	21.615	06.86	0	06	360	22.70	0.31	22.60	18.7	D	-	0
110327	0809 58.17	40.587	21.632	06.18	0	08	359	15.60	0.27	18.40	20.4	D	-	0
110402	0809 22.87	40.238	21.585	08.45	0	08	246	24.20	0.12	02.30	16	D	-	0
110402	0113 06.51	40.609	21.638	07.56	0	07	360	17.90	0.51	44.30	43.8	D		0
110407	0734 41.47	40.332	21.560	00.04	0	09	245	15.80	0.13	01.40	2.5	C	#	0
110407	1325 20.75	40.345	21.579	06.80	0	09	146	13.80	0.06	04.60	9.1	C	-	0
110408	1307 55.77	40.449	21.882	00.03	0	17	089	17.60	0.27	00.80	1.5	C	#	0
110409	0801 13.35	40.442	21.830	00.84	0	10	243	13.30	0.13	01.60	2.3	C		0
110410	0816 41.16	40.337	21.567	00.41	0	10	242	15.10	0.07	01.20	2	C		0
110413	1321 55.42	40.346	21.236	01.90	0	08	225	18.60	0.25	11.00	16.8	D		0
110414	0810 18.70	40.452	21.862	00.02	0	08	253	15.90	0.36	03.20	5.3	D	#	0
110415	0804 39.46	40.453	21.878	00.02	0	13	258	17.30	0.37	01.70	2.4	D	#	0
110415	0143 14.01	40.737	21.873	07.92	0	19	143	35.90	0.25	00.70	3.3	C	#	0
110416	0807 53.02	40.439	21.844	01.49	0	17	085	14.50	0.23	00.60	0.8	C		0
110416	1128 35.13	40.322	21.490	06.56	0	06	313	20.80	0.06	01.60	1	C		0
110417	0808 11.23	40.448	21.845	01.62	0	17	155	14.60	0.17	00.50	0.8	C		0
110417	1108 45.76	40.462	21.869	00.01	0	08	299	16.60	0.12	01.50	1.1	C	#	0
110417	1934 12.99	40.417	21.535	07.08	0	11	310	12.20	0.07	07.90	6.7	D	-	0
110418	1215 32.07	40.455	21.853	00.03	0	12	251	15.20	0.23	01.30	1.7	C	#	0
110419	0816 29.40	40.342	21.568	00.03	0	12	240	14.60	0.35	02.40	4.8	D	#	0
110419	0823 5.55	40.594	21.973	08.56	0	13	256	40.50	0.18	05.20	14.7	D	-	0

110420	0829 58.15	40.446	21.850	00.02	0	15	133	15.00	0.16	00.60	1	C	#	0
110420	1133 45.69	40.424	21.843	00.03	0	12	292	14.60	0.26	01.80	1.7	C	#	0
110420	2155 22.97	40.613	21.629	07.50	0	06	360	18.30	0.09	14.80	14.7	D		0
110421	0309 23.73	40.164	21.674	08.03	0	21	073	17.80	0.19	00.50	2.5	C		0
110421	0112 08.59	40.446	21.858	00.03	0	18	087	15.60	0.19	00.60	1.1	C	#	0
110422	0155 86.08	40.378	21.365	06.10	0	09	152	27.40	0.14	00.70	2.5	C		0
110423	1141 54.50	40.444	21.869	00.03	0	12	294	16.60	0.33	02.30	2.1	D	#	0
110424	1226 51.29	40.057	21.654	08.48	0	23	083	27.40	0.14	00.40	1.6	B		0
110425	0805 23.46	40.429	21.867	03.55	0	20	082	15.90	0.42	00.80	1	C		0
110425	0842 11.53	40.619	21.153	08.95	0	09	224	26.60	0.20	06.20	19.8	D	-	0
110427	0354 29.87	40.524	21.653	05.91	0	07	359	08.20	0.11	14.5	10.0	D		0
110427	0805 32.86	40.487	21.827	00.25	0	09	290	13.50	0.12	01.40	1.2	C		0
110427	1315 20.26	40.554	21.739	07.20	0	07	358	12.50	0.12	14.40	15.8	D		0
110428	0812 57.67	40.443	21.905	00.03	0	09	297	19.70	0.32	02.60	2.4	D	#	0
110428	1135 59.56	40.413	21.918	00.03	0	08	298	21.10	0.25	2 .6	1.8	D	#	0
110429	0642 07.84	40.618	21.424	28.53	0	10	141	18.80	0.23	01.10	3.4	C		0
110430	1115 28.12	40.472	21.869	00.02	0	09	303	16.80	0.34	03.10	2.2	D	#	0
110501	0736 29.99	40.541	21.959	06.00	0	07	324	26.20	0.06	07.20	11.2	D	-	0
110501	0817 22.29	40.452	21.849	00.00	0	06	293	14.80	0.05	12.30	1.6	D	-	0
110503	1130 53.46	40.343	21.554	08.42	0	07	298	15.30	0.09	02.10	14.4	D	-	0
110503	1323 10.13	40.438	21.841	02.24	0	19	124	14.20	0.17	00.40	0.4	C		0
110504	0606 32.33	40.602	21.583	18.95	0	20	085	18.50	0.13	00.50	0.9	A		0
110504	2334 43.27	40.537	21.644	07.05	0	05	359	09.90	0.32	26.70	20.4	D	-	0
110505	0013 32.80	40.589	21.632	07.22	0	05	359	15.70	0.22	20.70	22.2	D	-	0
110505	1018 17.20	40.492	21.905	08.06	0	08	313	20.20	0.11	05.20	14.7	D	-	0
110507	0135 43.62	40.343	21.242	28.17	0	27	087	18.20	0.30	00.70	1.3	B		0
110507	0151 53.69	40.368	21.272	25.78	0	20	077	19.60	0.34	00.80	1.9	B		0
110507	0211 35.86	40.350	21.269	28.09	0	27	078	20.00	0.27	00.60	1.1	B		0
110507	0348 29.13	40.357	21.269	28.76	0	22	077	19.80	0.27	00.70	1.5	B		0
110507	0931 43.67	40.444	21.868	00.05	0	13	087	16.50	0.35	01.00	2.1	C	#	0
110507	1520 29.27	40.290	21.801	07.63	0	12	291	03.10	0.06	01.20	0.4	C		0
110508	0807 39.06	40.453	21.863	00.72	0	09	253	16.10	0.15	01.20	1.4	C		0

110510	0408 38.17	40.059	21.532	15.23	0	21	089	18.50	0.33	00.70	3.4	C		0
110510	1958 44.99	40.700	21.386	07.06	0	11	158	09.30	0.32	13.80	19.2	D	-	0
110511	1205 49.79	40.439	21.856	00.44	0	16	086	15.50	0.25	00.70	1	C		0

Appendix IV : Epicenters derived from the Low velocities model.

Date	Time (HHMM SS.FF)	Lat	Lon										
110129	0310 39.43	40.499	21.664	04.24	0	05	360	05.40	0.79	67.10	65.00	D	0
110202	0844 58.47	40.418	21.675	01.01	0	05	360	03.20	0.66	56.30	47.40	D	0
110203	0437 33.83	40.505	21.630	12.41	0	07	357	06.90	0.04	12.10	04.60	D	0
110203	0926 58.13	40.486	21.367	12.67	0	21	108	26.30	0.33	00.90	02.90	C	0
110203	0934 03.41	40.488	21.368	10.06	0	20	108	26.30	0.37	00.80	05.70	C	0
110204	1713 12.03	40.492	21.376	12.32	0	21	106	25.60	0.30	00.80	02.80	C	0
110205	0305 32.00	40.290	21.730	12.68	0	11	197	03.90	0.08	01.40	01.60	C	0
110208	0739 51.67	40.156	21.645	04.12	0	10	123	19.90	0.18	00.70	02.40	C	0
110208	1221 31.83	40.440	21.832	01.39	0	16	084	13.40	0.30	00.70	01.30	C	0
110210	0906 58.31	40.439	21.802	04.00	0	09	272	10.90	0.46	06.30	03.80	D	# 0
110210	1229 12.49	40.456	21.840	00.54	0	05	291	14.00	0.37	30.20	24.20	D	0
110212	0911 12.95	40.393	21.710	04.30	0	06	183	06.70	0.13	13.50	14.90	D	0
110212	1220 18.73	40.437	21.842	04.21	0	17	084	14.30	0.58	01.20	02.20	D	# 0
110213	0751 16.40	40.226	21.736	11.72	0	07	249	09.50	0.06	03.10	03.60	D	0
110213	0906 13.86	40.435	21.802	04.02	0	08	270	10.90	0.43	05.70	03.60	D	# 0
110213	1713 03.67	40.301	21.694	07.04	0	10	173	06.60	0.11	09.00	10.70	D	0
110214	0903 19.16	40.413	21.774	00.65	0	10	220	09.30	0.31	01.60	00.50	D	# 0
110215	1225 47.34	40.453	21.842	04.00	0	19	086	14.20	0.91	01.90	03.00	D	# 0
110215	1833 26.35	40.204	21.650	10.44	0	12	227	15.40	0.37	02.10	13.00	D	# 0
110215	2351 16.16	40.209	21.620	09.33	0	09	220	16.80	0.29	02.30	08.10	D	# 0
110216	1203 25.77	40.463	21.675	03.68	0	04	360	01.30	0.05	13.20	01.20	D	0
110216	1402 36.91	40.459	21.716	07.69	0	04	267	03.70	0.06	10.30	08.60	D	0
110218	1244 43.71	40.458	21.668	03.58	0	04	347	00.90	0.05	13.00	01.00	D	0
110227	0214 53.72	40.354	21.272	01.83	0	10	158	20.90	0.15	00.80	00.80	B	0
110228	0910 33.30	40.401	21.555	15.01	0	06	358	11.30	0.10	12.30	09.80	D	0
110302	1222 44.66	40.441	21.545	15.91	0	06	357	10.90	0.04	11.10	08.90	D	0
110306	0314 44.34	40.680	21.935	10.55	0	13	111	33.70	0.24	00.80	05.90	C	# 0

110306	1225 00.41	40.424	21.766	04.06	0	09	245	08.20	0.62	10.10	07.30	D	# 0
110306	1608 21.60	40.529	21.668	15.49	0	10	289	08.50	0.04	01.20	00.70	C	0
110311	1621 26.33	40.574	21.654	10.40	0	17	099	13.60	0.20	00.60	01.20	B	0
110314	0911 14.77	40.523	21.768	00.36	0	07	348	11.20	0.07	11.70	00.80	D	0
110315	1233 43.47	40.482	21.797	01.21	0	07	348	10.90	0.11	07.60	00.80	D	0
110318	0141 15.06	40.495	21.700	04.38	0	07	357	05.10	1.23	53.40	88.60	D	0
110318	1725 01.75	40.455	21.676	01.69	0	06	333	00.30	0.02	12.10	01.80	D	0
110320	0915 28.14	40.630	21.731	07.20	0	10	253	20.20	1.08	10.60	10.90	D	# 0
110321	1222 57.96	40.440	21.782	00.22	0	09	285	09.20	0.09	01.00	00.10	C	0
110327	0804 19.67	40.436	21.767	00.67	0	07	322	08.00	0.10	07.70	01.30	D	# 0
110327	0806 59.90	40.587	21.646	10.57	0	06	360	15.30	0.31	28.60	25.60	D	0
110327	0809 58.12	40.382	21.610	05.53	0	07	359	09.00	0.18	13.60	15.50	D	0
110402	0809 22.40	40.355	21.477	08.42	0	08	181	19.60	0.19	18.30	19.50	D	0
110402	1130 06.52	40.545	21.643	06.85	0	07	359	10.70	0.51	31.90	30.80	D	0
110407	0734 40.93	40.360	21.622	03.90	0	08	223	10.60	0.06	00.90	01.20	C	0
110407	1325 19.65	40.360	21.599	09.39	0	09	145	11.50	0.26	06.30	20.00	D	0
110408	1307 55.07	40.439	21.840	04.03	0	17	084	14.10	0.38	01.00	02.20	C	# 0
110409	0801 12.99	40.395	21.721	05.24	0	10	187	06.90	0.17	09.90	01.20	D	# 0
110410	0816 39.85	40.358	21.614	01.68	0	09	226	11.10	0.02	00.80	01.10	C	0
110413	1321 53.47	40.283	21.288	00.34	0	08	186	16.00	0.10	02.60	00.50	D	0
110414	0810 17.99	40.411	21.761	02.21	0	08	213	08.40	0.23	02.30	01.10	C	0
110415	0804 37.86	40.433	21.796	00.18	0	12	230	10.40	0.21	01.10	00.10	C	0
110415	1431 01.87	40.743	21.865	02.05	0	11	145	36.10	0.25	01.20	22.10	C	0
110416	0807 51.79	40.437	21.815	02.99	0	19	083	12.00	0.21	00.60	00.90	C	0
110416	1128 35.11	40.346	21.579	06.71	0	06	290	13.80	0.06	06.90	10.70	D	0
110417	0808 10.46	40.446	21.814	03.96	0	17	146	11.90	0.29	00.80	01.20	C	# 0
110417	1108 45.90	40.447	21.807	03.98	0	10	278	11.30	0.71	39.50	21.40	D	0
110417	1934 12.93	40.431	21.657	09.66	0	11	247	02.20	0.12	10.30	03.60	D	# 0
110418	1215 32.19	40.450	21.767	03.30	0	13	219	07.80	0.55	02.80	02.90	D	0
110419	0816 28.92	40.400	21.747	05.02	0	12	203	08.10	0.15	04.70	02.00	D	0
110419	0823 04.98	40.585	21.025	11.17	0	14	246	37.40	0.33	01.70	27.20	D	0
110420	0829 57.46	40.436	21.813	03.92	0	17	130	11.90	0.40	01.00	01.30	C	# 0

110420	1133 45.84	40.447	21.736	02.75	0	11	280	05.20	0.05	00.80	00.40	C	# 0
110420	2155 24.20	40.444	21.654	08.18	0	05	338	01.70	0.04	12.30	03.70	D	0
110421	0309 22.40	40.162	21.693	12.99	0	18	074	17.40	0.27	00.70	02.40	B	0
110421	1120 07.90	40.438	21.829	03.97	0	18	084	13.20	0.43	01.00	01.80	C	# 0
110422	1558 05.00	40.384	21.359	09.03	0	07	148	27.80	0.13	04.30	15.60	C	0
110423	1141 54.14	40.459	21.770	00.93	0	11	284	08.10	0.09	00.90	00.60	C	# 0
110424	1226 50.12	40.054	21.657	10.75	0	24	066	27.40	0.15	00.30	03.80	C	0
110425	0805 22.39	40.427	21.858	03.88	0	19	082	15.20	0.50	01.10	01.80	C	# 0
110425	0842 10.04	40.625	21.123	08.33	0	05	232	28.20	0.10	04.10	14.70	D	0
110427	0354 29.65	40.500	21.682	01.92	0	08	360	05.20	0.40	35.40	23.30	D	0
110427	0805 32.79	40.497	21.716	02.09	0	09	254	06.00	0.10	02.20	00.70	C	0
110427	1315 20.36	40.421	21.739	01.54	0	08	302	06.10	0.08	04.10	01.80	D	0
110428	0812 57.51	40.458	21.787	00.47	0	08	286	09.60	0.16	01.40	00.40	C	# 0
110428	1135 59.12	40.472	21.789	00.15	0	08	286	09.90	0.12	01.50	00.10	C	0
110429	0642 06.40	40.626	21.433	31.93	0	09	144	18.10	0.23	01.40	03.50	C	0
110430	1115 27.92	40.414	21.777	00.68	0	09	247	09.40	0.58	10.40	02.50	D	# 0
110501	0736 30.00	40.477	21.873	02.51	0	07	304	17.10	0.05	10.90	06.80	D	0
110501	0817 20.61	40.459	21.856	03.52	0	06	297	15.40	0.09	13.50	12.80	D	0
110503	1130 52.96	40.355	21.620	07.62	0	07	271	11.10	0.10	02.40	14.40	D	0
110503	1323 08.78	40.431	21.855	04.06	0	18	083	15.50	0.42	01.00	01.50	C	# 0
110504	0606 31.08	40.601	21.585	20.06	0	15	084	18.30	0.14	00.60	01.40	A	0
110504	2334 43.26	40.488	21.669	04.11	0	05	360	04.20	0.32	29.60	28.80	D	0
110505	0013 33.37	40.509	21.667	05.07	0	05	359	06.40	0.20	17.90	15.10	D	0
110505	1018 17.33	40.426	21.785	00.29	0	10	259	09.60	0.30	12.60	01.00	D	# 0
110507	0135 42.40	40.347	21.247	29.62	0	24	085	18.40	0.29	00.70	00.80	B	0
110507	0151 52.31	40.357	21.283	28.19	0	18	074	20.90	0.39	01.10	02.70	B	0
110507	0211 34.74	40.347	21.283	28.15	0	27	074	20.90	0.28	00.70	01.40	B	0
110507	0348 28.00	40.358	21.278	29.34	0	23	075	20.50	0.28	00.70	01.20	B	0
110507	0931 41.27	40.434	21.851	00.17	0	11	086	15.10	0.43	01.50	00.40	C	0
110507	1520 28.55	40.301	21.736	05.36	0	10	180	03.10	0.08	01.20	01.30	C	0
110508	0807 38.16	40.431	21.792	01.60	0	09	229	10.20	0.28	01.60	01.20	C	0
110510	0048 36.96	40.058	21.560	10.47	0	19	091	20.30	0.37	00.80	24.70	C	0

110510	1958 43.90	40.702	21.407	07.72	0	11	152	09.30	0.30	04.50	12.00	C	# 0
110511	1205 49.02	40.438	21.826	04.35	0	16	084	13.00	0.35	00.90	01.60	C	0

Appendix V : The FPPAGE output file in which are illustrated the Focal mechanisms of the seismic events, calculated for the *High velocity model*.

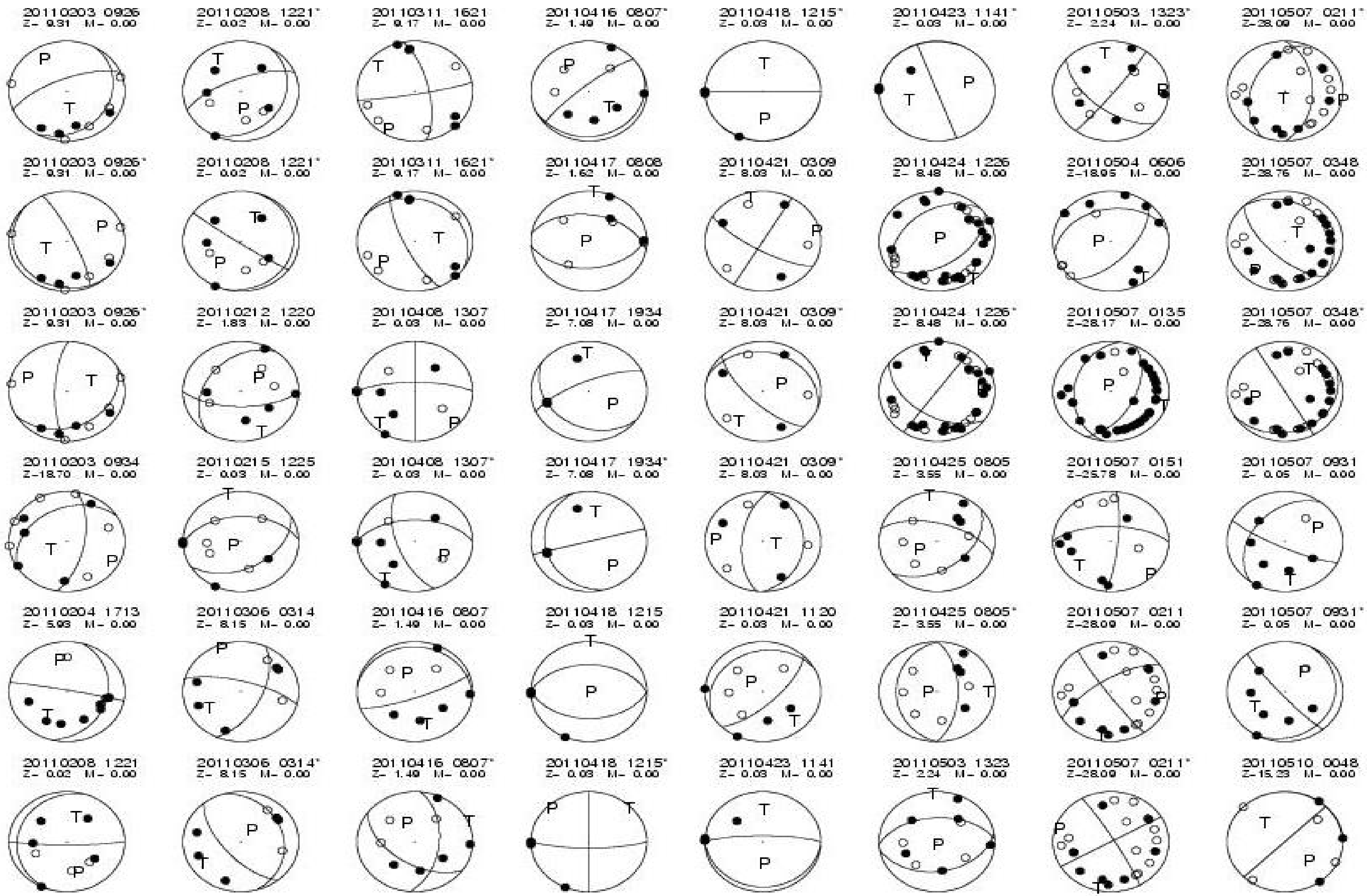

Appendix VI : The FPPAGE output file in which are illustrated the Focal mechanisms of the seismic events, calculated for the *Low velocity model*.

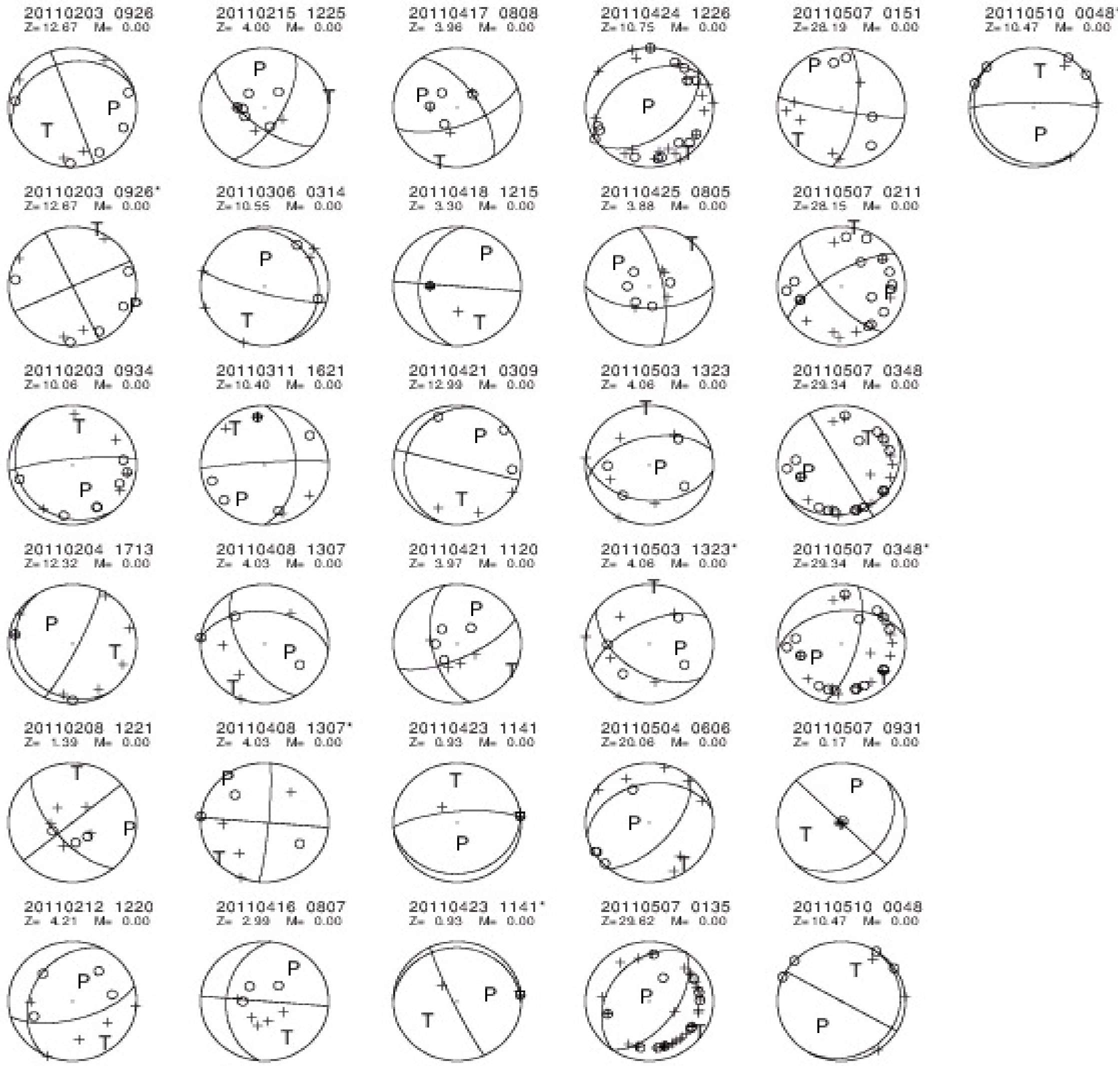

APPENDIX VII : ***Earthquake*** **recordings of the local seismological network.**

1. **110208_0739, 2.3**

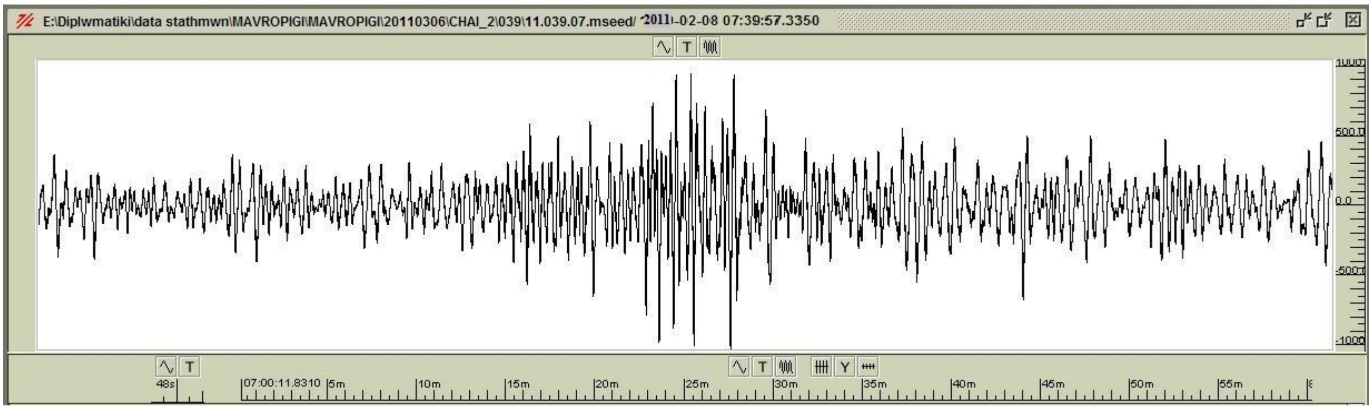

2. **110213_0751, 1.6**

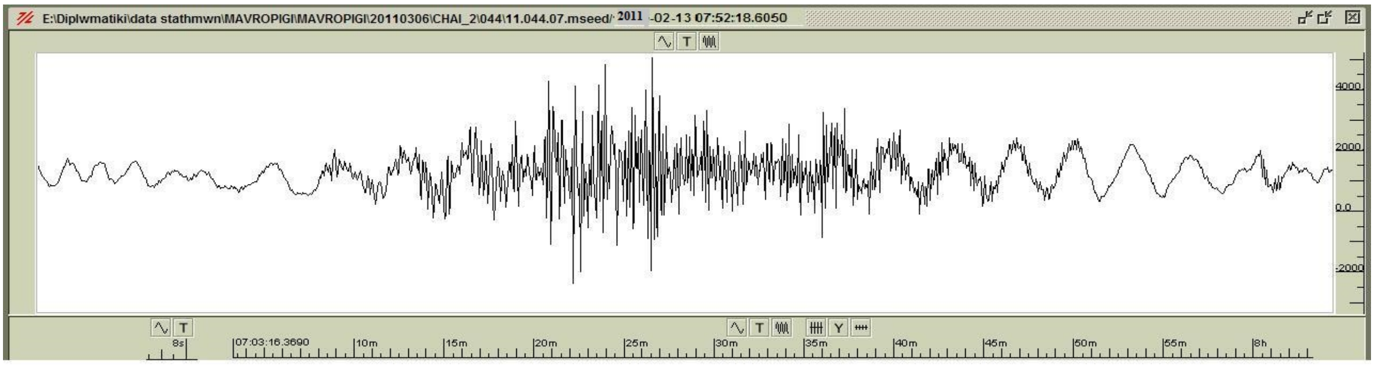

3. **110213_0906**

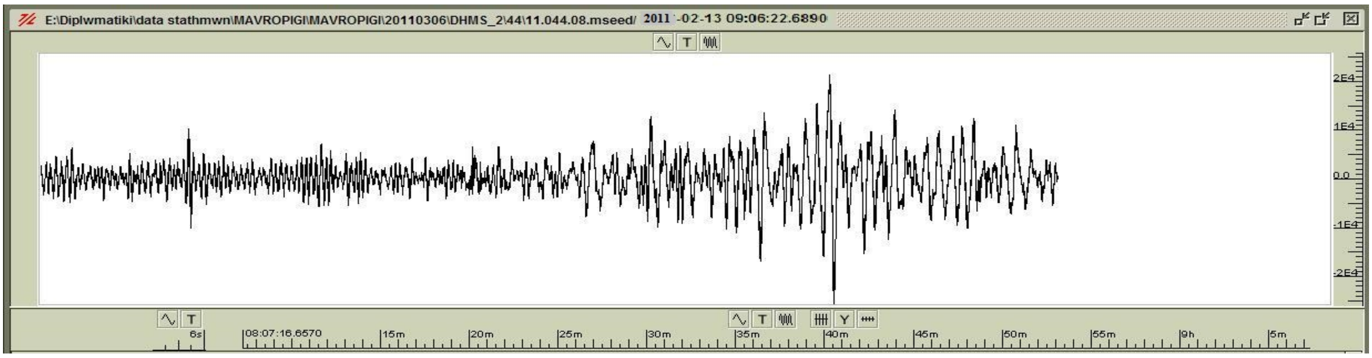

4. **110213_1713, 1.5**

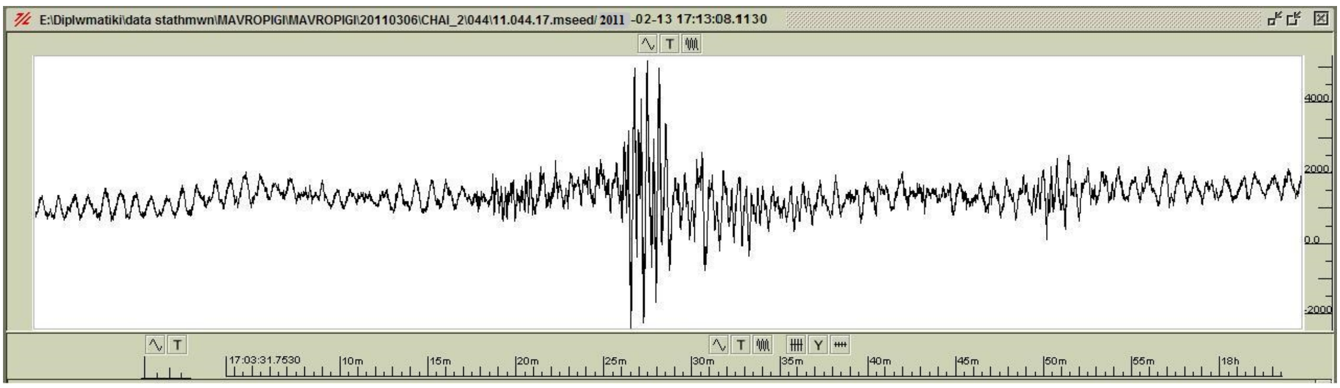

5. 110215_1833, 1.4

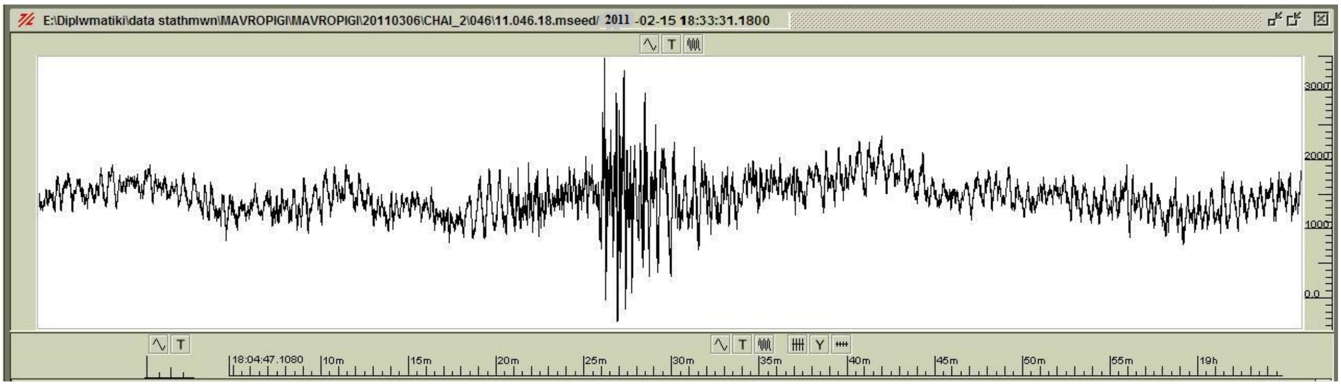

6. 110215_2351, 1.3

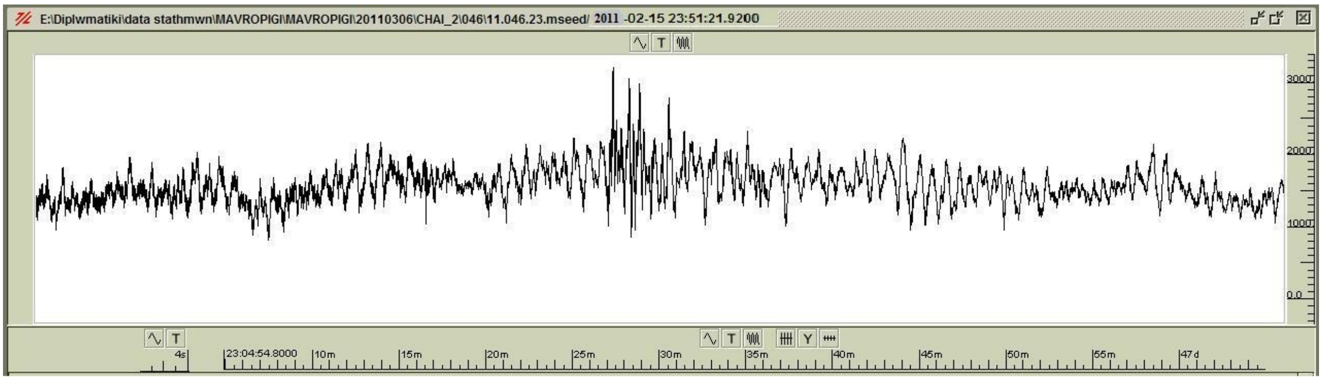

7. 110217_1434

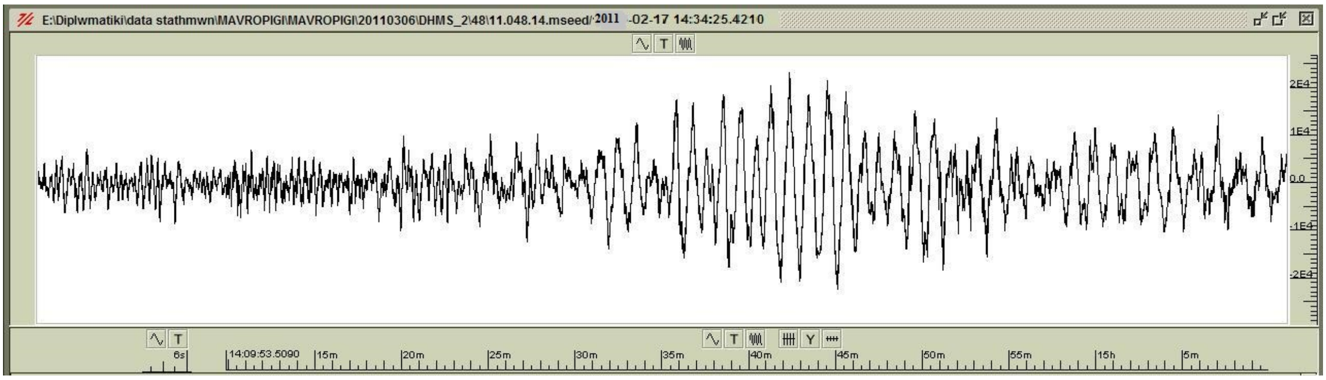

8. 110227_0214

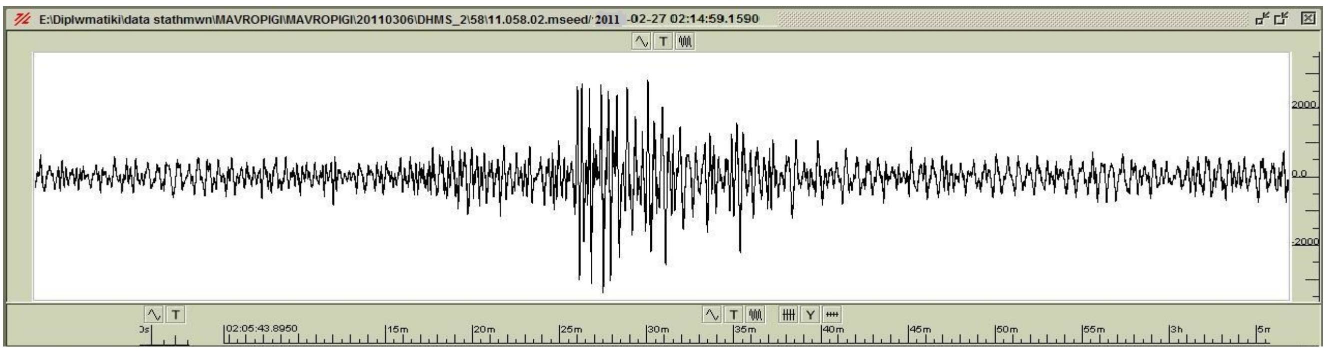

9. 110306_1608, 1.3

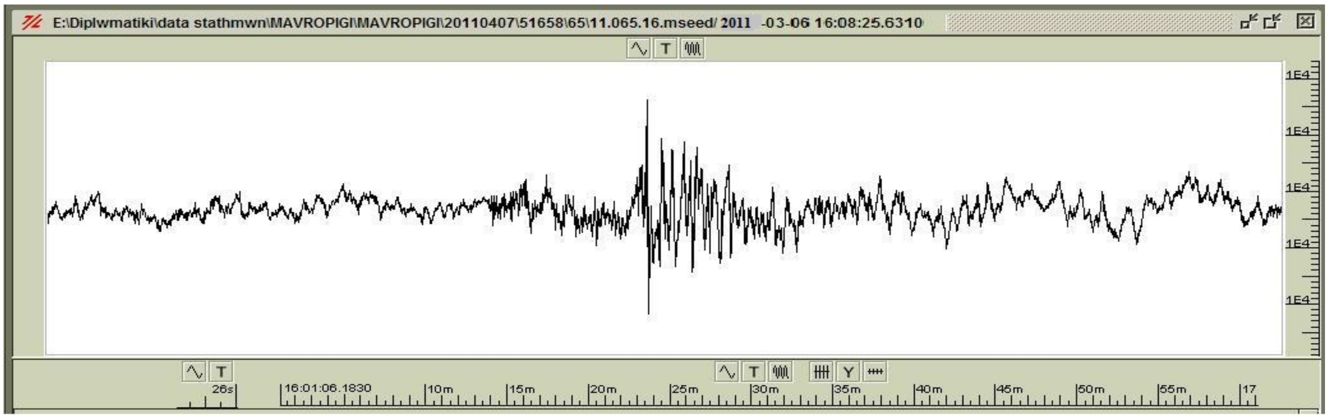

10. 110311_1621, 2.1

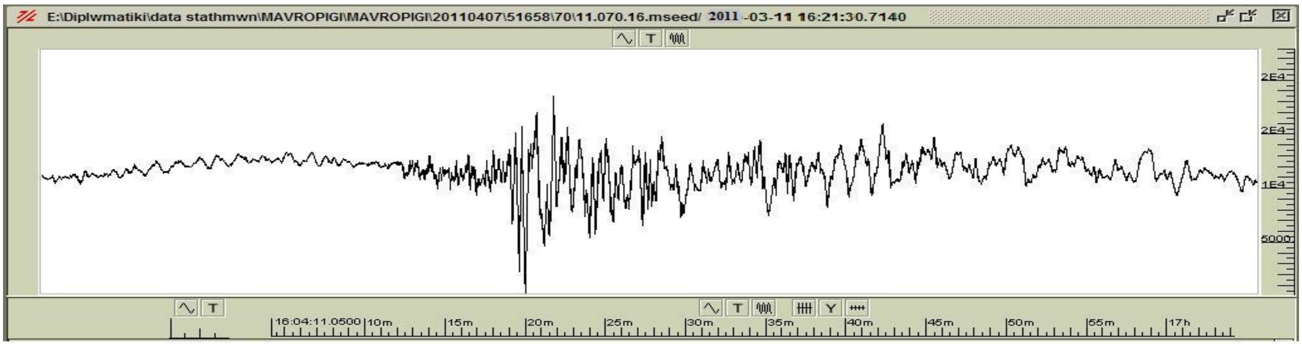

11. 110318_1725

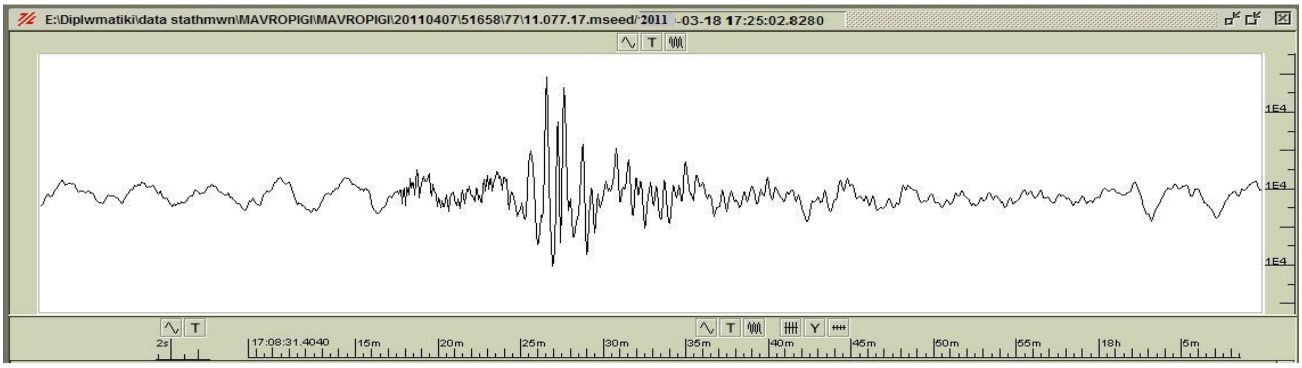

12. 110320_0915, 2.0

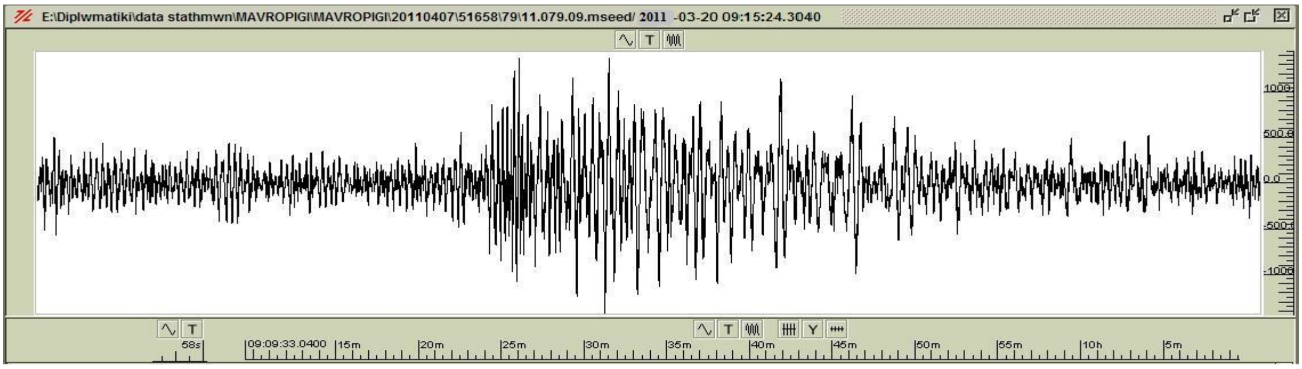

13. 110417_0808, 1.8

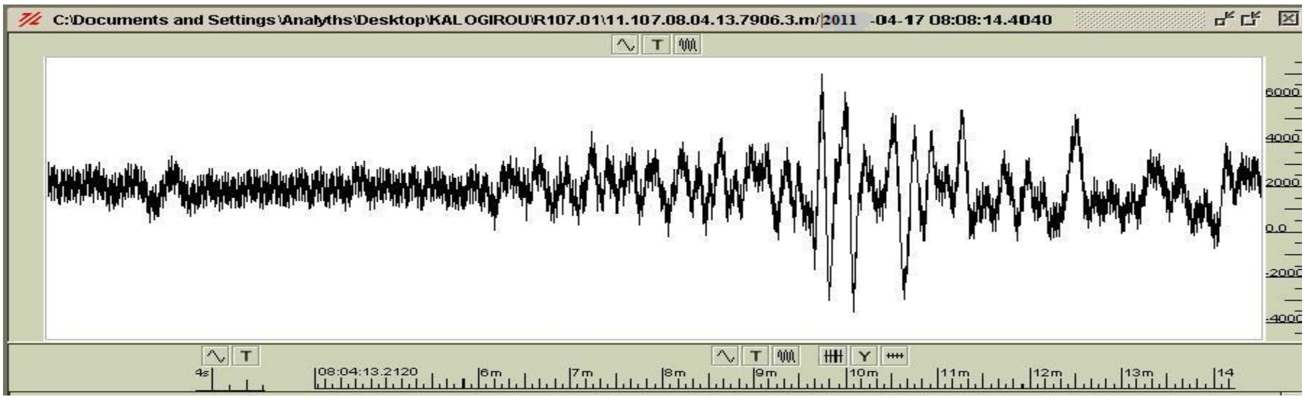

14. 110417_1934

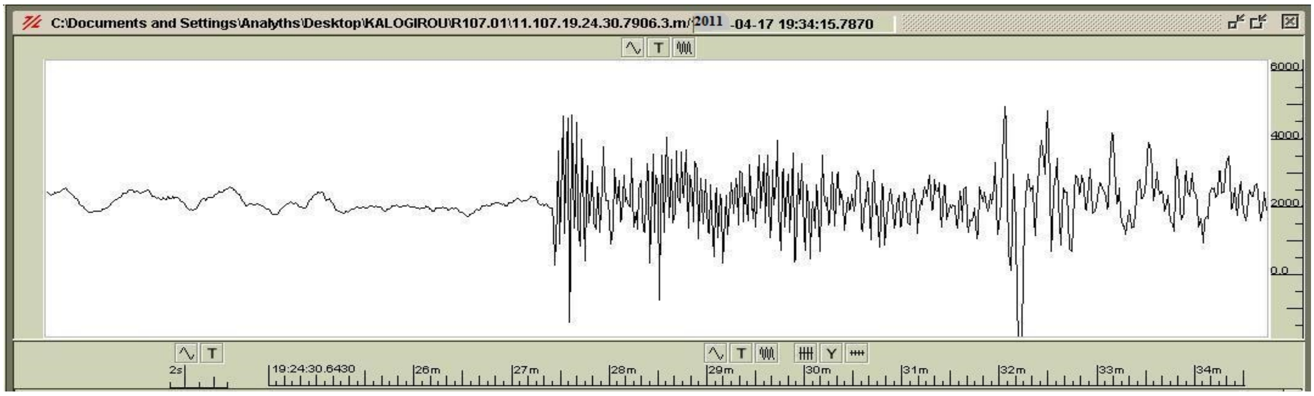

15. 110419_0823

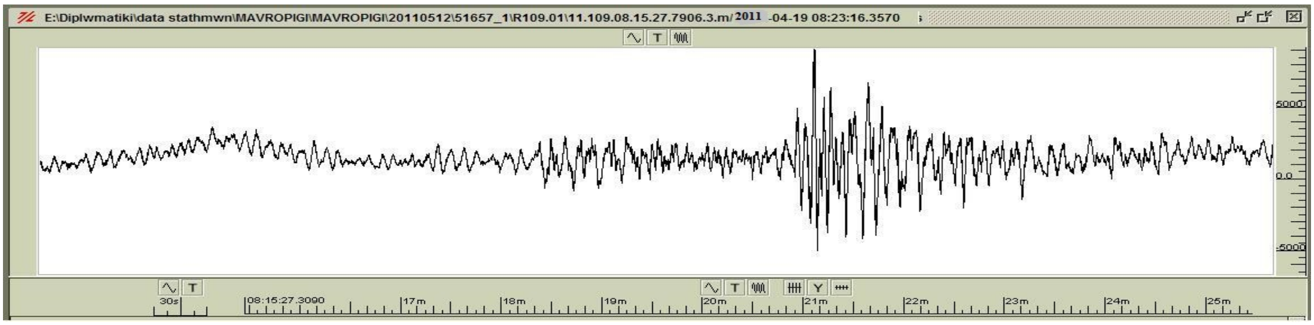

16. 110421_0309, 1.5

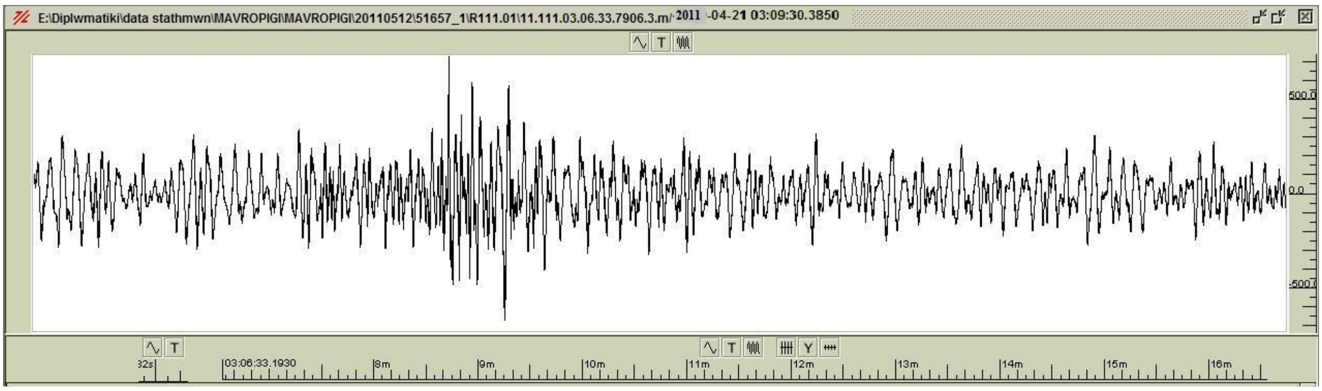

17. 110422_1558, 1.6

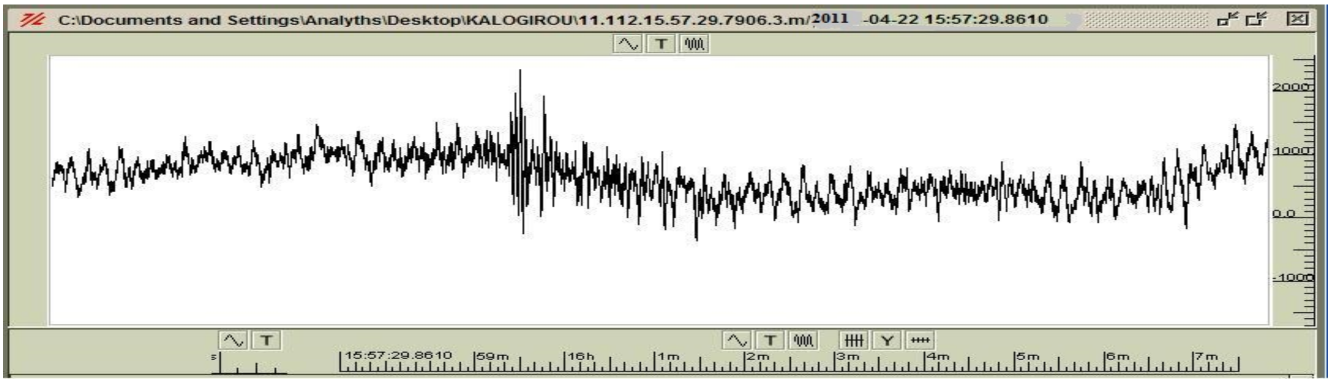

18. 110425_0842

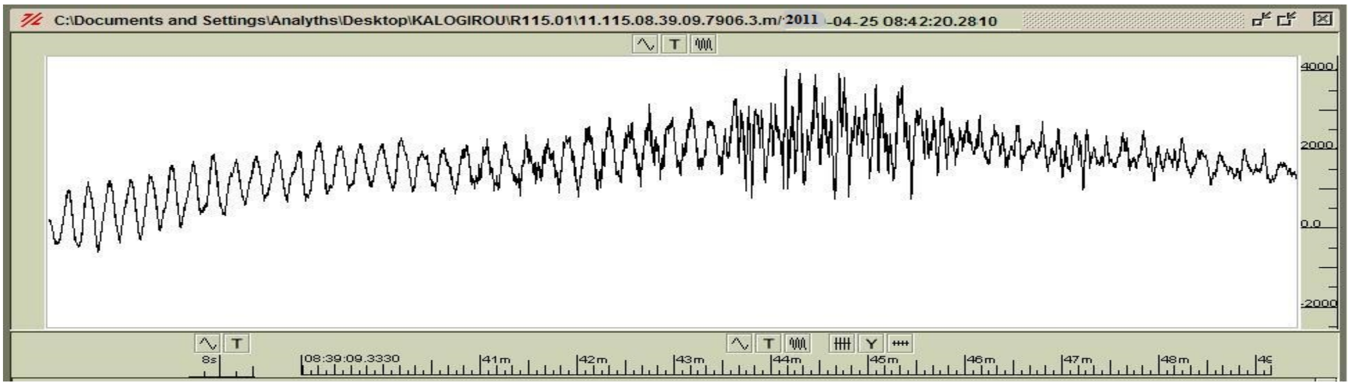

19. 110427_0805, 1.7

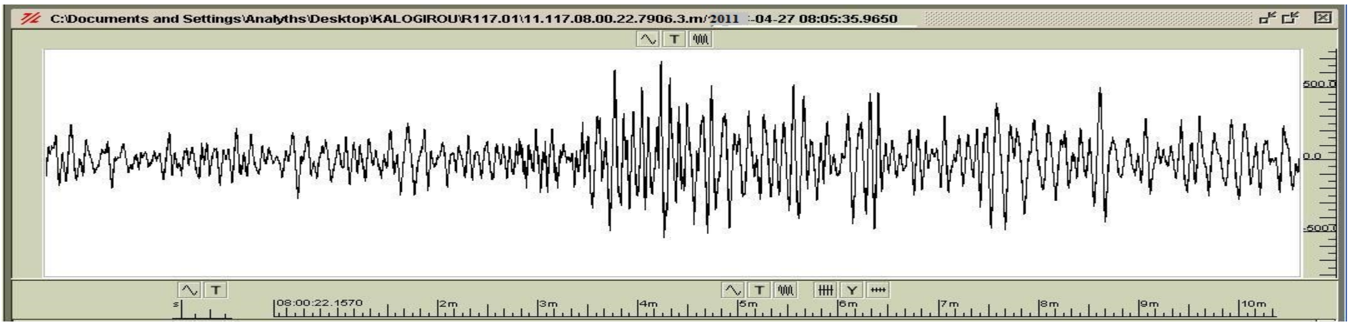

20. 110427_1315

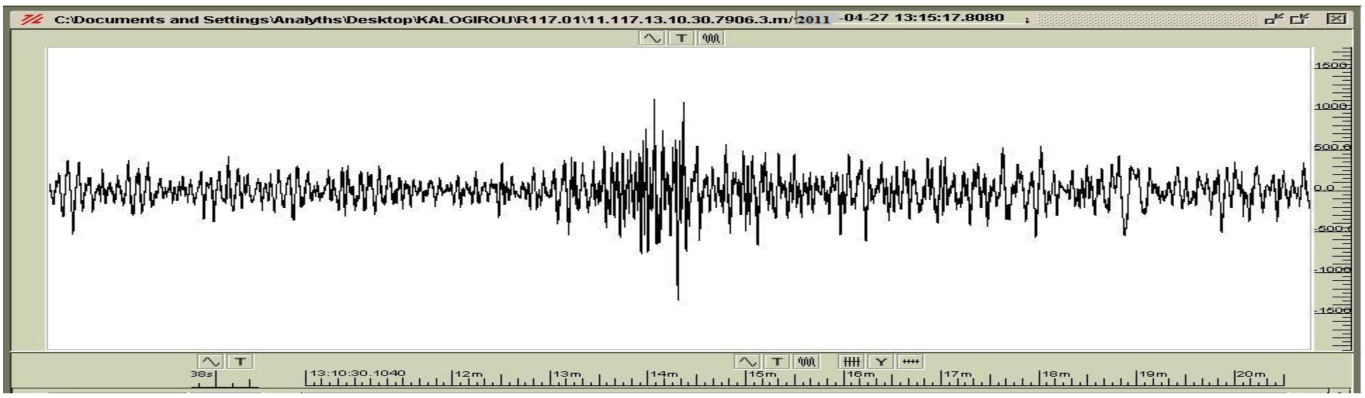

21. 110428_1135

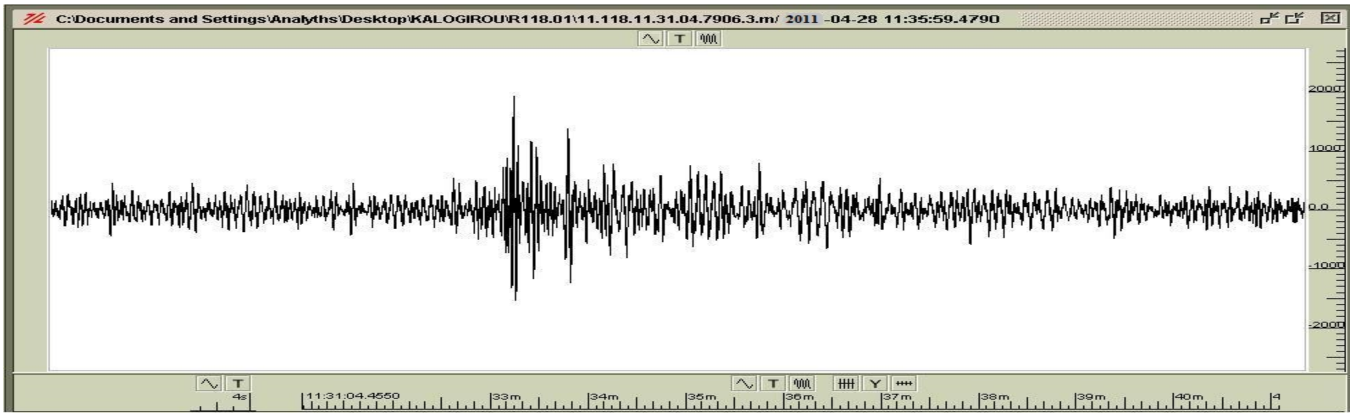

22. 110429_0642, 2.1

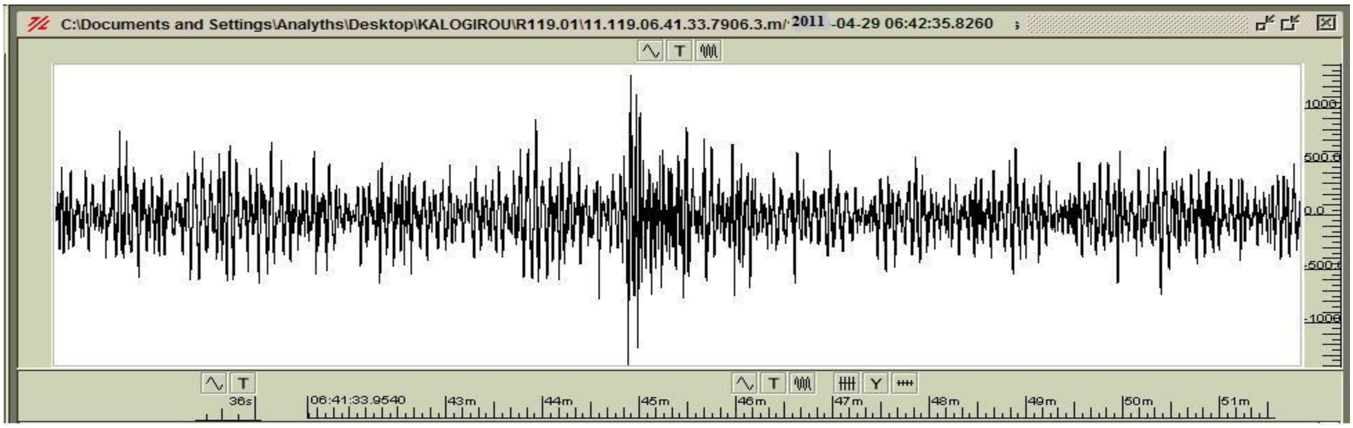

23. 110430_1115, 1.4

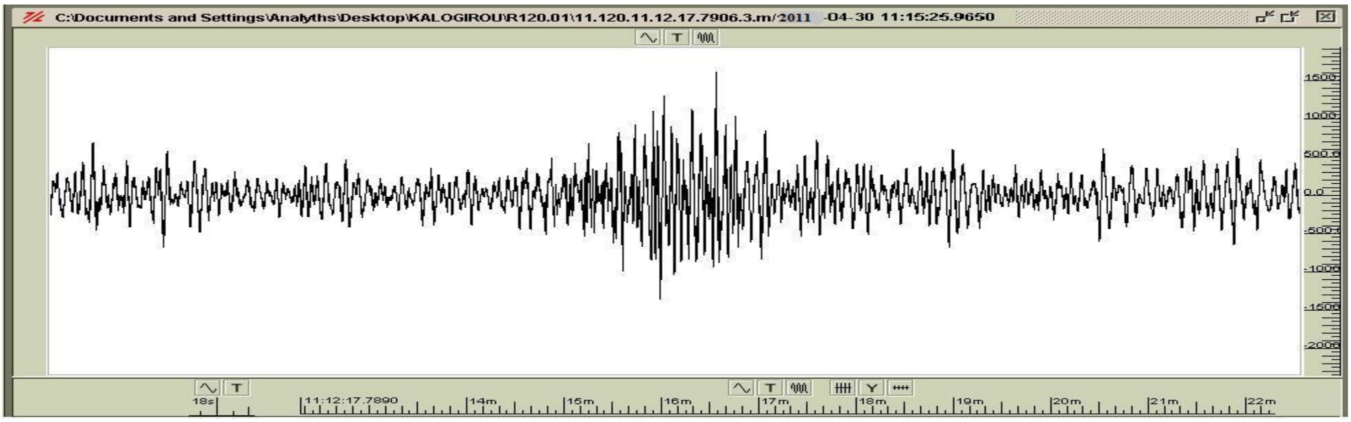

APPENDIX VIII : Explosion recordings of the local seismological network.

1. 110212_1220, 1.9

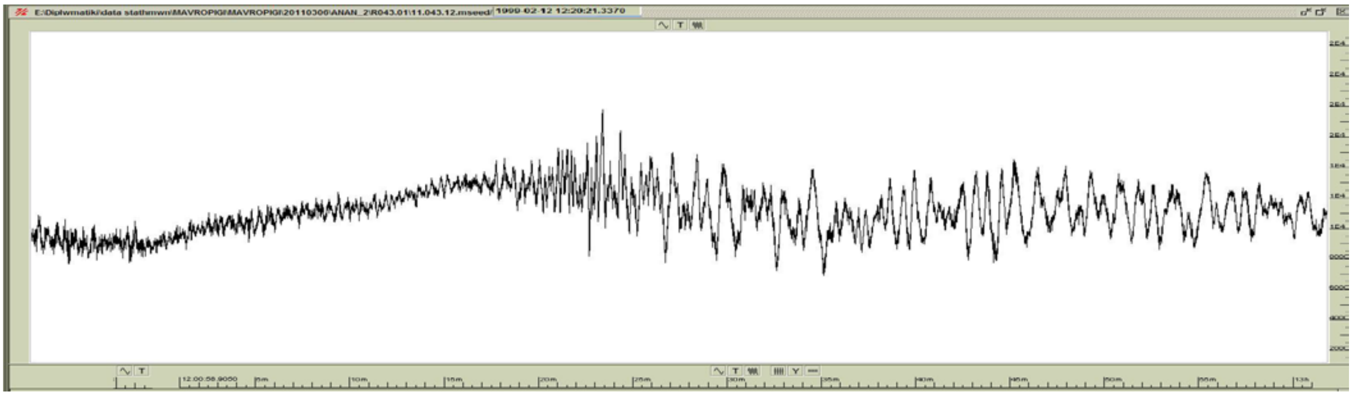

2. 110218_1244

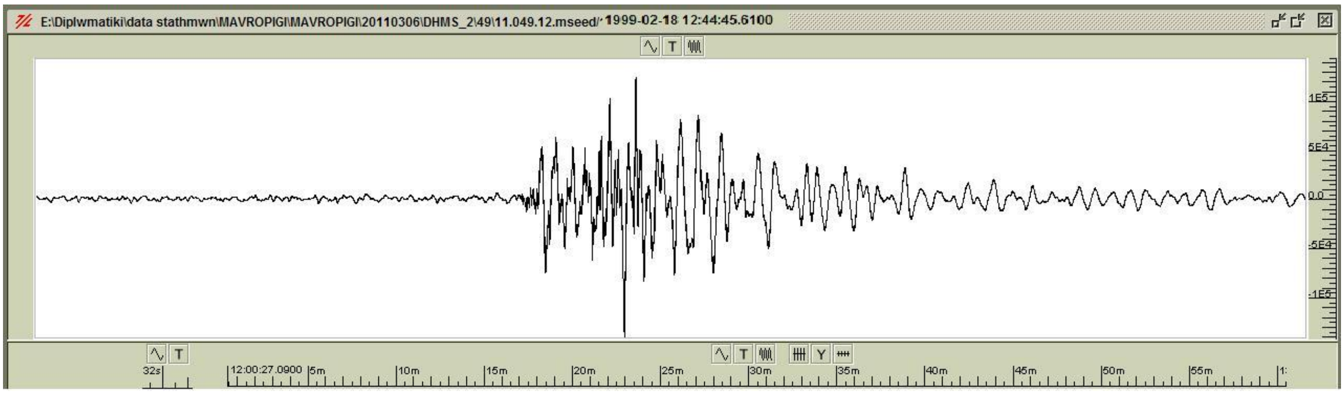

3. 110302_1222, 1.8

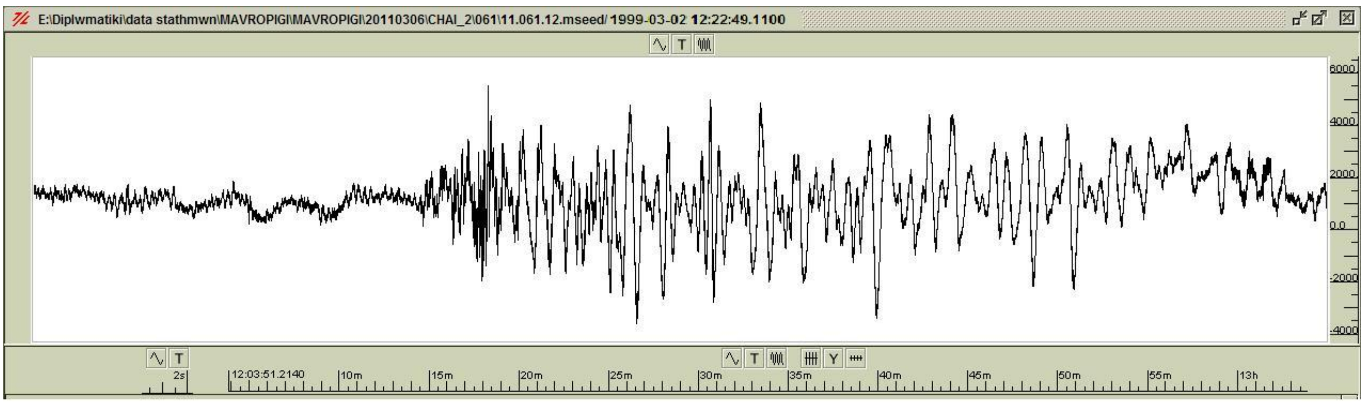

4. 110306_1225

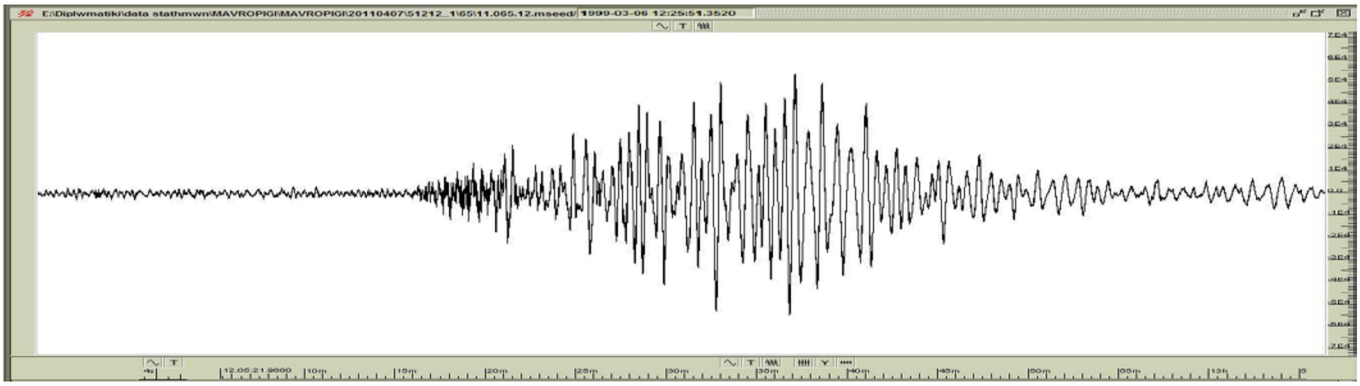

5. 110315_1233, 1.9

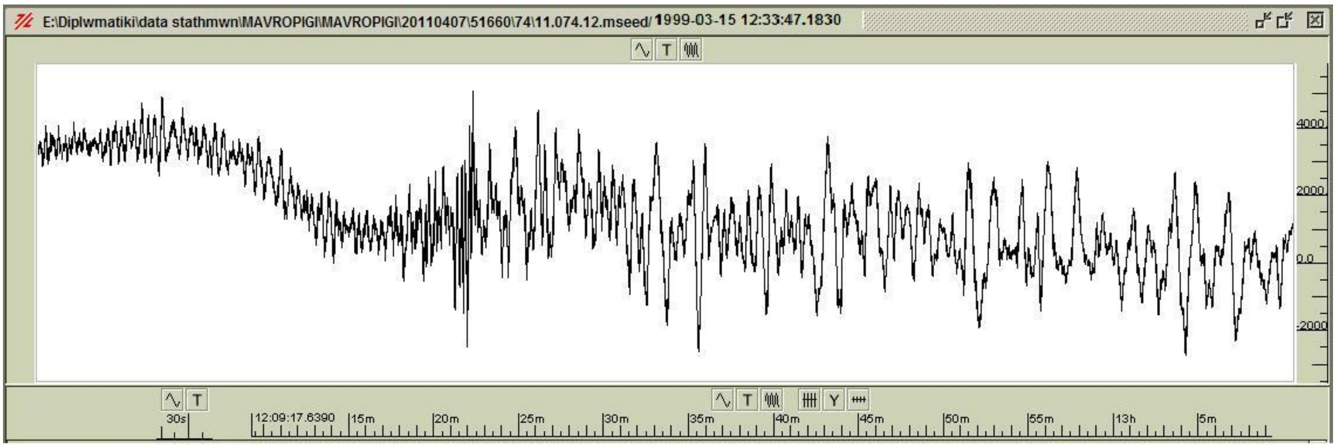

6. 110321_1222, 1.7

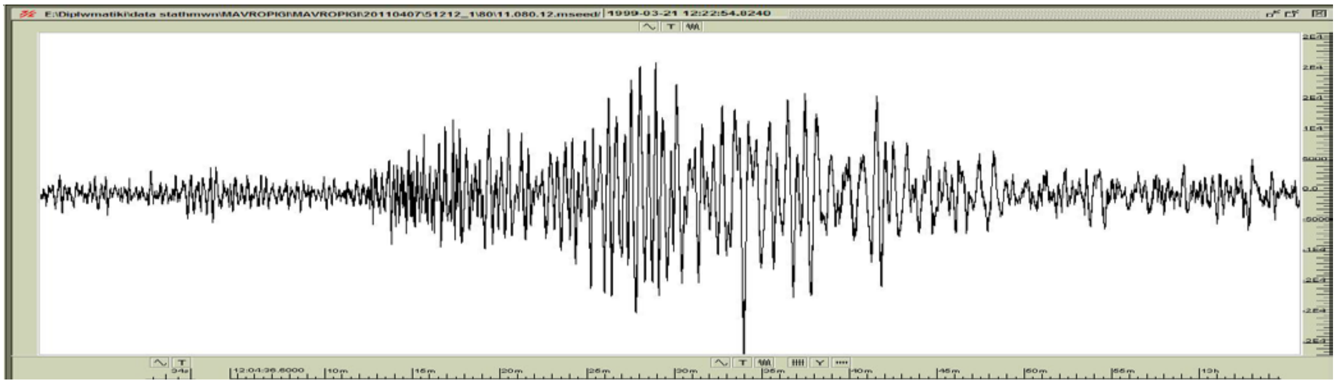

7. 110327_0804

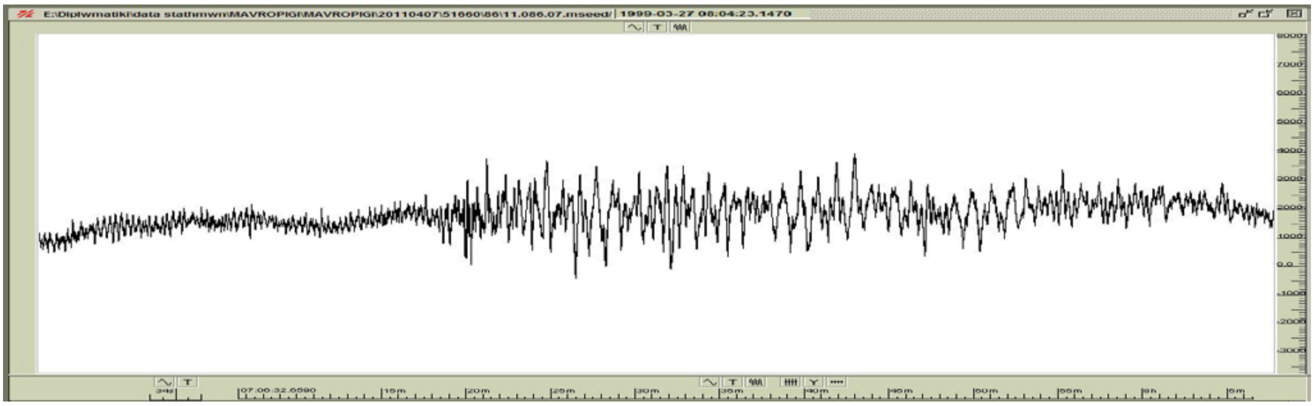

8. 110408_1307, 1.9

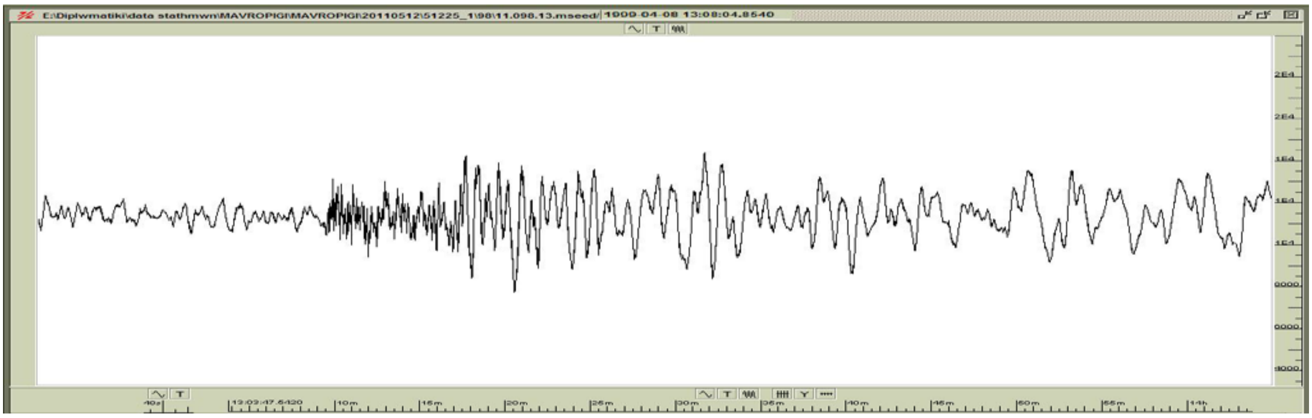

9. 110414_0810

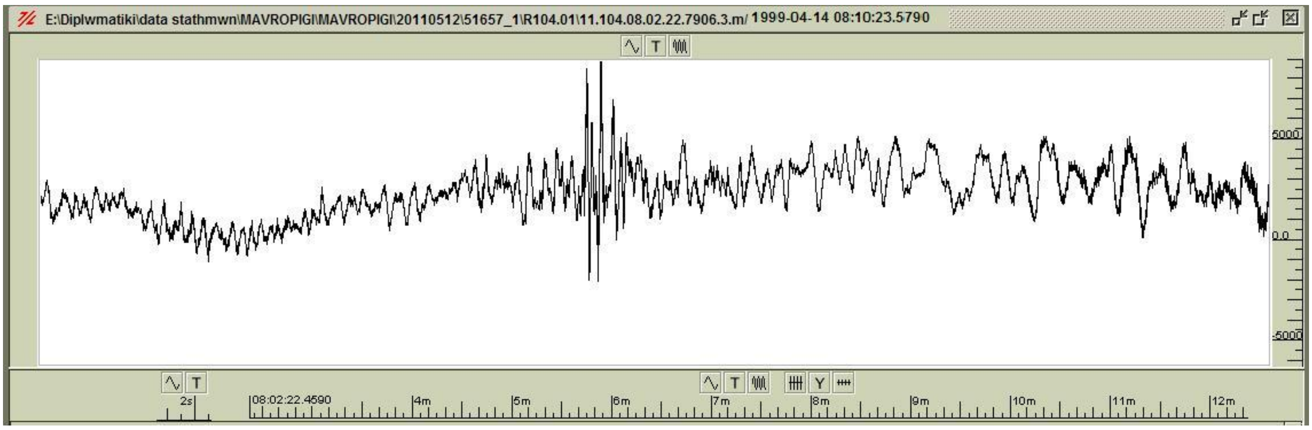

10. 110415_0804, 1.5

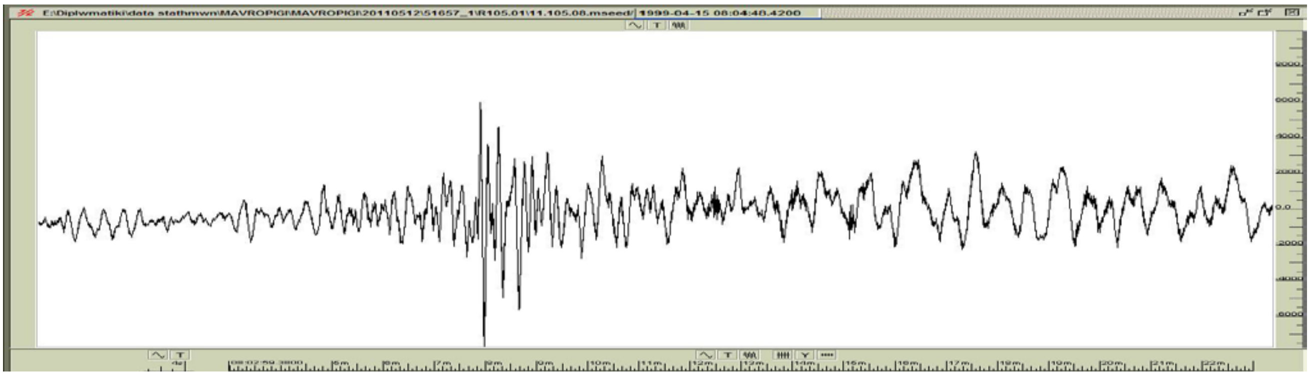

11. 110420_1133

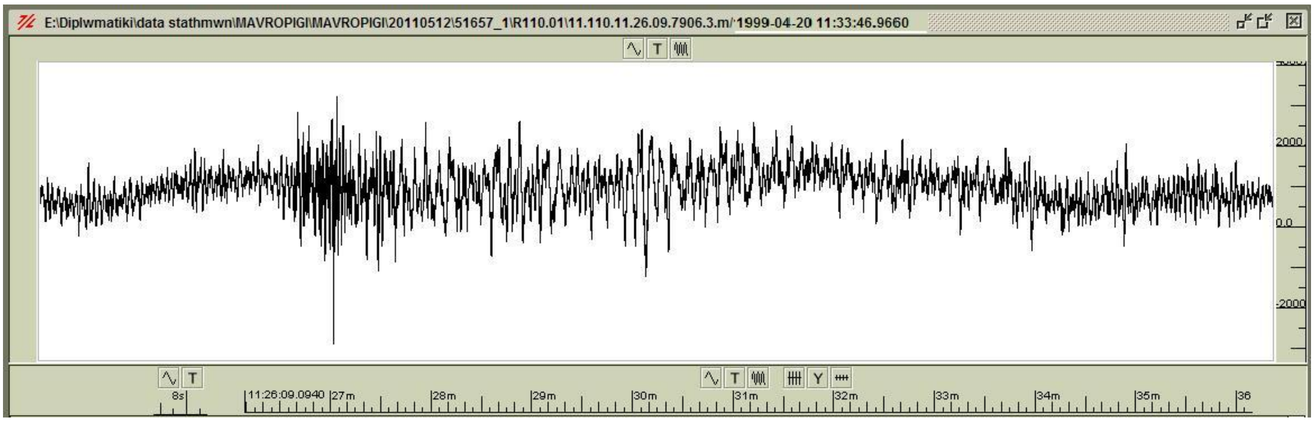

12. 110421_1120, 1.9

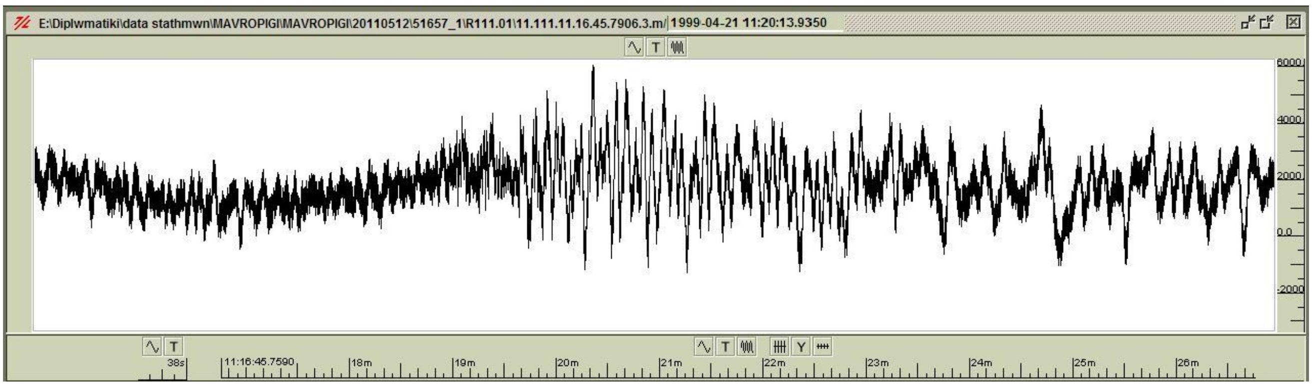

13.　　110423_1141

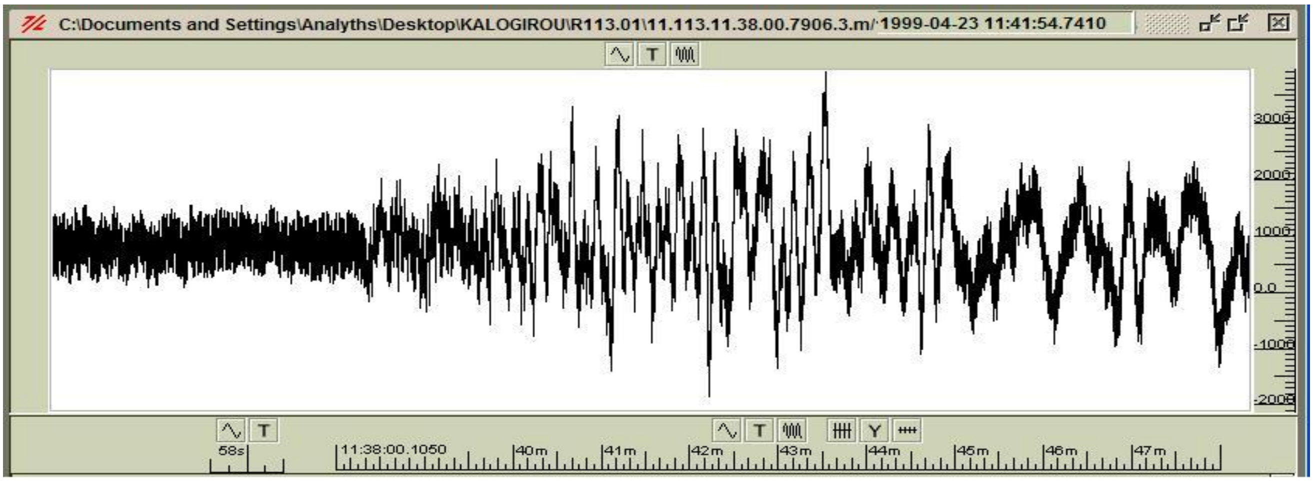

14.　　110425_0805, 1.7

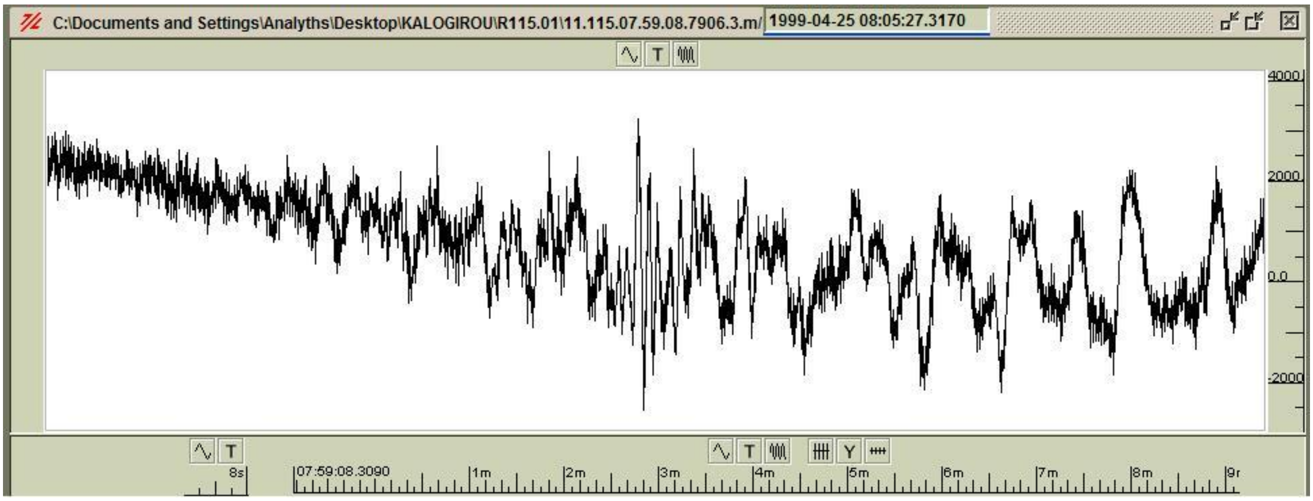

15.　　110428_0812, 1.4

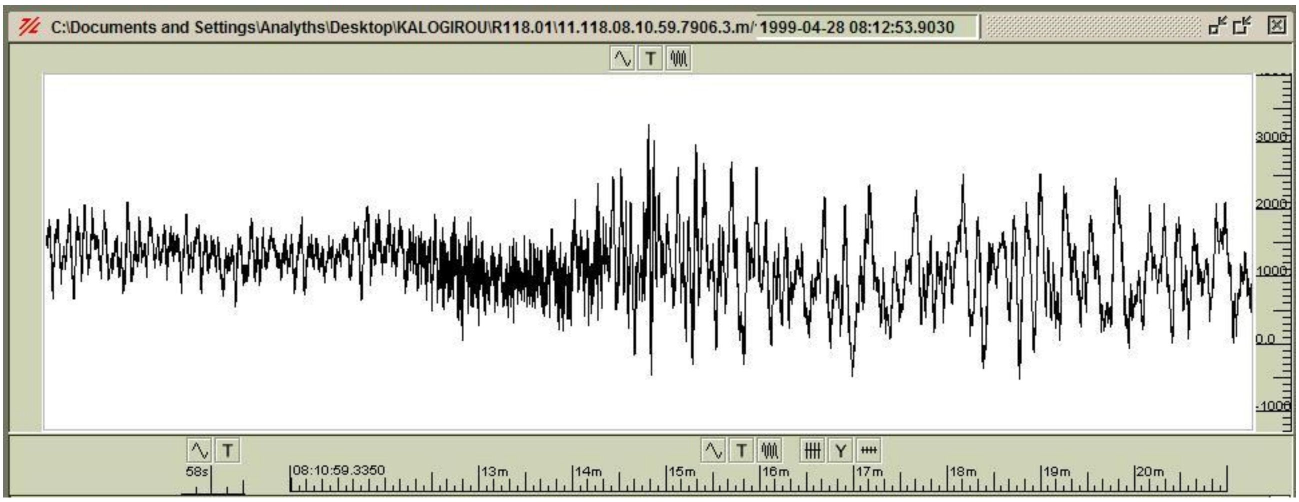

16. 110501_0817, 1.5